

UNIVERSITY OF CALIFORNIA SAN DIEGO

Throwing a wrench in the translational machinery:  
Discovery of RNA ligands by fluorescence techniques

A dissertation submitted in partial satisfaction of the requirements for the degree

Doctor of Philosophy

in

Chemistry and Biochemistry

by

Jerod Russell Parsons

Committee in charge:

Professor Thomas Hermann, Chair  
Professor Steve Briggs  
Professor Simpson Joseph  
Professor Ulrich Muller  
Professor Yitzhak Tor

2010

UMI Number: 3403450

All rights reserved

INFORMATION TO ALL USERS

The quality of this reproduction is dependent upon the quality of the copy submitted.

In the unlikely event that the author did not send a complete manuscript and there are missing pages, these will be noted. Also, if material had to be removed, a note will indicate the deletion.



UMI 3403450

Copyright 2010 by ProQuest LLC.

All rights reserved. This edition of the work is protected against unauthorized copying under Title 17, United States Code.



ProQuest LLC  
789 East Eisenhower Parkway  
P.O. Box 1346  
Ann Arbor, MI 48106-1346

©

Jerod Russell Parsons, 2010

All Rights Reserved

The Dissertation of Jerod Russell Parsons is approved, and it is acceptable in quality and form for publication on microfilm and electronically:

---

---

---

---

---

Chair

University of California, San Diego

2010



## TABLE OF CONTENTS

Signature Page.....	iii
Table of Contents.....	iv
List of Abbreviations.....	vi
List of Figures.....	vii
Acknowledgement.....	ix
Vita.....	x
Abstract of the Dissertation.....	xi
Chapter 1: Introduction.....	1
References.....	11
Chapter 2: Fluorescent pteridine nucleobase analogues as monitors of RNA structure in ribosomal decoding-site RNA.....	13
2.0: Abstract.....	14
2.1 Introduction.....	14
2.2 Results.....	17
2.3 Conclusions.....	24
References.....	26
Chapter 3: Using an oligonucleotide model to study ligand binding to two sites in ribosomal helix h44.....	27
3.0: Abstract.....	28
3.1: Introduction.....	28
3.2: Results.....	34
3.3: Conclusion.....	51

References.....	55
Chapter 4: Fluorescence Study of Hepatitis C Virus Internal Ribosome Entry Site	
(HCV IRES) Subdomain IIa .....	57
4.0: Abstract.....	58
4.1: Introduction.....	59
4.2: Results.....	66
4.3: Conclusions.....	73
References.....	75
Chapter 5: Förster Resonance Energy Transfer Studies of HCV IRES Subdomain IIa	
.....	79
5.0: Abstract.....	80
5.1: Introduction.....	80
5.2: Results.....	83
5.3: Conclusions.....	92
References.....	94
Chapter 6: Experimental methods and Appendix.....	
References.....	101
Appendix I.....	102
Appendix II.....	106

## LIST OF ABBREVIATIONS

HCV	Hepatitis C Virus
IRES	Internal Ribosome Entry Site
NTR	Non-translated Region
UTR	Untranslated Region
RNA	Ribonucleic acid
mg	milligram
mL	milliliter
NMR	nuclear magnetic resonance
2AP	2-aminopurine
FRET	Forster Resonance Energy Transfer
$E_{\text{FRET}}$	FRET efficiency
$EC_{50}$	Concentration of half-maximal effect
nt	nucleotide(s)
UV	ultraviolet

## LIST OF FIGURES

Figure 1.1a:	2-Deoxystreptamine and 3,5 diaminopiperidine.....	3
Figure 1.1b:	Paromomycin.....	3
Figure 1.2:	The 40S ribosomal subunit .....	6
Figure 1.3:	2-aminopurine. ....	7
Figure 2.1:	Nucleobase analogs .....	16
Figure 2.2a:	Thermal denaturation of RNA constructs with nucleobase analogs.	18
Figure 2.2b:	Oligonucleotide constructs .....	18
Figure 2.3a:	Titration of 3MI-labeled A-site RNA with Tobramycin. ....	20
Figure 2.3b:	Titration of 6MI-labeled A-site RNA with Tobramycin. ....	21
Figure 2.3c:	Titration of 3MI-labeled A-site RNA with Paromomycin. ....	22
Figure 2.3d:	Titration of 6MI-labeled A-site RNA with Paromomycin. ....	23
Figure 3.1a:	Chemical structures of neomycin and tobramycin. ....	30
Figure 3.1b:	Sequence of HX oligonucleotide construct. ....	31
Figure 3.1c:	Sequence of HX2-HX5 oligonucleotide constructs .....	31
Figure 3.2:	Magnesium titrations in HX RNA.....	35
Figure 3.3:	Ammonium sulfate titrations in HX RNA. ....	36
Figure 3.4:	Hygromycin B titrations in HX RNA .....	39
Figure 3.5:	Geneticin and Paromomycin titrations in HX RNA.....	40
Figure 3.6:	Hygromycin and paromomycin titrations in presence of Mg <sup>2+</sup> .....	43
Figure 3.7:	Tobramycin alone and in competition with magnesium.....	46
Figure 3.8:	Tobramycin competition with Hygromycin.....	48
Figure 3.9:	Melting Temperatures of HX RNA.....	49

Figure 3.10:	Model of A1492/A1493 positions .....	54
Figure 4.1:	Secondary Structure of IRES Ila RNA constructs .....	63
Figure 4.2a:	Crystal Structure of IRES Ila RNA .....	63
Figure 4.2b:	Secondary structure of HCV IRES.....	63
Figure 4.3:	IRES Ila hinge region.....	65
Figure 4.4a:	Neomycin Titrations in Ila-13-54 construct .....	67
Figure 4.4b:	Neomycin Titrations in Ila-13-57 construct .....	68
Figure 4.5:	P253.....	69
Figure 4.6:	P253 Titration in Ila-13-54 RNA.....	70
Figure 4.7:	P253 competition with magnesium.....	71
Figure 4.8:	Table of Ila-13-54 and Ila-13-57 titration results .....	72
Figure 5.1:	Equations of Förster Resonance Energy Transfer.....	81
Figure 5.2:	IRES Ila-2 construct .....	82
Figure 5.3:	IRES Ila-2 titrated with magnesium.....	83
Figure 5.4:	IRES Ila-2 titrated with P253.....	85
Figure 5.5:	Test of P253 as an NS5B polymerase inhibitor.....	87
Figure 5.6:	Compounds screened against the IRES Ila-2 RNA.....	90
Figure 5.7a:	Scaffold of Hydrazone compounds.....	91
Figure 5.7b:	Structure-Activity Relationship of Indole-class Hydrazones.....	91

## ACKNOWLEDGMENT

Research described in Chapter 2, has been published in *Tetrahedron*, Volume 63, Issue 17, 23 April 2007, Pages 3548-3552. Jerod Parsons was the primary investigator and first author of this paper, in collaboration with Prof. Thomas Hermann.

Research described in Chapter 3, in part, has been published in *Nucleic Acids Research*, 2010, 1–8. Jerod Parsons was the primary investigator and first author of this paper, in collaboration with Prof. Thomas Hermann and Dr. Sergey Dibrov.

Research described in Chapter 5, in part, has been published in *Nature Chemical Biology* 5, 11 823-825. Jerod Parsons was first author of this paper, in collaboration with Prof. Thomas Hermann, Dr. M. Paola Castaldi, Dr. Sanjay Dutta, Dr. Sergey Dibrov, and Dr. David Wyles.

## VITA

- 2005            Texas A&M University  
                  Bachelor of Science, Genetics
- 2010            University of California, San Diego  
                  Doctor of Philosophy, Chemistry and Biochemistry.

### Publications:

- J Comput Chem. 2005 Jul 30;26(10):1063-8.JSB (06)  
Practical conversion from torsion space to Cartesian space for in silico protein synthesis.
- J Struct Biol. 2006 Feb;153(2):103-12.  
Assessing methods for identifying pair-wise atomic contacts across binding interfaces.
- Tetrahedron, Volume 63, Issue 17, 23 April 2007, Pages 3548-3552  
Conformational flexibility of ribosomal decoding-site RNA monitored by fluorescent pteridine base analogues
- Nature Chemical Biology 5, 11 823-825 (Nov 2009).  
Conformational inhibition of the hepatitis C virus internal ribosome entry site RNA
- Nucleic Acids Research 2010; doi: 10.1093/nar/gkq159  
A model for the study of ligand binding to the ribosomal RNA helix h44
- Chembiochem 2010. *Accepted*.  
A Modular Approach to Synthetic RNA Binders of the Hepatitis C Virus Internal Ribosome Entry Site.

## ABSTRACT OF THE DISSERTATION

Throwing a wrench in the translational machinery:  
Discovery of RNA ligands by fluorescence techniques.

by

Jerod Russell Parsons

Doctor of Philosophy in Biochemistry and Biochemistry

University of California, San Diego, 2010

Professor Thomas Hermann, Chair

Ribonucleic acids (RNAs) are underexplored as targets for therapeutics. To date, drug research has focused primarily on protein targets. Inhibition of functional RNA is an alternative approach which can avoid some of the problems of resistance. A few RNAs of interest are the bacterial ribosome, HIV RRE and Tar, human thymidylate synthase mRNA, and the Hepatitis C Virus Internal Ribosome Entry Site.

Fluorescently-modified oligoribonucleotides are a relatively cheap method of quickly determining changes in the structure of the RNA. During chemical synthesis, fluorescent modifications can be placed in virtually any position and used to report on



local structural changes. This technique was applied to the ribosomal A-site, and expanded to encompass alternative fluorophores and RNA sites. To identify compounds bound to HCV IRES domain IIa, fluorescent and FRET-based constructs were designed. After screening a small compound library in these systems, several were identified as binding. A structure activity relationship based on one class of these binding compounds was determined for the IRES IIa.

In order to study the chemical components of RNA binding affinity, fluorescent methods for identifying RNA ligands to two RNA targets were devised. Extension of an oligonucleotide construct based on the ribosomal A site allows monitoring of an additional ligand binding site. FRET-based distance measurements in a viral RNA allow discrimination between functional and nonfunctional conformations, and therefore can be used to identify compounds that stabilize a nonfunctional conformation.

## **Chapter 1: Introduction**

## 1.0 Introduction

Unlike cellular Deoxynucleic acid (DNA) molecules, ribonucleic acids (RNAs) form complicated structural motifs that can be targeted by small molecules. These structural motifs form the basis for RNA folds, which are required for functional RNA molecules and are the targets of molecular recognition of RNA. RNA-binding molecules interact with RNA by mechanisms involving presentation of rigid hydrogen-bonding frameworks or by displacing structural metal ions by means of electrostatic compatibility provided by positively charged amino groups. (1).

Aminoglycoside antibiotics, originally isolated from bacteria, are a prime example of RNA-targeting drugs. Aminoglycosides bind to a wide variety of RNA targets. These antibiotics are built of amino sugars linked to a streptamine or 2-deoxystreptamine (2-DOS) heterocycle (figure 1.1a). (2) The charged nature of the dual amino groups in the 2-DOS core provides a large electrostatic component to RNA binding. The 2-DOS core is responsible for RNA affinity, while the sugars provide some measure of specificity (3). Even with this specificity, however, aminoglycosides can bind tightly to a plethora of RNA structures, including HIV TAR, HIV RRE, HDV ribozyme, and even poly(A) RNA, in addition to the ribosome. (3-8)

Attempts have been made to create mimetics of the 2-DOS core scaffold in order to improve specificity, affinity, and ease of synthesis, as well as to avoid inactivating chemical modifications in resistant bacteria. (9,10) One such 2-DOS mimetic is the 3,5

diaminopiperidine (DAP) heterocycle (Figure 1.1a), designed to maintain the cis-1,3 arrangement of amino groups from the 2-DOS ring.

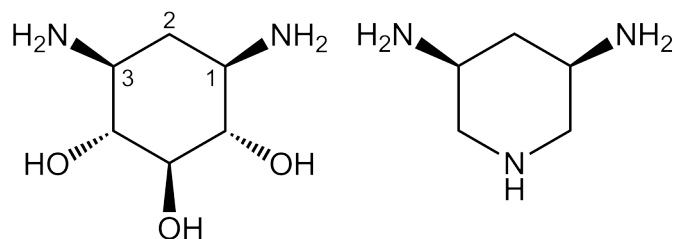


Figure 1.1a: (Left) 2-Deoxystreptamine (2-DOS). (Right) 3,5 diaminopiperidine (DAP).

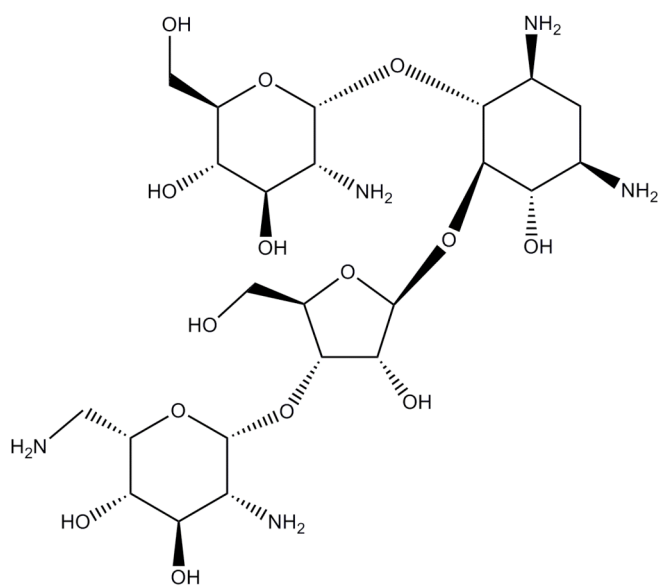


Figure 1.1b: Aminoglycoside antibiotic paromomycin.

### *The Ribosome:*

The ribosome is responsible for the synthesis of protein based on the information contained in messenger RNA (mRNA) template, through the process of translation. Ribosomes are around two-thirds RNA components and one-third protein components. Ribosomal proteins perform mostly supportive roles. The active site of the ribosome, where peptide bond formation occurs, is entirely composed of RNA. The bacterial ribosome is composed of two subunits of unequal size, the small (30S) subunit and the large (50S) subunit. The ribosomal subunits in eukaryotic cells are larger, with sedimentary coefficients of 40S and 60S. The process of protein synthesis can be broken into three steps: Initiation, elongation, and termination. Initiation of protein synthesis is described in detail in the introduction of Chapter 4. In the initiation process, the two ribosomal subunits join together with the mRNA template, reading the mRNA from 5' to 3' to create the corresponding protein N-terminus to C-terminus. An initiator tRNA, bound at the peptidyl transfer site (P site), begins the process. Additional tRNAs supply amino acids according to the genetic code to the aminoacyl site (A site). Elongation of the peptide occurs by attack from the free  $\alpha$ -amino group at the A site to the ester bond linking the P-site peptide to the tRNA. After this reaction occurs, the peptide chain remains at the A site. Translocation then cycles the A-site tRNA to the P site, and the P site tRNA to a third site, the exit site (E site). Additional cycles of peptidyl transfer occur, repeating until a stop codon is read. The termination step occurs as release factor proteins assist in the dissociation of the polypeptide from the tRNA. (11)

### *Ribosomal Structure*

The ribosome is a particle composed of RNA and protein that synthesizes protein using mRNA as template and aminoacyl-tRNA as substrate. The small (40S) ribosomal subunit forms a 3-dimensional structure resembling an upright duck (Figure 1.2) (28,32). The mRNA enters the subunit through the entry tunnel and exits at the other side, at the exit site. Conformational changes within the subunit can rotate the head relative to the shoulder and platform, or the entire 40S relative to the 60S. These conformational changes have been suggested to correlate with events in the initiation and translocation steps (32).

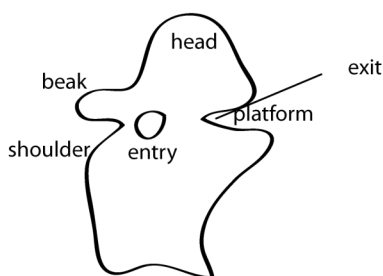


Figure 1.2: The 40S ribosomal subunit. The head, beak, shoulder and platform regions are marked, as well as the mRNA entry and exit tunnels.

### *The Ribosomal A Site*

The A-site of the small ribosomal subunit is the location of decoding during translation. The proper tRNA must be bound to the A site in order to translate the correct protein. High fidelity of translation from mRNA to protein is required for proper cellular function (12). One mechanism used to ensure translational fidelity occurs at the A site. Two flexible adenine bases, A1492 and A1493, are involved in this mechanism. These flexible bases can be stacked on neighboring bases inside the decoding loop or can be

located outside the loop, stabilizing the codon-anticodon interaction. These adenines interact with the tRNA and mRNA during the decoding process. During this process, the tRNA and mRNA form a codon-anticodon duplex, and the sensor adenines A1492-A1493 recognize this duplex by interacting with the minor groove.

Several aminoglycoside antibiotics target the A-site and bind within the decoding loop. They shift the equilibrium of 1492-1493 toward the tRNA-bound conformation – even in cases where the tRNA is non-cognate, leading to increased translational error as incorrect peptides are added to the nascent protein chain. This occurs due to a conformational change in the ribosome which precedes the peptidyl transfer reaction and is initiated due to the 1492-1493 interaction with the duplex RNA at the codon-anticodon site.

The A site of the ribosome has been intensely scrutinized. Crystal structures involving helix 44 show three distinct conformational possibilities for A1492 and A1493: The stacked, flipped-in conformation of an empty 30S, the stacked, flipped-out conformation of paromomycin-bound (or cognate tRNA bound), and a third ‘splayed-out’ conformation that occurs after IF-1 and S12 binding, or in the presence of hygromycin B). These conformational shifts propagate throughout the ribosome and are part of the concerted actions involved in the translation process (30-31).

The A-site loop in helix 44 of the small ribosomal subunit can be isolated from the native ribosomal context to form small RNA constructs (13-17). These constructs maintain the conformational flexibility of the 1492/1493 and are capable of binding

aminoglycosides. Being significantly smaller than the full ribosome makes the small RNA constructs suitable for high-resolution X-ray crystallography (15,16) and presents opportunities for selective chemical modifications.

### *2-aminopurine Modification*

The unnatural nucleobase 2-aminopurine (2AP) has been used extensively as a nucleobase analog due to its fluorescent properties and structural similarity to adenine. The fluorescence of 2AP reflects its chemical environment. When stacked with other bases, fluorescence output is quenched. When un-stacked, fluorescence output is increased. Therefore, alternative conformations of the 2-aminopurine base can be distinguished based on the differential fluorescence response. 2AP replacement is therefore very applicable to the sensor adenines in the ribosomal A-site (18-20), but can be applied in any setting where a conformationally flexible adenine can be found.

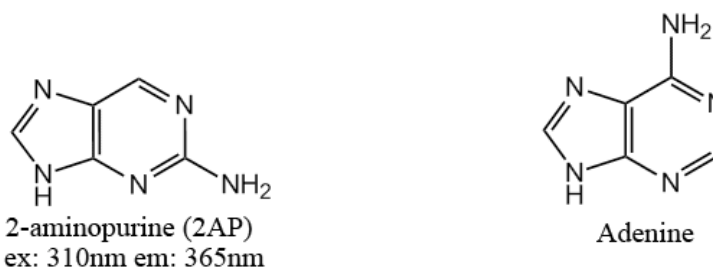


Figure 1.3: The 2AP nucleobase analog compared to adenine.

### *Non-ribosomal Targets*

Non-ribosomal RNA has only recently become the subject of pharmacological attention, but RNA frequently forms highly ordered functional 3D structures, which can be suitable for drug targeting. Messenger RNA (mRNA) production and translation in



the cell is highly regulated in order to produce the proper amounts of protein at the appropriate time. Regulation of translation can take the form of RNA degradation or sequestration (21). Riboswitches can attenuate or induce translation by hiding or exposing the expression platform, usually due to binding a target metabolite. (22,23) Internal Ribosome Entry Sites (24,25) allow cap-independent translation of viral proteins in eukaryotic cells, and allow some eukaryotic proteins to be expressed in the absence of initiation factors (26).

### *Internal Ribosome Entry Sites*

Viruses rely on host cells to replicate. Cellular defense mechanisms have evolved to shut down cellular translation after viral infection, in order to prevent viral spread. These defense mechanisms typically prevent initiation of translation (27). To combat these defenses, some viral mRNAs have evolved internal ribosome entry sites (IRESes) to begin translation. Over one hundred IRES sequences have been identified, with widely variable structures. One class of IRES structures is exemplified by the Hepatitis C Virus (HCV) IRES. HCV translation is driven by the IRES comprised of the 5' untranslated region (UTR) of the HCV mRNA. This sequence is over 350 nucleotides in length and folds into four independently structured domains. Chapter 4 describes the mechanism of IRES-driven initiation of translation in the Hepatitis C Virus. The sequence and structure of the HCV IRES are highly conserved relative to the rest of the viral genome. Thus, drugs targeting the IRES structure are less likely to develop resistant mutations than drugs targeting the viral proteins. Specific interactions between the IRES and ribosome are required for translation to occur, and these interactions may be

disrupted by the action of small molecules. A small molecule that alters the conformation of a specific fragment of the IRES RNA could be sufficient to disrupt the overall function of the IRES and preclude translation by this mechanism.

Structural studies of the HCV IRES (28) have shown that the HCV IRES complexes with the ribosome by forming extensive contacts. Preventing the association of the IRES with the ribosome would require overwhelming the positive interactions of a large surface area, a feat nearly impossible for small molecules. An alternative strategy involves making pinpoint disruptions at structurally important positions. Domain II of the IRES forms direct contacts with the ribosome at only a small interface, where apical loop IIb is positioned between the ribosomal head and platform. Nevertheless, the entirety of domain II is required for initiation of translation. It has been suggested that the function of domain II may be to position the single-stranded coding RNA of the virus inside the decoding site (28). A sharp kink in the RNA backbone is caused by subdomain IIa, and this structural disturbance serves to thread the remainder of domain II between the ribosomal head and platform and into the active site of the ribosome.

Work presented herein serves to further the goal of identifying RNA-targeting small molecules. Such compounds may serve as future antiviral, antibacterial, or even anticancer agents, and will certainly assist in future efforts to create such agents by guiding structure-based design. Fluorescence techniques that can be used to rapidly determine the RNA-binding characteristics of a compound in multiple systems are described.

In addition, the mechanism of action of a small molecule inhibitor of viral translation is described, highlighting the potential of such ligands to disrupt RNA-based molecular machines other than the ribosome.

## References:

1. Hermann, T. (2002). Rational ligand design for RNA: the role of static structure and conformational flexibility in target recognition. *Biochimie*. 84, 869–875
2. Gallego, J., and Varani, G. (2001). Targeting RNA with Small-Molecule Drugs: Therapeutic Promise and Chemical Challenges. *Acc. Chem. Res.* 34, 836-843
3. Arya, D. P.; Xue, L., and Willis, B. (2003). Aminoglycoside (Neomycin) Preference Is for A-Form Nucleic Acids, Not Just RNA: Results from a Competition Dialysis Study. *J. Am. Chem. Soc.* 125: 10148.
4. Xi H, Gray D, Kumar S, Arya DP. (2009) Molecular recognition of single-stranded RNA: neomycin binding to poly(A). *FEBS Lett.* 7; 583(13): 2269-75.
5. Wang, S., Huber, P.W., Cui, M., Czarnik, A.W., and Mei, H.Y. (1998). Binding of neomycin to the TAR element of HIV-1 RNA induces dissociation of Tat protein by an allosteric mechanism, *Biochemistry* 37:5549–5557.
6. Zapp, M.L., Stern, M.S., and Green, M.R. (1993). Small molecules that selectively block RNA binding of HIV-1 Rev function and viral production. *Cell* 74: 969–978.
7. Stage, T.K., Hertel K.J., and Uhlenbeck, O.C.. (1995). Inhibition of the hammerhead ribozyme by neomycin, *RNA* 1: 95–101.
8. Rogers, J., Chang, A.H., Ahsen, U., Schroeder, R., and Davies, J. (1996). Inhibition of the self-cleavage reaction of the human hepatitis delta virus ribozyme by antibiotics, *J. Mol. Biol.* 259:916–925.
9. Silva, J.G., and Carvalho, I. (2007). New insights into aminoglycoside antibiotics and derivatives. *Curr Med Chem.* 2007; 14(10): 1101-19.
10. Ye, X.-S., and Zhang, L.-H (2002). Aminoglycoside Mimetics as Small-Molecule Drugs Targeting RNA . *Curr. Med. Chem.* 9,9, 929-939.
11. Simonović, M., and Steitz, T.A. (2009) A structural view on the mechanism of the ribosome-catalyzed peptide bond formation. *Biochim Biophys Acta*; 1789(9-10): 612-23.
12. Ogle, J.M., and Ramakrishnan, V. (2005) Structural insights into translational fidelity. *Annu Rev Biochem*; 74:129-77.
13. Purohit P., and Stern, S. (1994). Interactions of a small RNA with antibiotic and RNA ligands of the 30S subunit. *Nature.* 25:370(6491): 659-62.
14. Shandrick, S., Zhao, Q., Han, Q., Ayida, B. K., Takahashi, M., Winters, G.C., Simonsen, K.B., Vourloumis, D., and Hermann, T. (2004). Monitoring Molecular Recognition of the Ribosomal Decoding Site. *Angew. Chem.* 116, 3239; *Angew. Chem. Int. Ed.* 2004, 43, 3117.
15. Vicens, Q., and Westhof, E. (2001). Crystal structure of paromomycin docked into the eubacterial ribosomal decoding A site. *Structure*, 9, 647-658.
16. Vicens, Q., and Westhof, E., (2002). Crystal Structure of a Complex between the Aminoglycoside Tobramycin and an Oligonucleotide Containing the Ribosomal Decoding A Site *Chemistry & Biology*, Vol. 9, 747–755.
17. Hermann, T. (2006). A-site model RNAs. *Biochimie*, 88, 1021–1026.

18. Hermann, T. (2005). Drugs targeting the ribosome. *Curr. Opin. Struct. Biol.* 15: 355–366.
19. Yang, G., Trylska, J., Tor, Y., and McCammon, J.A. (2006). Binding of Aminoglycosidic Antibiotics to the Oligonucleotide A-Site Model and 30S Ribosomal Subunit: Poisson-Boltzmann Model, Thermal Denaturation, and Fluorescence Studies. *Med. Chem.*, 49, 5478-5490
20. Dibrov, S.M., Parsons, J., and Hermann, T. (2010). A model for the study of ligand binding to the ribosomal RNA helix h44. *Nucleic Acids Research*; doi: 10.1093/nar/gkq159
21. Liang, R., Bates, D.J., and Wang, E. (2009). Epigenetic Control of MicroRNA Expression and Aging. *Curr Genomics.* 10(3): 184-93.
22. Serganov, A. (2009). The long and the short of riboswitches. *Current Opinion in Structural Biology* 19, 3, pp. 251-259
23. Scott, W.G., Martick, M., and Chi, Y. (2009) Structure and function of regulatory RNA elements: Ribozymes that regulate gene expression. *Biochimica et Biophysica Acta (BBA)* 1789, 9-10, pp 634-641
24. C.U.T. Hellen. (2009). IRES-induced conformational changes in the ribosome and the mechanism of translation initiation by internal ribosomal entry. *Biochimica et Biophysica Acta* 1789. 558–570
25. Saffran, H.A., Read, G.S., and Smiley, J.R.J. (2010). Evidence for translational regulation by the herpes simplex virus virion host shutoff protein. *Virology*. doi:10.1128/JVI.01819-09 Mar 31.
26. Allam, H., and Ali, N. (2010). Initiation factor eIF2-independent mode of c-Src mRNA translation occurs via an internal ribosome entry site. *J. Biol. Chem.* Feb 19; 285(8): 5713-25.
27. Balvay, L., Soto Rifo, R., Ricci, E.P., Decimo, D., and Ohlmann, T. (2009) Structural and functional diversity of viral IRESes. *Biochim. Biophys. Acta.* 1789(9-10): 542-57.
28. Spahn, C.M., Kieft, J.S., Grassucci, R.A., Penczek, P.A., Zhou, K., Doudna, J.A., and Frank, J. (2001). Hepatitis C virus IRES RNA-induced changes in the conformation of the 40s ribosomal subunit. *Science* 291, 1959–1962.
29. Beales, LP, Rowlands, DJ, and Holzenburg, A. (2001). The internal ribosome entry site (IRES) of hepatitis C virus visualized by electron microscopy. *RNA*; 7: 661–670.
30. Carter, A.P., Clemons, W.M., Brodersen, D.E. (2000). Functional insights from the structure of the 30S ribosomal subunit and its interactions with antibiotics. *Nature.* 2000; 407: 340–348
31. Ogle, J.M., Brodersen, D.E., Clemons, W.M. (2001) Recognition of cognate transfer RNA by the 30S ribosomal subunit. *Science.* 2001; 292: 897–902.
32. Schmeing, T. and Ramakrishnan, V. (2009) What recent ribosome structures have revealed about the mechanism of translation. *Nature* 461, 1234-1242.

**Chapter 2:**

**Fluorescent pteridine nucleobase analogues  
as monitors of RNA structure  
in ribosomal decoding-site RNA**

Parts of this work are published in:

“Conformational flexibility of ribosomal decoding-site RNA monitored by  
fluorescent pteridine base analogues.”  
Tetrahedron. April 2007, V63, 17, 23 pp. 3548-3552

## 2.0 Abstract:

Pteridine nucleobase analogues 3-methylisoxanthopterin (3MI) and 6-methylisoxanthopterin (6MI) are viable alternative red-shifted fluorophores for use in fluorescence experiments involving compounds spectrally incompatible with 2-aminopurine (2AP), the nucleobase analog typically used to monitor conformational transitions in ribosomal decoding-site RNA constructs. The use of pteridine analogs requires careful structural validation, as the bases are more distant chemically than 2AP.

(1)

## 2.1 Introduction

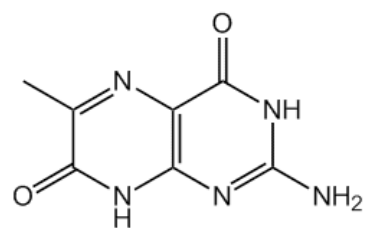
Helix h44 of the 16S rRNA constitutes the majority of the bacterial decoding site. This internal loop contains two key adenosine residues, A1492 and A1493. These two conformationally flexible residues monitor interactions between the mRNA codon and tRNA anticodon in the A site and are key to maintaining fidelity during protein synthesis. Oligonucleotides containing subsequences of this internal loop adopt structures similar to the native ribosomes, making them useful as model systems. (2-4) Making chemical modifications to the short oligonucleotides in these models is relatively straightforward. The fluorescent nucleobase analog, 2AP, has been used in such a fluorescently labeled decoding site model. (5, 6) In this system, ligand binding can be identified by selectively exciting the 2AP nucleoside and monitoring the emission changes, which reflect the changes in the local environment of the nucleoside. (7) In the context of the ribosomal

decoding site, the 1492 and 1493 nucleotides are displaced from the internal loop in the presence of either a proper tRNA: mRNA match or an aminoglycoside antibiotic. This displacement from the internal loop corresponds to a significant change in local environment and therefore a change in the quantum yield of 2AP fluorescence.

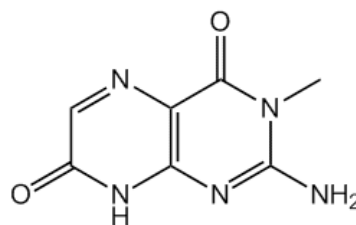
2AP excitation and emission spectra are fairly short wavelength, with 310nm excitation and 370nm emission peaks. These wavelengths introduce complications with highly conjugated organic compounds, which may also absorb or emit in the same wavelength range. Spectral overlap with 2AP precludes usage in 2AP-based binding assays for compounds with strong absorbance or emission in the overlapping range. Nucleotide analogs that are red-shifted relative to 2AP widen the scope of such assays.

Spectral overlap issues can be overcome in fluorescence screens by reproducing the RNA construct with alternative fluorophores using excitation and emission wavelengths orthogonal to those of other molecules in the solution. One of the main benefits of 2AP is its structural similarity to natural nucleoside bases, which makes it a relatively safe alternative to adenine in a large number of structural contexts. Caution must be observed to ensure that fluorophores do not disturb the overall fold of the RNA. Pteridine analogues had previously been applied to DNA (8-9), where they are useful as guanosine analogs. Structural environments that are amenable to pteridine fluorescence have been described by this group.

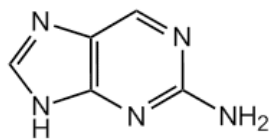




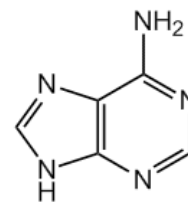
6-methylisoxanthopterin (6MI)  
ex: 345nm em: 431nm



3-methylisoxanthopterin (3MI)  
ex: 348nm em: 430nm



2-aminopurine (2AP)  
ex: 310nm em: 365nm



Adenine

Figure 2.1: Nucleobase analogs. Shown are 2AP, Adenine, 3MI, and 6MI, as well as their fluorescence excitation and emission peaks.

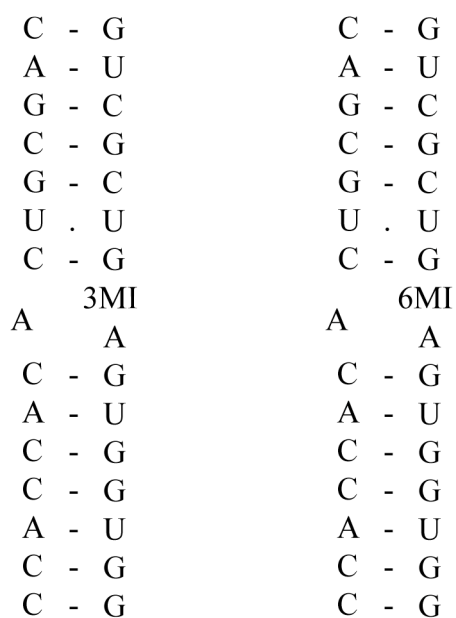
## 2.2 Results:

To determine relative stability of constructs differing only in the type of nucleobase analog, thermal denaturation experiments (Figure 2.2) were performed on RNA constructs based on the sequence of the ribosomal A-site in helix h44. These constructs were chemically synthesized with analogs at position 1493. In 10mM cacodylate buffer, the melting temperatures are 44.2°C for 3MI, 45.2°C for 6MI, and 47.4°C for 2AP-labeled A-site RNA constructs. DNA oligos containing 3MI and 6MI substitutions display similar shifts in  $T_m$ , due to 6MI forming slightly stronger interactions with other bases (9). In the presence of 1mM  $MgCl_2$ , all three constructs have a  $T_m$  of 65.5°C. Adding 1mM paromomycin to RNA in the presence of 1mM  $MgCl_2$  stabilizes each construct by approximately 2°C to 67.8°C, 67.5°C, and 66°C for 3mi, 6mi, and 2AP, respectively.

To demonstrate the differences between the alternative labels, fluorescence titrations were performed. Stepwise addition of increasing amounts of compound results in a sigmoidal dose response curve, with a fluorescence shift indicative of the change in local environment around the fluorescent base. Binding of ligands such as tobramycin (Figure 2.3) in the two constructs show that RNA labeled at the 1493 position with either 3MI or 6MI responds to titration by being quenched with an  $EC_{50}$  of  $1.8\mu M \pm 0.7\mu M$  in 3MI and  $2.2\mu M \pm 1.1\mu M$  in 6MI. Paromomycin titrations of the two constructs show that 3MI-labeled RNA fluorescence is very slightly increased in the presence of the compound, while 6MI RNA is quenched to 70% with an  $EC_{50}$  of  $800nM \pm 300nM$ .

Nucleobase Analog:	RNA T <sub>m</sub> (°C)	RNA + 1 mM Mg <sup>2+</sup> T <sub>m</sub> (°C)	RNA + Mg <sup>2+</sup> , Paromomycin (1mM each) T <sub>m</sub> (°C)
2AP	47.4	65.5	66
3MI	44.2	65.5	67.8
6MI	45.2	65.5	67.5

Figure 2.2a: Thermal denaturation of RNA constructs with nucleobase analogs. RNA constructs containing either 2AP, 3MI, or 6MI at the 1493 position had UV absorption measurements made at every 1° from 20C to 85C. Reported is the T<sub>m</sub> for each construct in 10mM cacodylate buffer, (left) in 1mM magnesium, (center), and in 1mM paromomycin and 1mM magnesium (Right).



### 3MI construct    6MI construct

Figure 2.2b: Oligonucleotide constructs used for fluorescence and thermal denaturing experiments. 3MI or 6MI nucleobase analogs replace an adenosine in an RNA construct based on the ribosomal A-site.

For titration figures, relative fluorescence response (bottom) to addition of compound is plotted. RNA alone is given a fluorescence value of 1. Values are averages of 3 replicate experiments, with error bars representing 1 standard error. Error margins of  $EC_{50}$  values are fit errors. Normalization of RNA (top) is done such that  $I_{min}=0$  and  $I_{max}=1$ . In cases such as tobramycin, where a maximum fluorescence intensity is achieved after addition of compound, the fraction bound plots can be misleading.

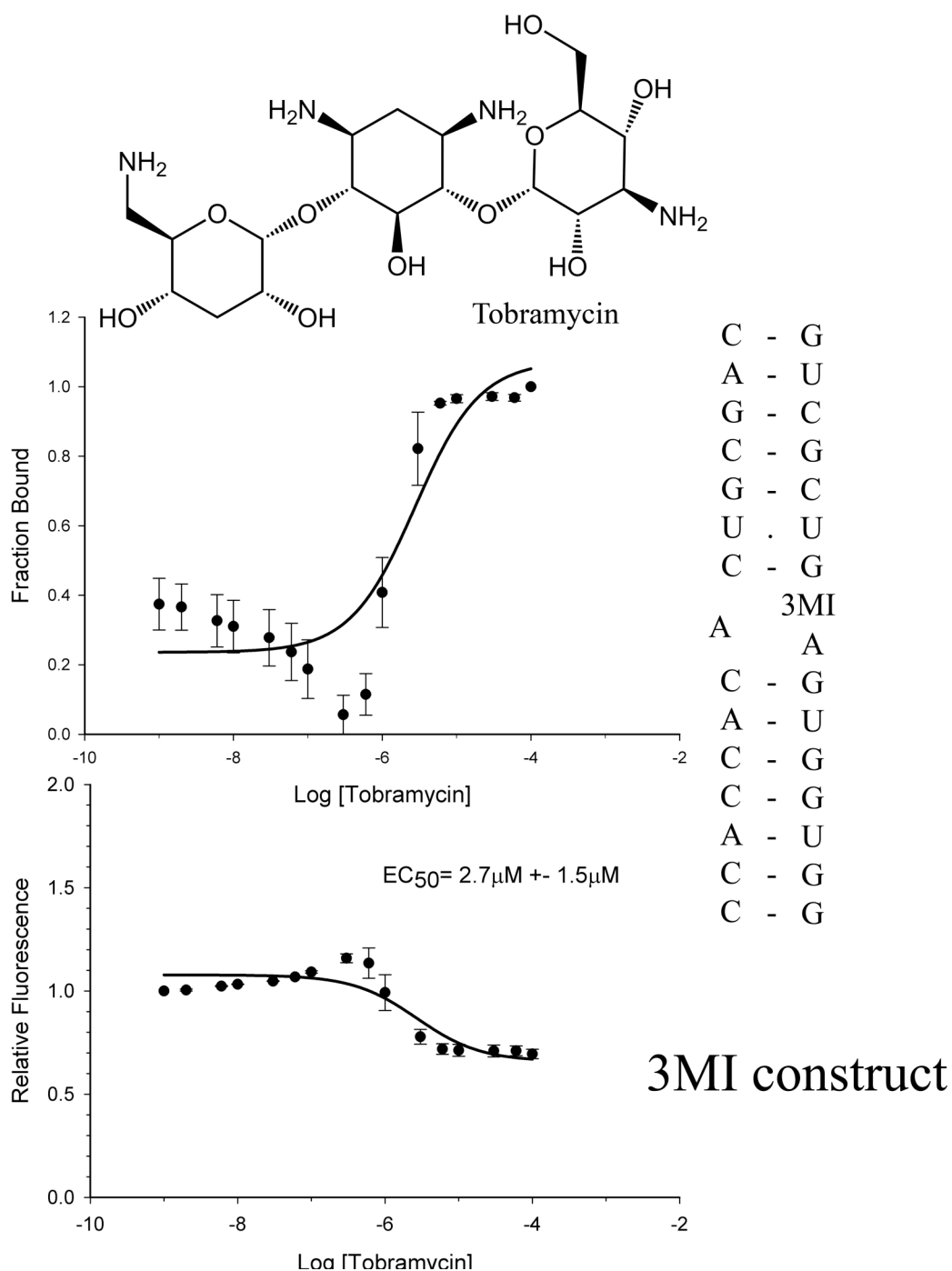


Figure 2.3a: Titration of 3MI-labeled A-site RNA with Tobramycin. The  $EC_{50}$  of the quenching phase of the biphasic response is  $1.8\mu\text{M} \pm 0.7\mu\text{M}$ . The initial increase in fluorescence intensity at sub-micromolar concentrations is discussed more in Chapter 3. Fitting both phases of this response results in the calculations shown above.

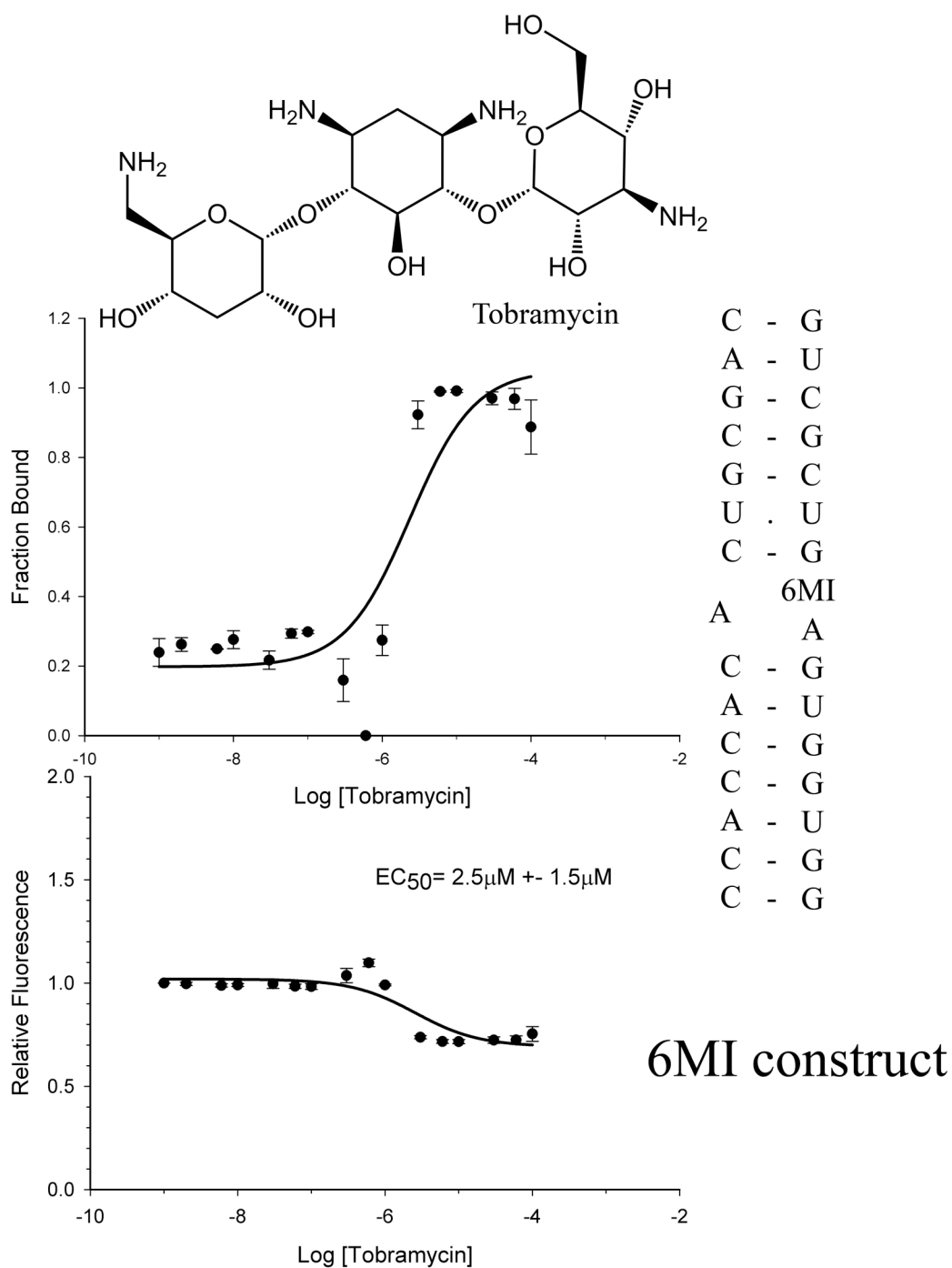


Figure 2.3b: Titration of 6MI-labeled A-site RNA with Tobramycin. The  $EC_{50}$  of the quenching phase of this biphasic response is  $2.2\mu\text{M} \pm 1.1\mu\text{M}$ . The biphasic effect of tobramycin binding is responsible for the disparity between the calculated  $EC_{50}$  for the quenching phase (in the legend) and for the entire titration (above the titration). This biphasic effect is explored in chapter 3.

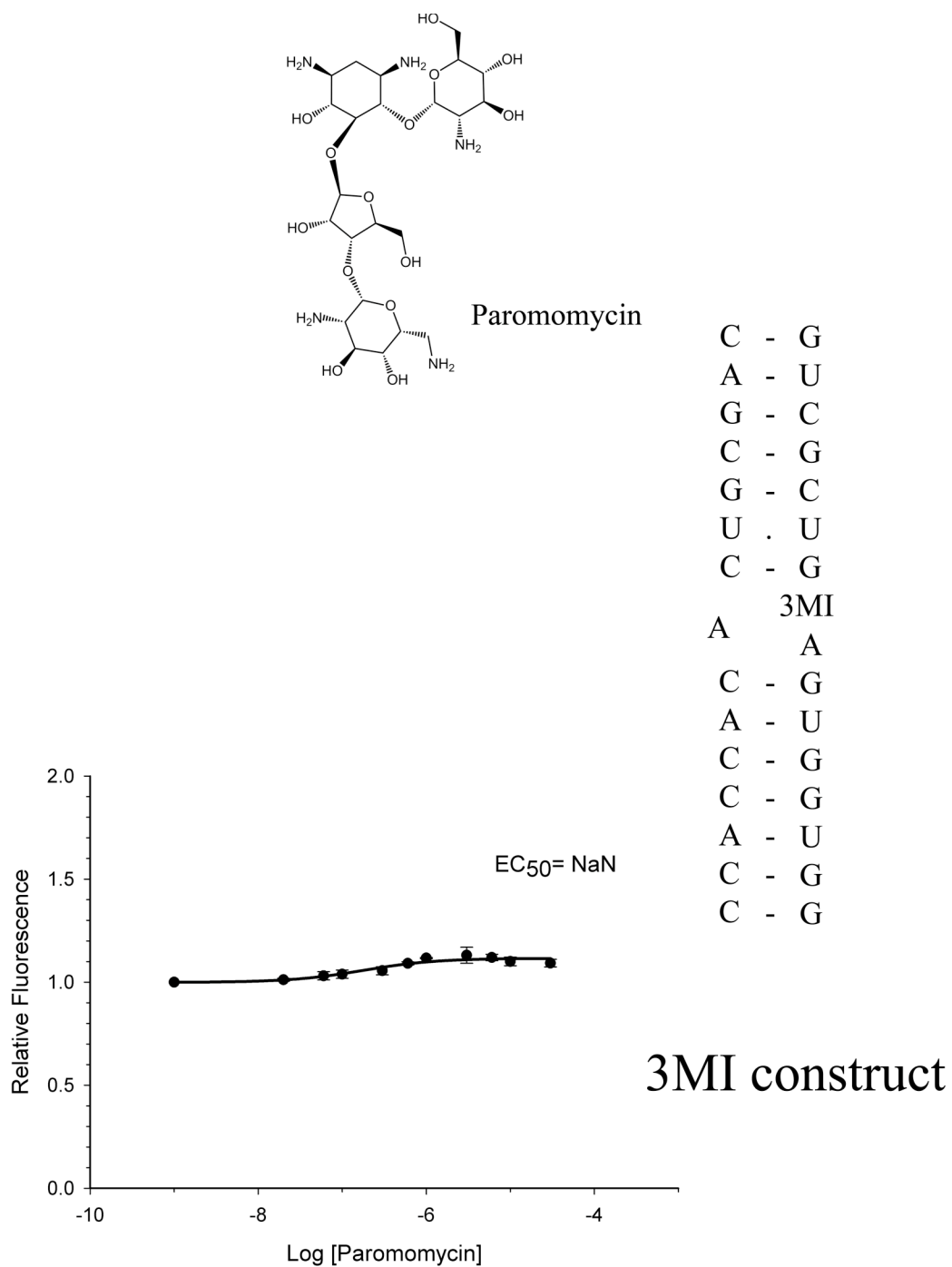


Figure 2.3c: Titration of 3MI-labeled A-site RNA with Paromomycin

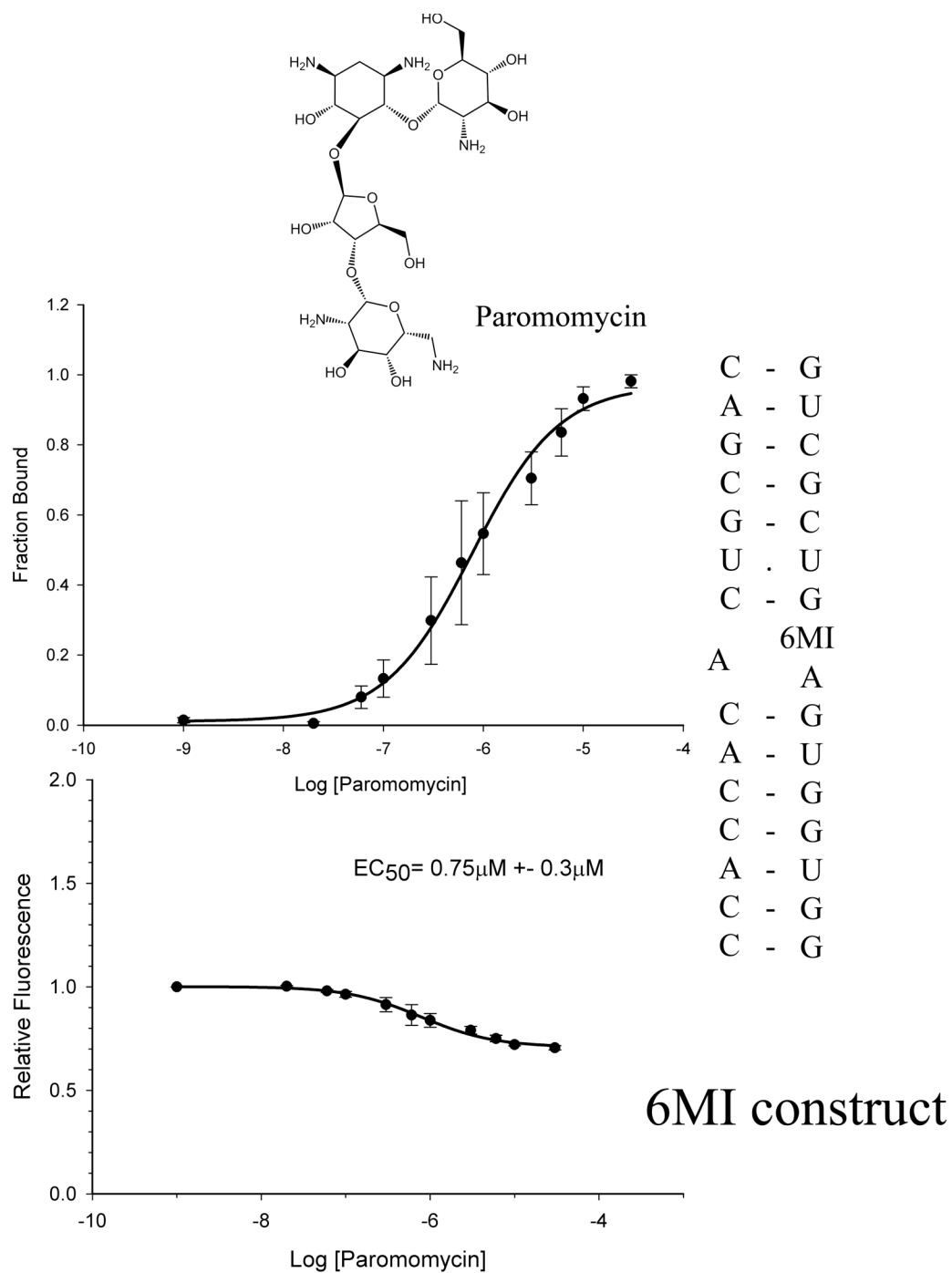


Figure 2.3d: Titration of 6MI-labeled A-site RNA with Paromomycin



### 2.3 Conclusions:

Pteridine-based nucleobase analogs for fluorescent labeling are a tool that can be used instead of 2AP. However, the pteridine bases 3MI and 6MI have less structural similarity to adenine and require careful validation in the context of constructs. The difference in thermal stability of the 3 constructs in the absence of magnesium suggests that the pteridine analogs, especially 3MI, do not form as favorable of stabilizing interactions with the A1408 base. However, in the presence of magnesium or aminoglycosides, interactions between A1493 and A1408 are abolished due to A1493 being locked outside of the helix (A-site and  $Mg^{2+}$  state, Fig 3.11). The pteridine analogs 3MI and 6MI are similar to 2AP in the absence of these interactions, when the nucleobases are fully exposed to solvent.

The 3MI label showed insignificant fluorescent change in the presence of paromomycin, highlighting the need to validate such constructs. As modifying the absorption spectra is coupled with modifying the biophysical properties of the base, any fluorescently modified base analog would ideally be capable of maintaining the chemical interactions of the native base. 2AP has been well studied in this respect. Pteridine bases such as 3MI and 6MI are capable of maintaining some hydrogen-bonding interactions, but should be carefully validated in the context of each construct. 6MI may seem strictly better, but has a slightly lower quantum yield and is more susceptible to photobleaching than 3MI so it may prove less useful in certain experimental designs.

Research described in Chapter 2, has been published in *Tetrahedron*, Volume 63, Issue 17, 23 April 2007, Pages 3548-3552. Jerod Parsons was the primary investigator and first author of this paper, in collaboration with Prof. Thomas Hermann.

## References:

1. Parsons, J., and Hermann, T. (2007). Conformational flexibility of ribosomal decoding-site RNA monitored by fluorescent pteridine base analogues. *Tetrahedron*, Volume 63, Issue 17, 23. Pp.3548-3552
2. Vourloumis, D., Winters, G.C., Simonsen, K.B., Takahashi, M., Ayida, B.K., Shandrick, S., Zhao, Q., Han, Q. and Hermann, T. (2005). Aminoglycoside-hybrid ligands targeting the ribosomal decoding site. *Chembiochem*, 6, 58–65.
3. Wong, C. H., Hendrix, M., Priestley, E. S., and Greenberg, W. A. (1998). Specificity of aminoglycoside antibiotics for the A-site of the decoding region of ribosomal RNA. *Chem. Biol.* 5, 397–406.
4. Purohit P, and Stern S. (1994). Interactions of a small RNA with antibiotic and RNA ligands of the 30S subunit. *Nature*. 25; 370(6491): 659-62.
5. Shandrick, S Zhao, Q., Han, Q., Ayida, B. K., Takahashi, M., Winters, G. C., Simonsen, K. B., Vourloumis, D. and Hermann, T. (2004). Monitoring Molecular Recognition of the Ribosomal Decoding Site *Angew. Chem.* 116, 3239; *Angew. Chem. Int. Ed.* 2004, 43, 3177.
6. Kaul, M., Barbieri, C.M., and Pilch, D.S. (2005). Defining the basis for the specificity of aminoglycoside-rRNA recognition: a comparative study of drug binding to the A sites of *Escherichia coli* and human rRNA. *J Mol Biol.* Feb 11; 346(1): 119-34.
7. Jean, J.M., and Hall, K.B. (2001). 2-Aminopurine fluorescence quenching and lifetimes: Role of base stacking. *PNAS*, vol. 98, no. 1. Pp. 37-41
8. Hawkins, M.E. (2001). Fluorescent pteridine nucleoside analogs: a window on DNA interactions. *CellBiochem.Biophys.* 34,257–281.
9. Hawkins, M.E., Pfeleiderer, W., Balis, F.M., Porter, D., and Knutson, J.R. (1997). Fluorescence properties of pteridine nucleoside analogs as monomers and incorporated into oligonucleotides. *Anal Biochem.* 1; 244(1): 86-95.

## **Chapter 3:**

### **Using an oligonucleotide model to study ligand binding to two sites in ribosomal helix h44**

Parts of this work are published as:

“A model for the study of ligand binding to the ribosomal RNA helix h44”  
Nucleic Acids Research 2010; doi: 10.1093/nar/gkq159

### 3.0 Abstract:

An oligonucleotide construct monitoring two distinct ligand binding sites within helix h44 of the 16S ribosomal RNA was designed. The oligonucleotide construct (HX) was fluorescently labeled with 2AP to elicit fluorescent response to binding-induced structural changes. A high-resolution crystal structure of the construct was solved, showing that the HX RNA construct is an accurate structural model of the ribosomal binding sites. Fluorescent responses to both binding sites are demonstrated and differentiated. (1)

### 3.1 Introduction:

The interactions of aminoglycoside antibiotics with the ribosomal decoding site have been intensely studied in the recent past (2-9). A number of crystal structures of ribosomal subunits in complex with these drugs have been determined (2,3,5,6,8). Aminoglycosides are a diverse family of natural products, which interfere with bacterial translation by binding to the small ribosomal subunit. The central scaffold of aminoglycosides is a 2-deoxystreptamine (2-DOS) ring. (Ring II, figure 3.1) The 2-DOS core alone provides considerable affinity for RNA (10,11). The substitution pattern of amino sugars around the 2-DOS ring provides differentiation within the family. Aminoglycosides bind to at least 4 sites in the 30S ribosome, but those within the two largest subclasses bind at the ribosomal decoding site (A-site) within helix h44.

Neomycin and kanamycin (Figure 3.1a) are examples of 4,5 and 4,6 disubstituted 2-DOS aminoglycosides.

Hygromycin B (Figure 3.1a) is a unique aminoglycoside that binds to a distinct region of h44, higher within the decoding site loop (12) (Figure 3.1c). The 2-DOS ring of hygromycin is substituted only at the 5 position. The glucosamine sugar, attached at carbon 4 in most aminoglycosides, (13-15) is absent in hygromycin.

The Hygromycin B binding site (Figure 3.1c) is very near the decoding site. Upon binding, hygromycin elicits conformational changes in the universally conserved adenosines A1492 and A1493, consistent with the other aminoglycosides(13). However, the conformation of A1492 and A1493 adopted in the presence of hygromycin is quite different from those adopted in the presence of other aminoglycosides, such as paromomycin. (13) In the presence of hygromycin, A1492 undergoes only a minor transition, while A1493 migrates into a position where it could potentially act as a steric block to tRNA movement between the A and P sites. This steric block is thought to be the mechanism by which hygromycin interferes with translocation and reverse translocation. (13,16)

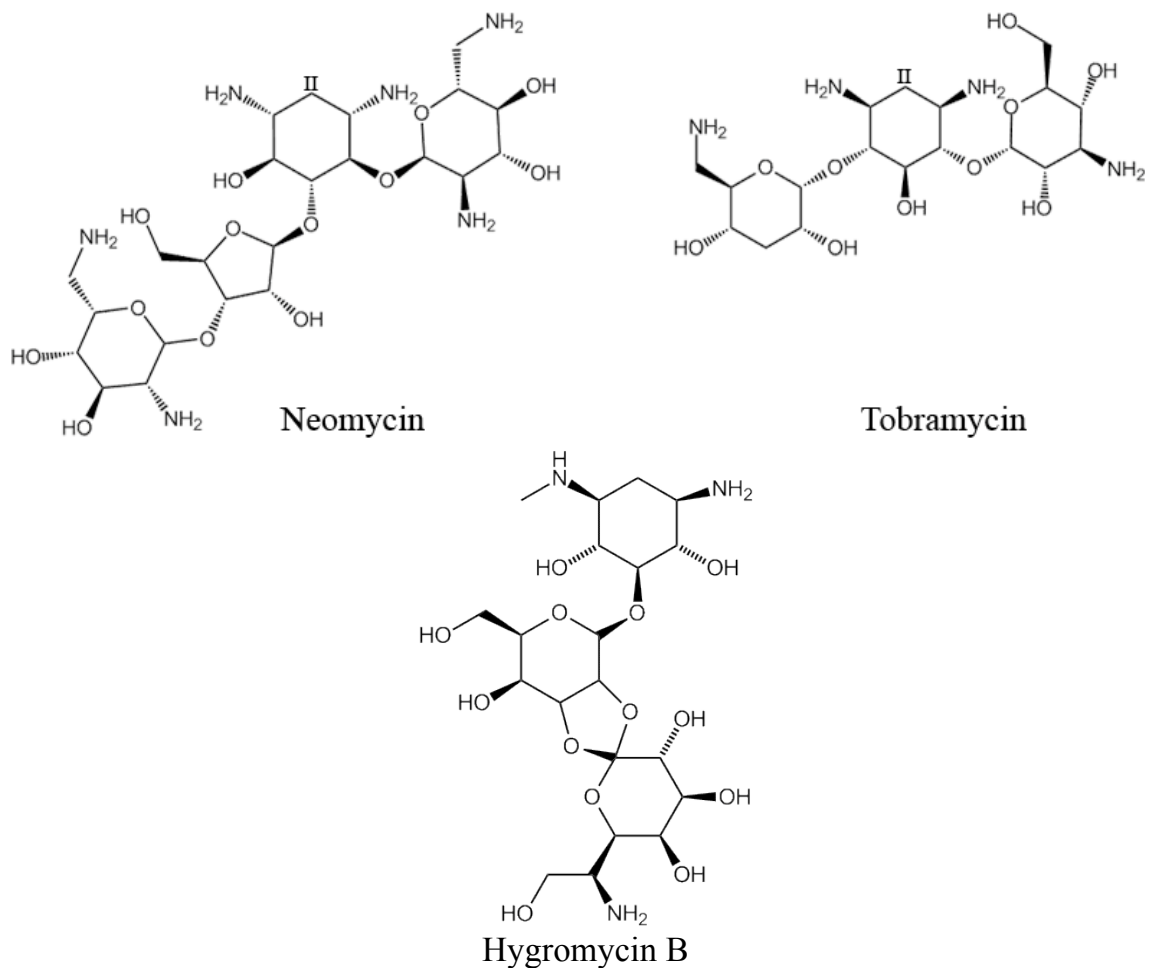
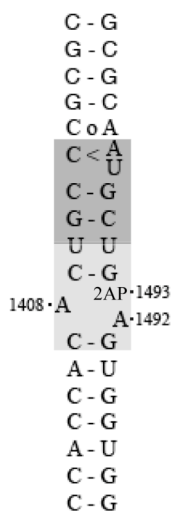


Figure 3.1a: Chemical structures of neomycin and tobramycin, presented as typical aminoglycosides of the 4,5 and 4,6 disubstituted 2-DOS families. The 2-DOS ring (labeled as II) provides RNA binding affinity. Also shown is the chemical structure of hygromycin B; an aminoglycoside antibiotic isolated from *Streptomyces hygroscopicus*. This unique structure contains a 2-DOS ring substituted only at the 5 position.



## HX RNA

Figure 3.1b: Sequence of HX oligonucleotide construct. Binding regions for aminoglycosides are shaded: the lower region contains the A site and binds neomycin and gentamycin families, while the upper region binds hygromycin B. Note the 2AP replacement at base 1493.

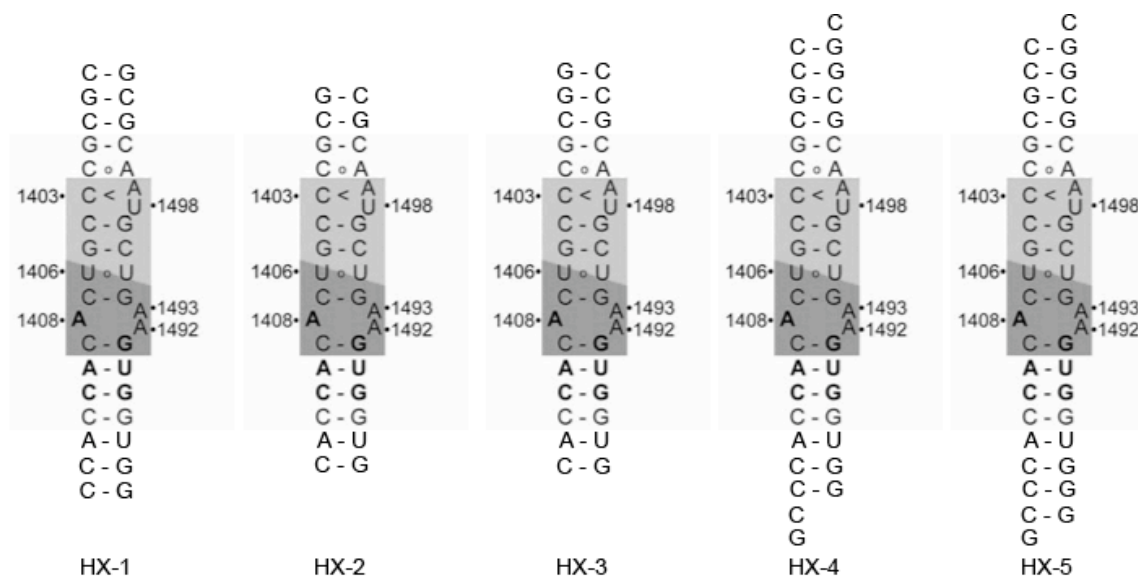


Figure 3.1c: Sequence of HX2-HX5 oligonucleotide constructs. Binding regions for aminoglycosides are shaded: the lower (blue) region contains the A site and binds neomycin and gentamycin families, while the upper (orange) region binds hygromycin B



Hygromycin B is frequently used as a selection agent in cell culture. It targets eukaryotic and prokaryotic ribosomes by inhibiting translocation and slightly decreasing translational fidelity. (4,16,17) Several resistance mutations to hygromycin have been characterized. (18,19) RNA mutations conferring resistance to Hygromycin B occur at nucleotides U1406, C1496, U1495 and U1498. All of these bases are conserved from archaea to humans, making hygromycin medically useless. Nevertheless, the proximity of the hygromycin site to the A-site raised the possibility of gaining specificity and affinity by creating hybrid molecules to bridge between the two sites. (14)

Investigations of aminoglycoside binding to constructs with the decoding-site sensor adenosines A1492 and A1493 replaced by the fluorescent nucleobase analog 2-aminopurine (2AP) have shown the constructs to be robust indicators of drug interactions. (20) The base flipping of 1492/1493 is important to the biological function of the decoding site (21). When the conserved adenosines are positioned outside h44, they are able to interact favorably with the major groove of the RNA helix formed by the joining of the mRNA codon with the proper tRNA anticodon in the A site (22). Aminoglycosides act by reducing the energy barrier between the two conformations of the sensor adenines, thereby reducing discrimination between near-cognate and cognate tRNAs. Without this discrimination, the error rate of protein synthesis becomes unacceptably high, and cells die due to accumulation of mistranslated and misfolded protein (23). Hygromycin, however, has a much less pronounced effect on misreading, acting mostly by inhibiting translocation (13,17).

2AP fluorescence output is a powerful indicator of the environment around the nucleotide base. 2AP fluorescence is quenched primarily due to stacking interactions with neighboring bases (24). A1492 and A1493 are ideal candidates for 2AP replacement in oligonucleotide constructs, as they are known to undergo dramatic changes in local environment. The transition of the sensor adenines from stacking with other bases inside the RNA helix to being solvent-exposed outside the helix results in major changes in fluorescence. The alternative conformations adopted by these adenine bases in the presence of aminoglycosides is reflected by the change of fluorescence signal. The conformations seen in crystal structures in complex with hygromycin can be differentiated from the conformations seen in crystal structures in complex with other aminoglycosides such as paromomycin by means of these fluorescence changes.

## 3.2 Results:

### *Characterization of hygromycin-site binding by 2-aminopurine fluorescence*

The Hygromycin-site (HX) RNA construct was designed based on the sequence of helix h44 of the bacterial ribosome. For crystallization studies, five sequences (HX1-HX5, figure 3.1d) were used. The addition of single nucleotide overhangs in the HX5 construct aided greatly in crystal growth, allowing large crystals to grow quickly. Fluorescence studies used the HX sequence. A1493 (*E. Coli.* numbering) was replaced with 2AP during synthesis to create the HX construct. The 1493-labeled RNA was first exposed to magnesium in order to cause global stabilization of the structure and to determine a baseline fluorescence response. (Figure 3.2) This increase in fluorescence is in accord with data that shows that the 1493 base is preferentially outside the helix in the native conformation. Magnesium addition enhances stability of structured RNA, yielding a greater proportion of natively folded, high fluorescence RNA. (25 26) Monovalent ions such as  $K^+$  or  $NH_4^+$  tend to produce curves similar to magnesium, although with less affinity. (Figure 3.3)

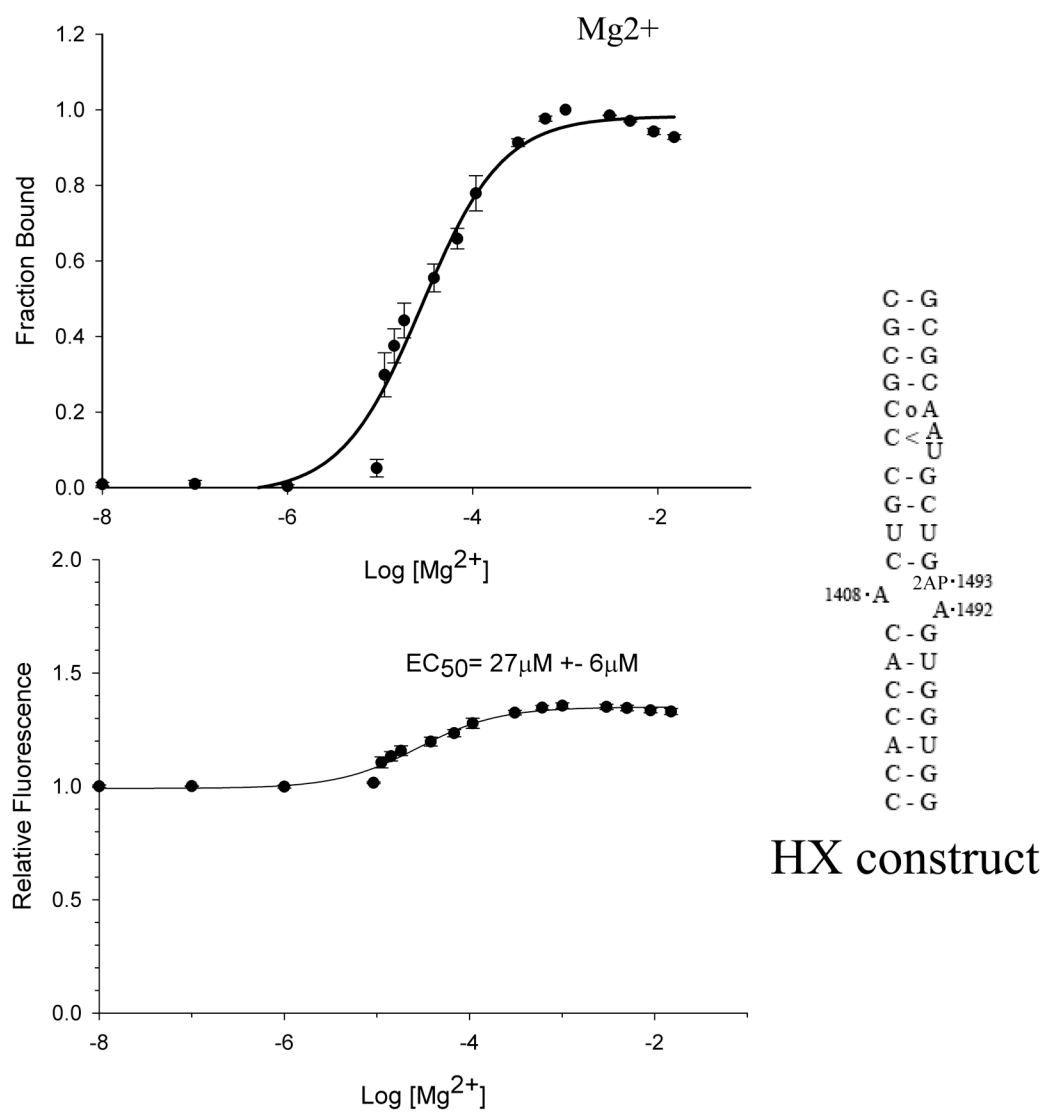


Figure 3.2: Magnesium titrations in HX RNA. Normalized 2AP fluorescence in HX-RNA is plotted against the concentration of magnesium chloride present. The EC<sub>50</sub> of this fluorescence increase is (3.9 μM ± 1.2 μM) Error bars in this and all subsequent titration figures indicate standard deviations in three independent titrations.

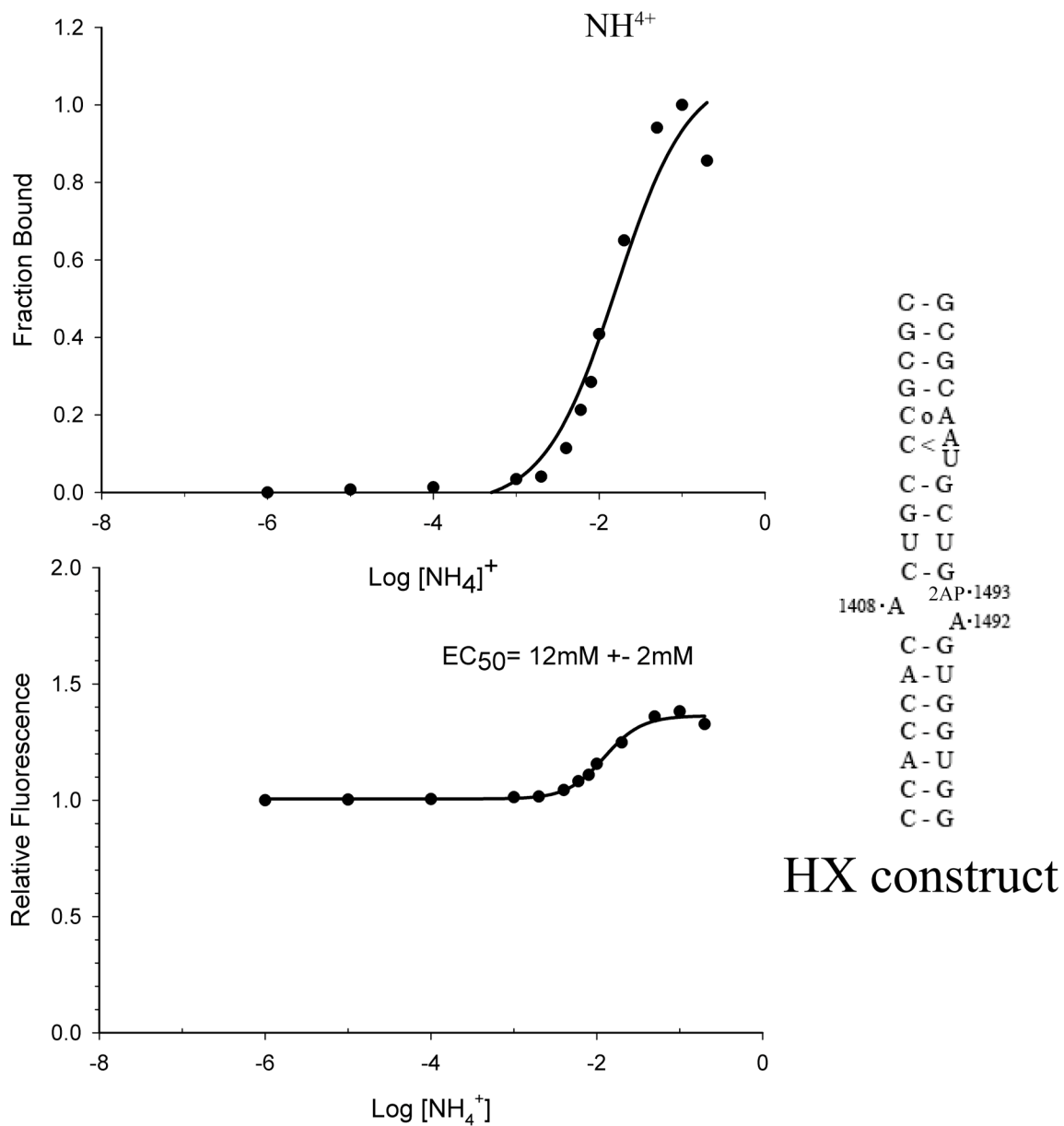


Figure 3.3: Ammonium sulfate titrations in HX RNA. Shown is the fluorescence response of HX-RNA to titration with ammonium sulfate. The EC<sub>50</sub> of this fluorescence increase is (12mM±2mM).

Next, the impact of hygromycin B binding to the construct was studied.

Oligonucleotide constructs containing only the sequences forming the A-site show no affinity for hygromycin B (9). In the HX construct, titration of hygromycin increases fluorescence of the 1493 label at micromolar concentrations. (Figure 3.4) The fluorescence increase is in contrast to the decrease caused by typical aminoglycosides, such as paromomycin, which bind to the A-site proper. (Figure 3.5) These compounds act by stabilizing a lower-fluorescence conformation where 1492 is expelled from the helix and stacked with 1493, partially quenching it. The stacking of 1492 and 1493 is not observed in co-crystal structures of hygromycin and the ribosome (4 13).

Aminoglycosides gentamycin (g418) and paromomycin (figure 3.5) were chosen as representatives of the two major classes of aminoglycosides, 4,6 and 4,5 disubstituted deoxystreptamines. Other aminoglycosides in these classes were tested and behaved similarly (not shown). Previously reported affinities of aminoglycosides for A-site constructs (9,27) are similar to that seen in the HX construct. Paromomycin binds at 140nM  $\pm$  60 (200nM previously reported), tobramycin 2 $\mu$ M  $\pm$ (1.5 $\mu$ M) and gentamycin 1.0 $\pm$ 0.2 $\mu$ M (1.7 $\mu$ M). This assay was then used for competitive binding experiments to determine the possibility of discriminating between A-site binders and hygromycin-site binders by virtue of fluorescence response patterns.

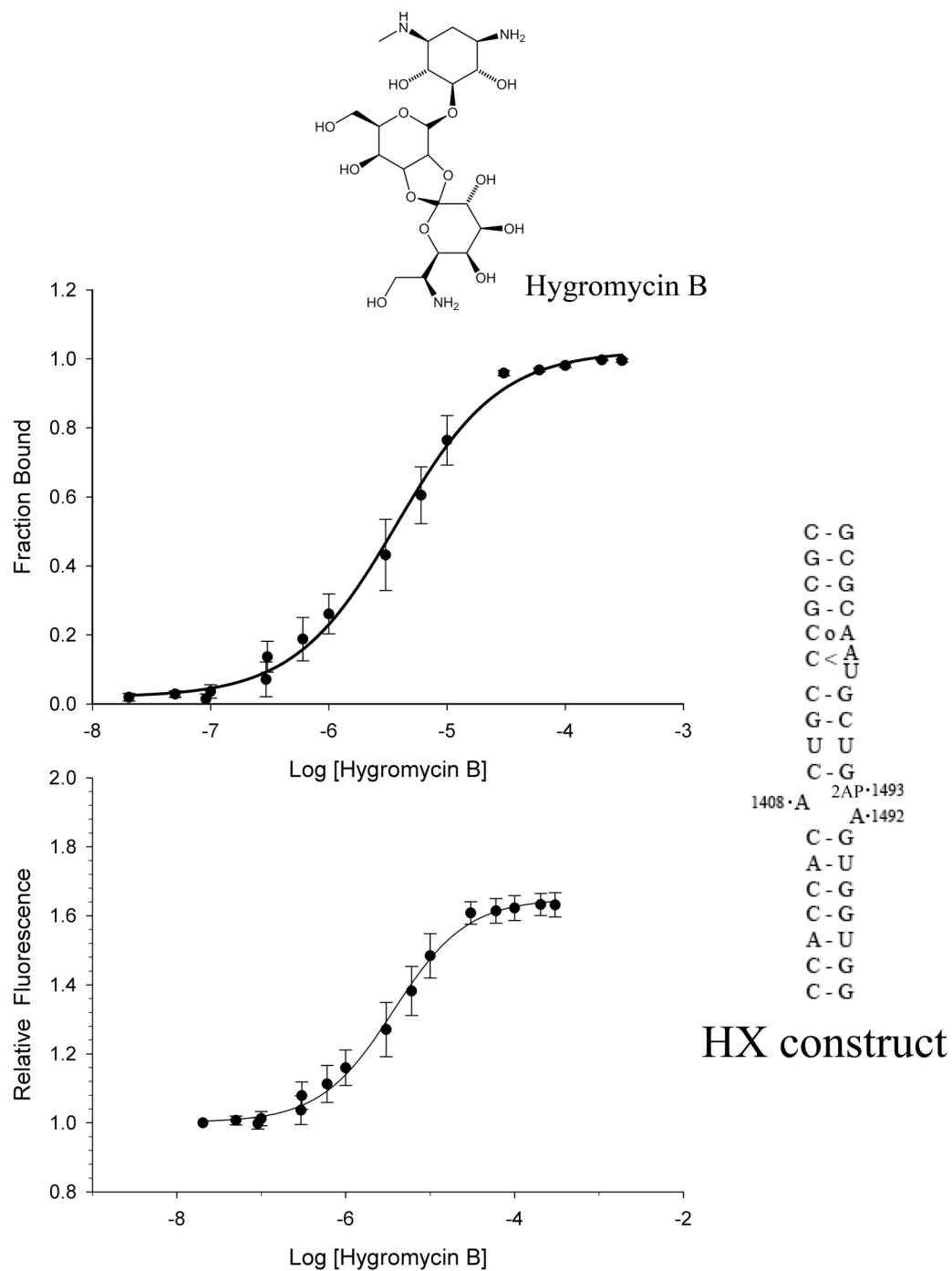


Figure 3.4: Hygromycin B titrations in HX RNA. The  $EC_{50}$  of this fluorescence increase is  $3.7\mu\text{M} \pm 1.2\mu\text{M}$ .



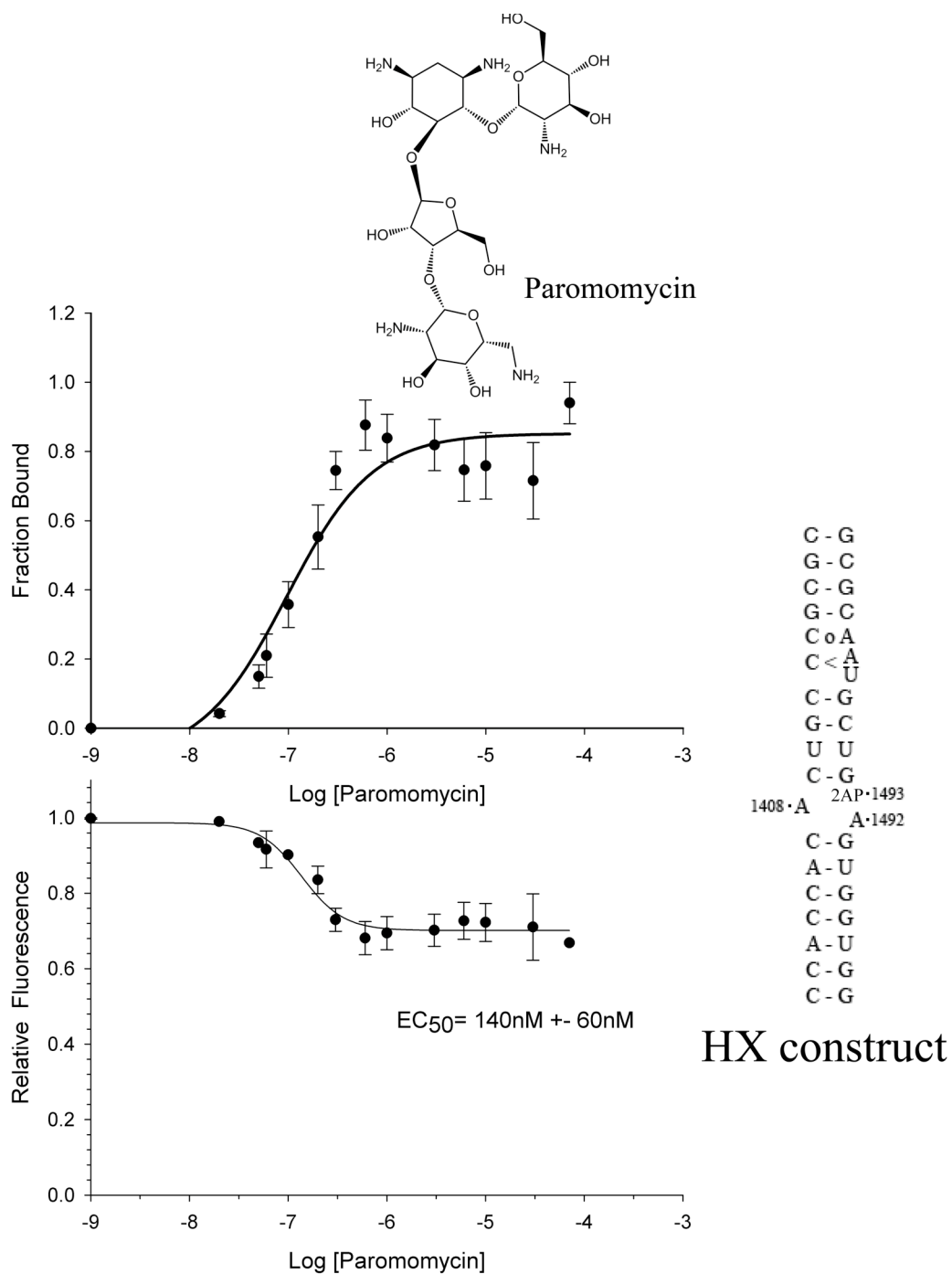


Figure 3.5a: Paromomycin titration in HX RNA. The EC<sub>50</sub> of this fluorescence decrease is (140nM ± 60nM).

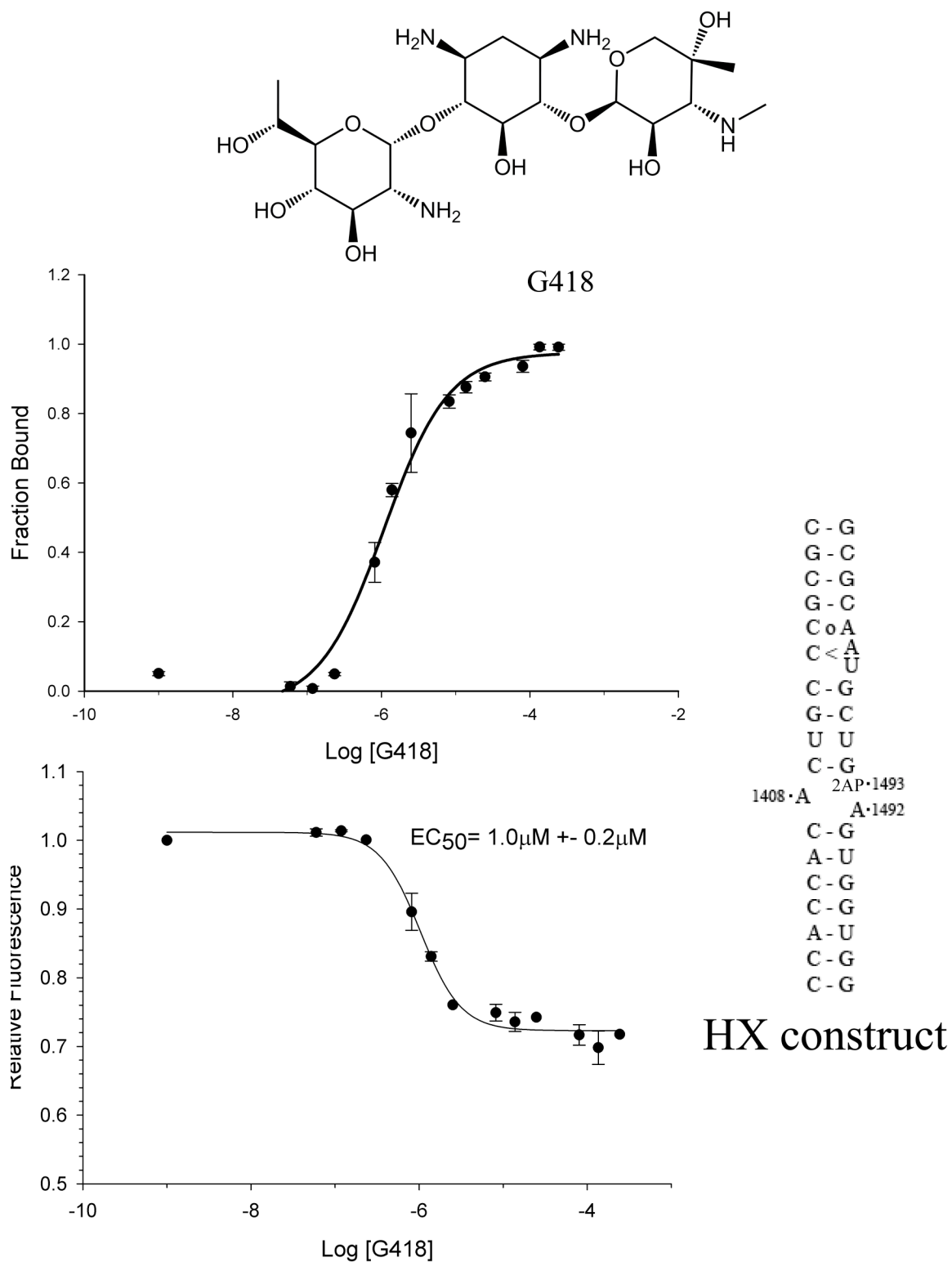


Figure 3.5b: HX-RNA titrated with geneticin (G418). The EC<sub>50</sub> of this fluorescence decrease is (1 μM ± 0.2 μM).

*Binding in the presence of magnesium:*

The presence of magnesium stabilizes the RNA structure and increases the fluorescence of A1493. In the background of at least 100 $\mu$ M magnesium, the hygromycin effect on fluorescence is reduced in magnitude from a 1.6-fold increase to a 1.25-fold increase (Figure 3.6a). Paromomycin binding is unaffected by the presence of magnesium (Figure 3.6b). Tobramycin competition with magnesium is characterized by the reduction or removal of the first phase of its biphasic response. This first phase consists of a fluorescence increase at around 100nM. The removal of this first phase of the tobramycin fluorescence curve can be seen in the presence of sodium and spermidine as well as in magnesium. (Figure 3.7).

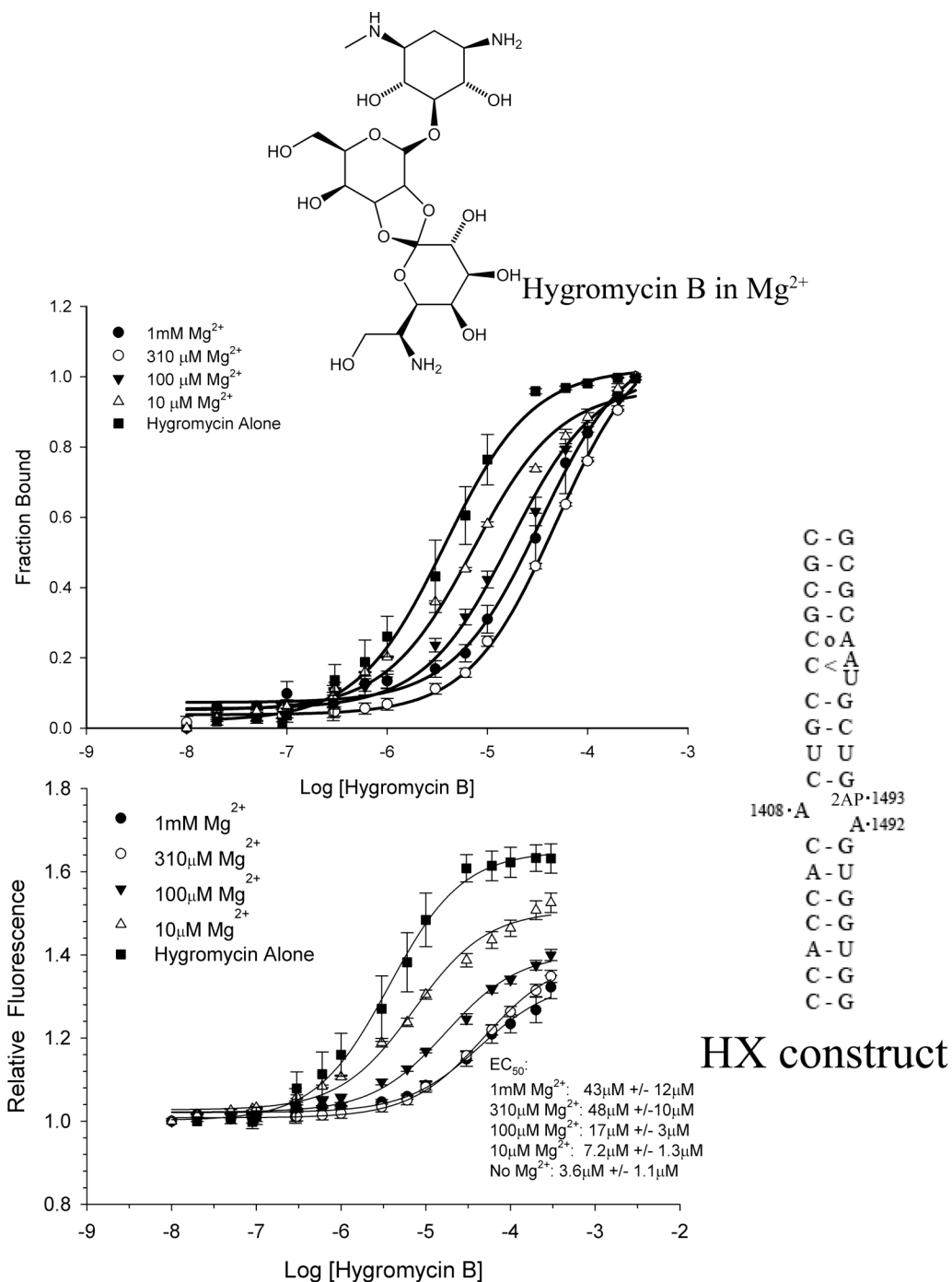


Figure 3.6a: Titrations of HX-RNA with hygromycin B in the presence of Mg<sup>2+</sup> (Squares: 0; open triangles: 10 μM; closed triangles: 100 μM; open circles: 320 μM; closed circles: 1000 μM). EC<sub>50</sub> of the fluorescence increase shifts from 3.7 μM ± 1.2 μM in 0 magnesium to 43 μM ± 12 μM in 1M magnesium.

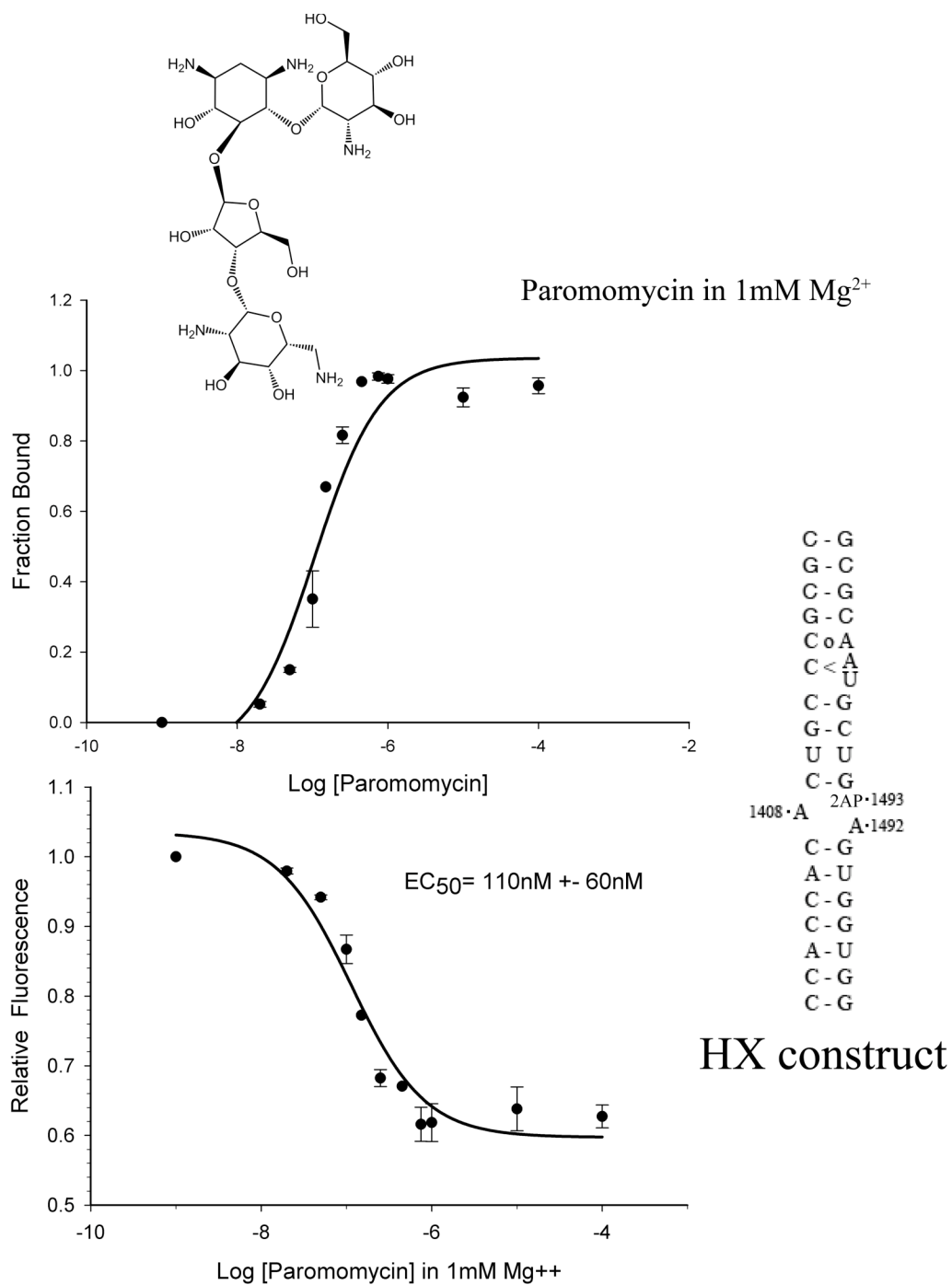


Figure 3.6b: Titrations of HX-RNA with paromomycin in the presence of 1mM Mg<sup>2+</sup>. The EC<sub>50</sub> of the fluorescence decrease is 110nM ± 60nM in 1mM magnesium. In the absence of magnesium, EC<sub>50</sub> is 140nM ± 60nM.

*Competition Binding Experiments:*

When tobramycin is titrated into a paromomycin-saturated solution or vice versa, the final fluorescence state is the same. In other words, with tobramycin bound or paromomycin bound, fluorescence is the same and displacing one with the other does not impact the fluorescence. However, Figure 3.8 shows that tobramycin and hygromycin compete, but only in regards to the first binding phase.

This biphasic response of tobramycin with the RNA construct is in keeping with the dual binding sites noted in the ribosome (9). The first portion of this response is

competitive with magnesium, sodium, and spermidine (Figure 3.7).

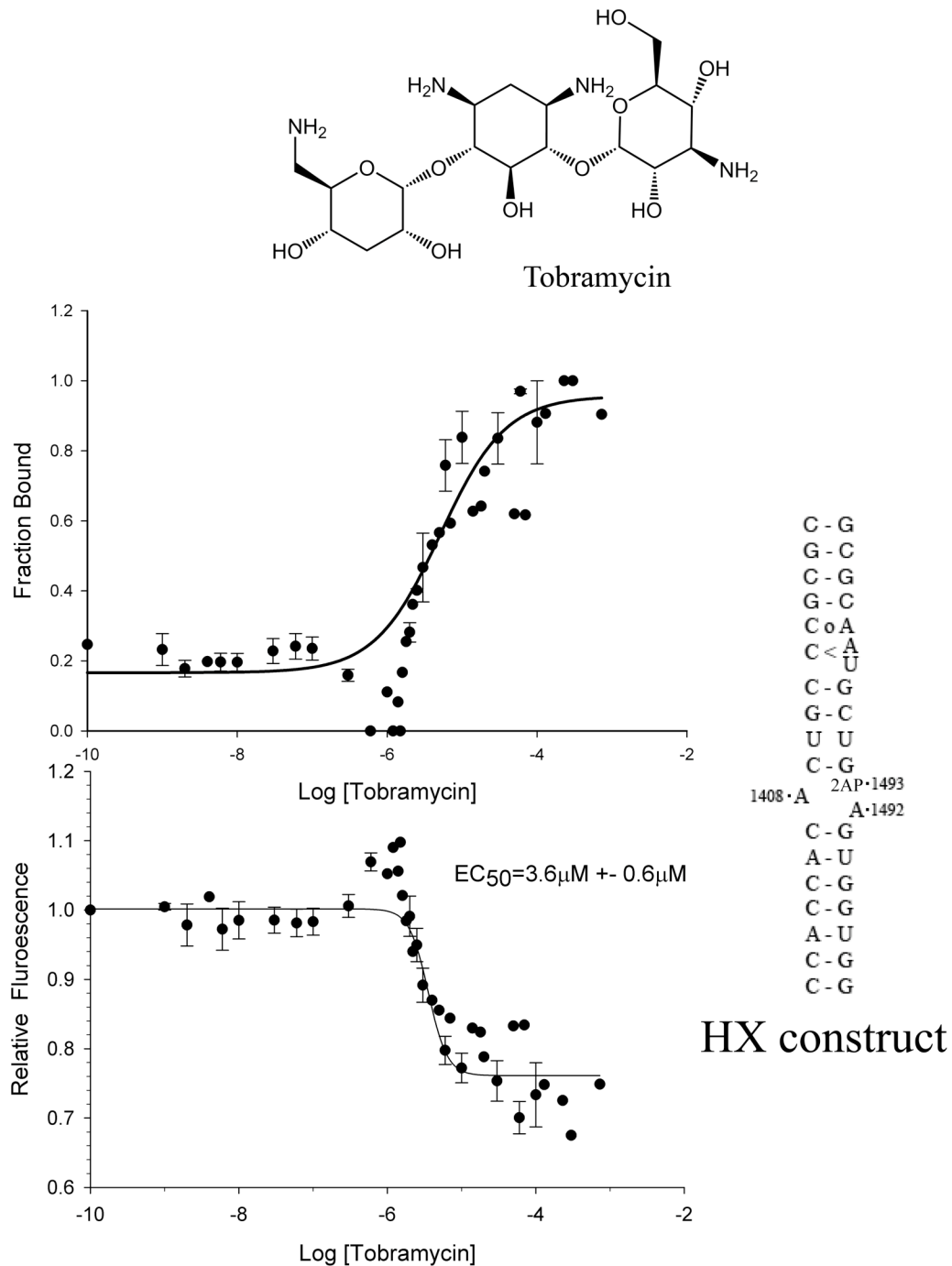


Figure 3.7a: Titration of HX-RNA with tobramycin. The fluorescence increase at sub-micromolar concentrations is part of a biphasic response and is omitted from the curve fitting. The biphasic response is described in the text.

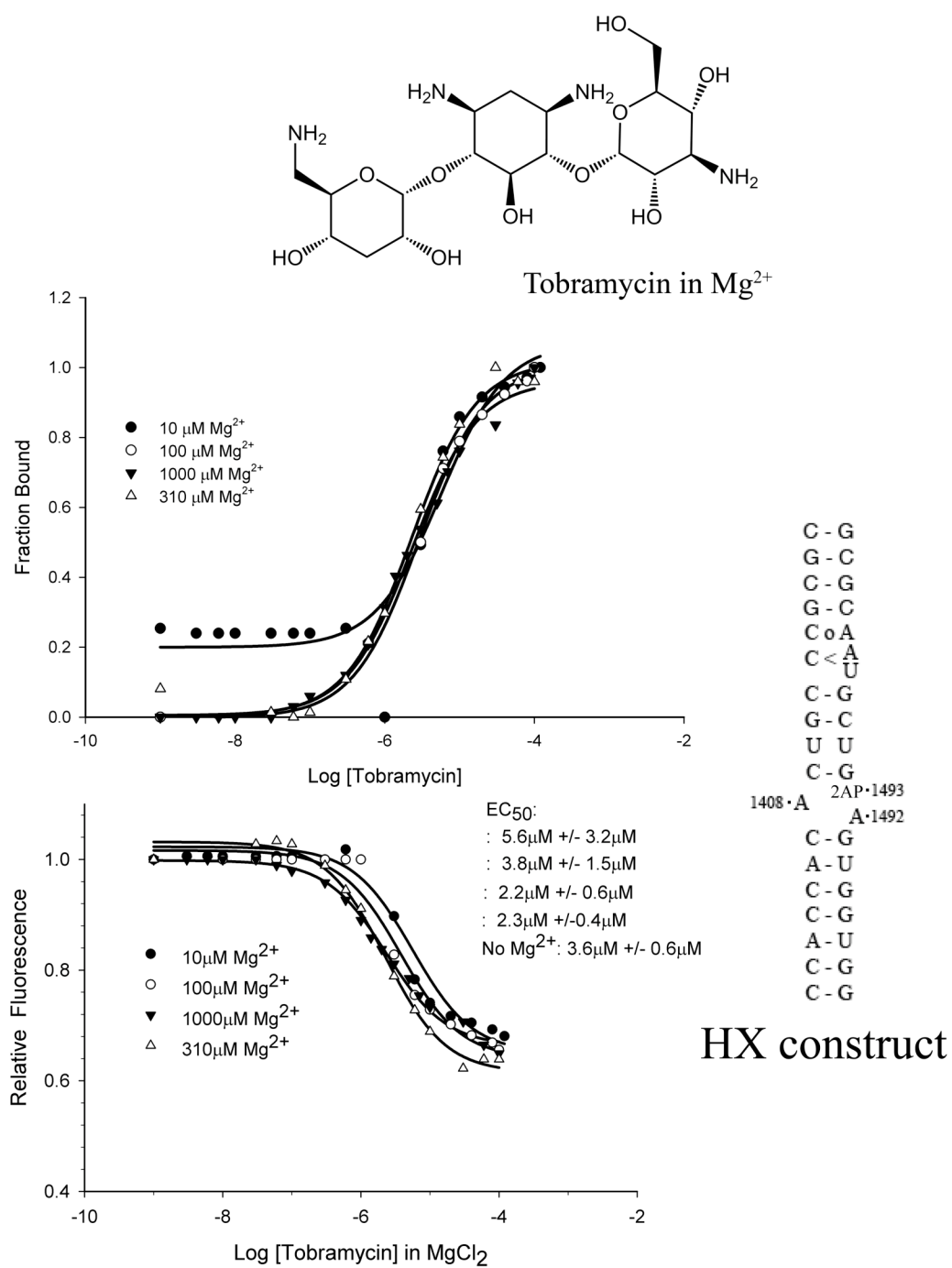


Figure 3.7b: Titrations of HX-RNA with tobramycin in the presence of magnesium. At concentrations of magnesium above 10  $\mu M$ , the fluorescence increase is ablated.



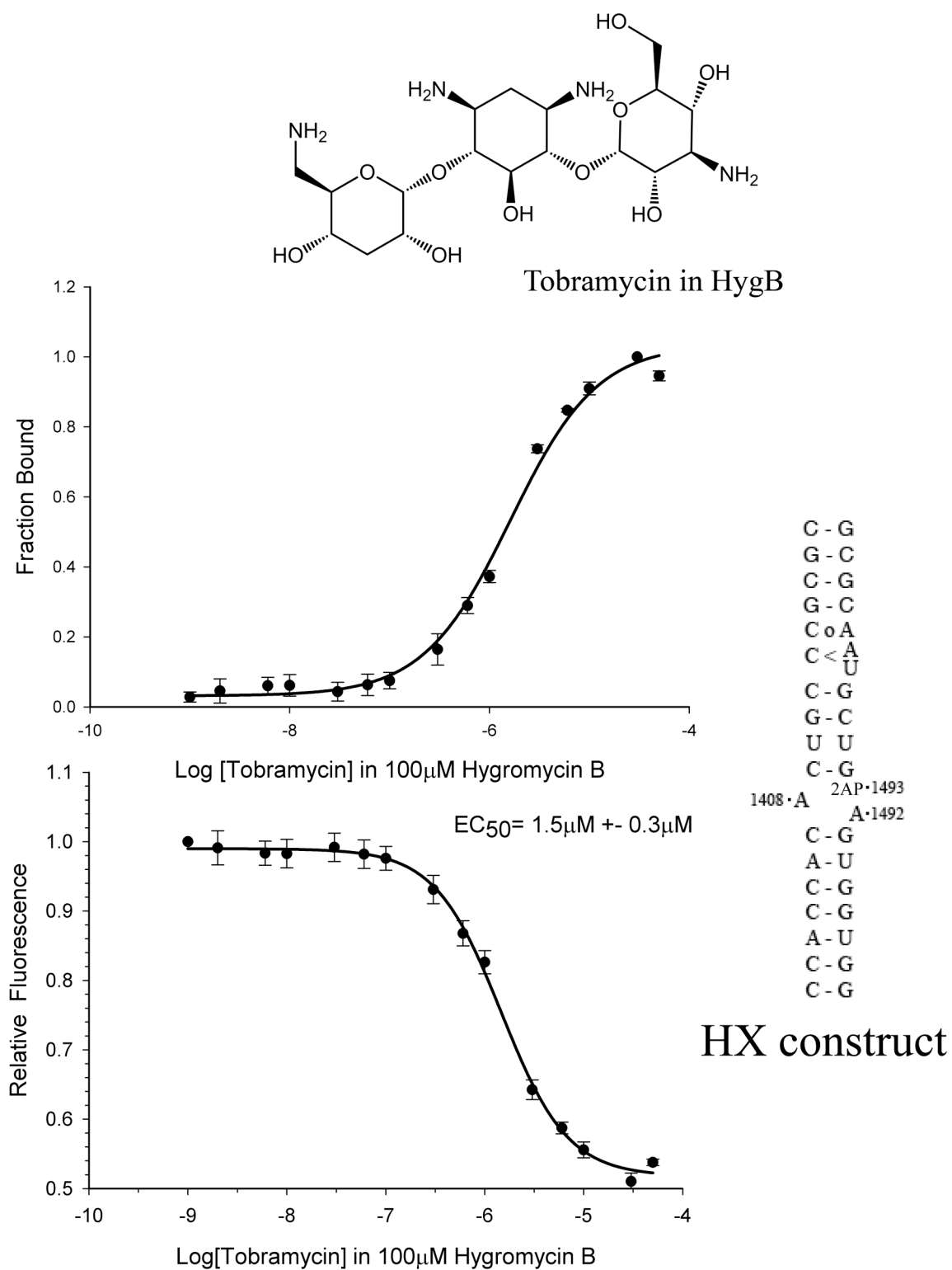


Figure 3.8: Titration of HX-RNA with tobramycin in the presence of hygromycin.

### *RNA Thermal Denaturation*

Hygromycin construct HX RNA was thermally denatured in presence of aminoglycosides in order to determine the degree of stabilization each of these compounds causes. (Figure 3.9) In the absence of magnesium, Hygromycin, paromomycin, and tobramycin raise the  $T_m$  by 5°, 8°, and 12° K, respectively. The addition of 1mM magnesium to untreated construct increases melting temperature by 16°. Further addition of hygromycin, paromomycin, or tobramycin at 10 $\mu$ M concentration further increases the melting temperature by 0°, 2.4°, or 4.5°.

	compound	Concentration	$T_m$ , °C	$\delta T(\text{RNA})$	$\delta T(\text{Mg})$
RNA Alone	NA	NA	40	0	
RNA	Hygromycin	10 $\mu$ M	45	5	
RNA	Paromomycin	10 $\mu$ M	48	8	
RNA	Tobramycin	10 $\mu$ M	52	12	
RNA	Magnesium	1mM	56	16	0.0
RNA, Mg <sup>2+</sup>	Hygromycin	1mM, 10 $\mu$ M	56		-0.6
RNA, Mg <sup>2+</sup>	Paromomycin	1mM, 10 $\mu$ M	59		2.4
RNA, Mg <sup>2+</sup>	Tobramycin	1mM, 10 $\mu$ M	61		4.6

Figure 3.9: Melting Temperatures of HX RNA in the presence of aminoglycosides.

### *Crystallization*

RNA constructs HX through HX5 were screened against the Natrrix™ screen (Hampton Research). The first four constructs produced only small and non-diffracting crystals. Optimization of the construct, particularly the addition of 5' overhanging bases, increased the likelihood of crystallization. The fourth construct (HX4) made small, non-diffracting crystals in several conditions despite containing mismatched overhangs. Fixing this issue in the HX5 construct produced large crystals in a wide variety of conditions of the Natrrix screen after two days. Optimization of the crystals in this screen decreased diffraction limits from 3.5Å to 2.3Å. Crystal growth conditions are described in (1). Crystals were prepared in the presence of millimolar concentrations of hygromycin B, but were without density corresponding to the bound ligand, perhaps due to the overwhelming (1.95M) concentration of ammonium salt. (1)

### 3.3 Discussion:

Hygromycin B does not share its bactericidal mechanism with typical A-site binding aminoglycosides, despite the proximity of the binding sites. Hygromycin binding does not have the dramatic effect on A1492 and A1493 that forces them outside of H44 and results in mistranslation. This is reflected in the differing response of 2AP fluorescence in response to binding at either site. The effect of hygromycin on 2AP93 is an increase similar to that seen in magnesium, implying that the hygromycin binding stabilizes the construct in a state with 1493 more frequently exposed to solvent (Figure 3.10). Magnesium in fact competes with hygromycin in causing this response. The effect of paromomycin binding, a decrease in 2AP93 fluorescence, is exemplary of both 4,5 and 4,6 substituted DOS aminoglycosides. Binding affinities in this construct are similar to previously reported affinities. (9,27).

Tobramycin binding in this construct shows a biphasic response, suggesting two binding sites in this short construct. Earlier studies (9) had shown that two equivalents of tobramycin bind to the ribosome with similar affinity. In 1493-labeled HX RNA (HX), these two events have opposite effects on fluorescence. The tighter event increases fluorescence slightly and can be competed away by hygromycin or high concentrations of spermidine and magnesium. The second binding event decreases fluorescence to an extent similar to other A-site binding aminoglycosides.

Discrimination between A-site and Hygromycin-site binding can be achieved by means of fluorescence screening in this oligonucleotide construct. Hygromycin-site binding is characterized by competition with magnesium and ablating the first phase of tobramycin binding. Binding at this site causes an increase in 1493 fluorescence as A1493 is positioned both outside the helix and far away from A1492. (Fig 3.10)

The fluorescence response of HX RNA is modeled in figure 3.10. In low concentrations of magnesium, A1493 adopts a more flexible conformation, occasionally adopting a conformation in the interior of the helix. After magnesium, hygromycin, or A-site aminoglycosides bind to the RNA, however, this flexibility is reduced. In the case of A-site aminoglycoside binding but not hygromycin binding, the reduction in flexibility of A1493 is accompanied by stacking with A1492, resulting in reduced fluorescence. Crystal structure data of the ribosome in complex with hygromycin suggests that A1493 adopts a conformation that is outside of the RNA helix but in an orientation that interferes with tRNA translocation. This is in contrast to the orientation that interacts with the tRNA:mRNA hybrid, such as that adopted by the base in presence of A-site binding aminoglycosides.

The HX construct can be used as a tool for discovery of novel ligands binding to the bacterial A-site, either in the decoding loop or at the hygromycin site. Potential antibacterial compounds bridging the hygromycin binding site and the decoding site can be screened in this construct.

Research described in Chapter 3, in part, has been published in *Nucleic Acids Research*, 2010, 1-8. Jerod Parsons was the primary investigator and first author of this paper, in collaboration with Prof. Thomas Hermann and Dr. Sergey Dibrov.

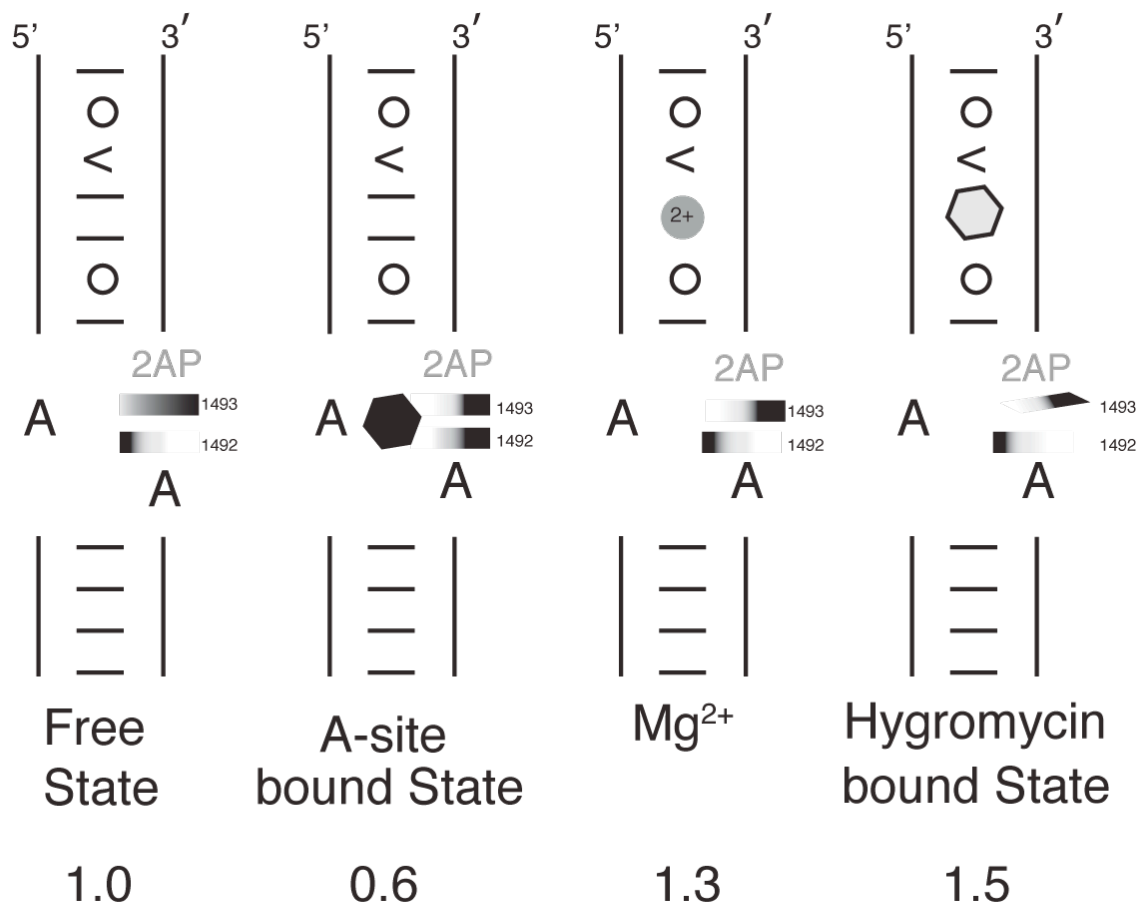


Figure 3.10: Model depicting conformational states of A1492 and A1493 in HX RNA, free and after binding of magnesium, neomycin-type aminoglycosides, and hygromycin. Shaded rectangles represent estimated probabilistic location of A1492 and A1493 in relation to the RNA helix, based on crystal structures and fluorescence results. (Black = higher probability) Numerical values represent normalized (Free = 1.0) fluorescence intensity from HX RNA experiments.

## References:

1. Dibrov, S.M., Parsons, J., and Hermann, T. (2010) A model for the study of ligand binding to the ribosomal RNA helix h44. *Nucleic Acids Research*; doi: 10.1093/nar/gkq159
2. Borovinskaya, M.A., Pai, R.D., Zhang, W., Schuwirth, B.S., Holton, J.M., Hirokawa, G., Kaji, H., Kaji, A., and Cate, J.H.D. (2007). Structural basis for aminoglycoside inhibition of bacterial ribosome recycling. *Nat. Struct. Mol. Biol.* 14:727–732.
3. Francois, B., Russell, R.J., Murray, J.B., Aboul-ela, F., Masquida, B., Vicens, Q. and Westhof, E. (2005). Crystal structures of complexes between aminoglycosides and decoding A site oligonucleotides: role of the number of rings and positive charges in the specific binding leading to miscoding. *Nucleic Acids Res.*, 33, 5677–5690
4. Brodersen, D.E., Clemons, W.M.Jr., Carter, A.P., Morgan-Warren, R.J., Wimberly, B.T. and Ramakrishnan, V. (2000). The structural basis for the action of the antibiotics tetracycline, pactamycin, and hygromycin B on the 30S ribosomal subunit. *Cell*, 103, 1143–1154.
5. Vicens, Q. and Westhof, E. (2002). Crystal Structure of a Complex between the Aminoglycoside Tobramycin and an Oligonucleotide Containing the Ribosomal Decoding A Site. *Chemistry & Biology*, 9:747–755.
6. Vicens, Q. and Westhof, E. (2001). Crystal structure of paromomycin docked into the eubacterial ribosomal decoding A site. *Structure*, 9:647–658.
7. Woodcock, J., Moazed, D., Cannon, M., Davies, J., and Noller, H.F. (1991). Interaction of antibiotics with A- and P-site-specific bases in 16S ribosomal RNA. *EMBO J.*, 10,10:3099-3103.
8. Wirmer, J., Westhof, E. (2006). Molecular Contacts Between Antibiotics and the 30S Ribosomal Particle. *Methods Enzymology*. 415, 180-200.
9. Wong, C. H., Hendrix, M., Priestley, E. S., and Greenberg, W. A. (1998). Specificity of aminoglycoside antibiotics for the A-site of the decoding region of ribosomal RNA. *Chem. Biol.* 5, 397–406.
10. Busscher, G.F., Rutjes, F.P. and vanDelft, F.L. (2005). 2-Deoxystreptamine: central scaffold of aminoglycoside antibiotics. *Chem. Rev.*, 105, 775–791.
11. Liu, X.; Thomas, J. R.; Hergenrother, P. J. (2004). Deoxystreptamine dimers bind to RNA hairpin loops. *J. Am. Chem. Soc.* 2004, 126, 9196.
12. Moazed, D. and Noller, H.F. (1987). Interaction of antibiotics with functional sites in 16S ribosomal RNA. *Nature*, 327, 389–394.
13. Borovinskaya, M.A., Shoji, S., Fredrick, K. and Cate, J.H. (2008). Structural basis for hygromycin B inhibition of protein biosynthesis. *RNA*, 14, 1590–1599.
14. Vourloumis, D., Winters, G.C., Simonsen, K.B., Takahashi, M., Ayida, B.K., Shandrick, S., Zhao, Q., Han, Q. and Hermann, T. (2005). Aminoglycoside-hybrid ligands targeting the ribosomal decoding site. *Chembiochem*, 6, 58–65.
15. Konno, T., Takahashi, T., Kurita, D., Muto, A., and Himeno, H. (2004). A minimum structure of aminoglycosides that causes an initiation shift of trans-translation. *Nucleic Acids Res.* 32: 4119–4126



16. Peske, F., Savelsbergh, A., Katunin, V.I., Rodnina, M.V., and Wintermeyer, W. (2004). Conformational changes of the small ribosomal subunit during elongation factor G-dependent tRNA-mRNA translocation. *J Mol Biol.* 5;343(5):1183-94.
17. Eustice, D.C., and Wilhelm J.M. (1984). Mechanisms of action of aminoglycoside antibiotics in eucaryotic protein synthesis. *Antimicrob Agents Chemother.* 26(1):53-60.
18. Spangler, E. A., and E. H. Blackburn. (1985). The nucleotide sequence of the 17S ribosomal RNA gene of *Tetrahymena thermophila* and the identification of point mutations resulting in resistance to antibiotics the paromomycin and hygromycin. *J. Biol. Chem.* 260:6334–6340.
19. Pfister, P., Risch, M., Brodersen, D.E., and Böttger, E.C. (2003). Role of 16S rRNA Helix 44 in Ribosomal Resistance to Hygromycin B. *Antimicrob Agents Chemother.* 47(5):1496-502.
20. Shandrick, S Zhao, Q., Han, Q., Ayida, B. K., Takahashi, M., Winters, G. C., Simonsen, K. B., Vourloumis, D., and Hermann, T. (2004). Monitoring Molecular Recognition of the Ribosomal Decoding Site *Angew. Chem.* 116, 3239 ; *Angew. Chem. Int. Ed.*, 43, 3177.
21. Ogle, J.M. and Ramakrishnan, V. (2005). Structural insights into translational fidelity. *Annu. Rev. Biochem.*, 74, 129–177.
22. Ramakrishnan V. (2002). Ribosome structure and the mechanism of translation. *Cell.* 22;108(4):557-72.
23. Hermann, T. (2005). Drugs targeting the ribosome. *Curr. Opin. Struct. Biol.*, 15, 355–366.
24. Jean, J.M., and Hall, K.B. (2001). 2-Aminopurine fluorescence quenching and lifetimes: Role of base stacking. *PNAS*, 98,1:37-41
25. Brion, P., and Westhof, E., (1997). Hierarchy and dynamics of RNA folding, *Annu. Rev. Biophys. Biomol. Struct.* 26, pp. 113–127.
26. Ferre-D'Amare, A.R. and Doudna, J.A. (1999). RNA folds: insights from recent crystal structures, *Annu. Rev. Biophys. Biomol. Struct.* 28, pp. 57–73.
27. Griffey, R.H., Hofstadler, S.A., Sannes-Lowery, K.A., Ecker, D.J., and Crooke, S.T. (1999). Determinants of aminoglycoside-binding specificity for rRNA by using mass spectrometry. *Proc. Natl. Acad. Sci. USA*, 96, 10 129.

**Chapter 4:**  
**Fluorescence Study of Hepatitis C Virus Internal Ribosome**  
**Entry Site (HCV IRES) Subdomain IIa**

#### 4.0 Abstract:

The hepatitis C virus (HCV) is a substantial health concern, infecting three out of every one hundred individuals worldwide. The virus is translated by host cell ribosomes using an internal ribosome entry site (IRES). Subdomain IIa, a short RNA sequence within the IRES, acts as a mechanical hinge to properly position the viral RNA in the ribosome. Here, we investigate the hinge domain IIa by using 2AP modified fluorescent oligonucleotide constructs. A 'hit' compound known to have sub-micromolar affinity IIa RNA was tested and found to exhibit competitive binding with magnesium ions. The competition, combined with other biochemical and structural results, suggests a specific binding site for this compound in the IIa hinge region.

#### 4.1 Introduction:

##### *Hepatitis C Virus.*

HCV is a significant health burden. 170 million people worldwide and nearly 3 million Americans have been diagnosed with the virus (1), and the majority develop chronic infection, ultimately leading to liver disease. Forty percent of liver cancers test positive for HCV antibodies (2), suggesting that the HCV virus, which replicates exclusively in the liver, is a significant contributor to the third-leading cause of cancer-related deaths. Current HCV treatments consist of multi-month treatment regimens of immuno-stimulation with ribavirin and pegylated interferon. No direct antiviral treatments or vaccines are available. Less than 40 percent of patients who receive this treatment undergo sustained viral response (SVR) and clear the virus (3). This number is even lower in patients with genotype 1 of the virus, which is found mostly in North America (2). Novel protease inhibitors and polymerase inhibitors are currently in phase III clinical trials (4,5), but it is widely accepted that multi-drug combination therapies will be required to keep the virus in check.

##### *Viral Life Cycle*

HCV is a positive-sense, single-strand RNA virus. It is directly translated by cellular ribosomes by a cap-independent mechanism (6-9) to create viral proteins. HCV is translated as a polyprotein, which is then cleaved into ten proteins by cellular and viral proteases. (10) Three of the ten are viral structural proteins: the core protein, E1, and E2. Six of the remaining seven proteins are nonstructural (NS). Nonstructural proteins NS2,

NS3, and NS4A are predominantly proteases, involved in cleavage of the HCV polyprotein and cellular signaling proteins. Another nonstructural protein, NS5b, is an RNA-dependent RNA polymerase, (RdRP) which catalyzes replication of the viral RNA (11). The final protein is an ion-channel protein required for production of infectious virus(12,13).

The cap-independent, IRES-driven mechanism of HCV translation stands in stark contrast to eukaryotic cap-mediated translation, which is responsible for translation of the vast majority of cellular proteins. Cap-mediated translation is a complicated process requiring several host initiation factor proteins (eIFs) in addition to the ribosome. The process begins by formation of a Met-tRNA-MetI-eIF2.GTP complex, which joins with an association of the 40S ribosomal RNA, eIF3, eIF1A, and eIF1 to form the 43S pre-initiation complex. After binding the 5' m<sup>7</sup> guanosine cap on the mRNA in association with eIF4, the complex scans down the mRNA to the initiation codon. The initiation complex, which is now 48 sedimentation units in size, is joined by the 60S ribosomal subunit to form an elongation-competent holo-ribosome. (4, 14-20).

HCV translation, on the other hand, occurs by a cap-independent mechanism, which is driven by the highly structured RNA in the 5' nontranslated region (NTR) of the viral mRNA. This structured region forms an internal ribosome entry site (IRES). IRES initiation bypasses the majority of translation initiation factors, although the exact factor requirement depends on experimental conditions (21-24). In contrast to cap-dependent translation, IRES-driven translation bypasses the scanning step. Instead, the 40S ribosomal RNA is recruited directly to the viral start codon (25,26). This association is

mediated by the structural RNA of the viral IRES. The 40S subunit recruitment is performed mostly by domain III of the IRES. In particular, the pseudoknot structure formed by subdomain IIIf is necessary for 40S recruitment (27). Further 40S interaction surface is provided by subdomains IIIc, IIId, and IIIe (8, 28-30). After the IRES recruits the 40S rRNA, the 60S subunit joins and forms an intact 80S ribosome which performs translation in the same manner as those formed by cap-driven methods.

The sequence of the HCV IRES, especially domain IIa, is well conserved in the viral genome (31-34). The function of the IRES structure can be significantly reduced or even completely obliterated by single base mutations (35). Disrupting IRES function by targeting the complex RNA structure has been proposed as a potential route for therapeutic treatment of HCV infections (36).

*HCV IRES Domain II:*

While domains III and IV of the HCV IRES form the primary interaction surface for the 40S ribosome and eIF3, domain II deletion substantially diminishes translational activity (26,37-39). This can be attributed to the involvement of domain II in subunit joining (22,37). The apical loop IIb forms a contact with the 40S ribosome (28,43), which leads to a large conformational rearrangement in the 40S prior to subunit joining (40,41). Several structural studies (40,42-44) probed the rationale behind the domain II function.

The global architecture formed by domain II came by a long, winding road. Various models were proposed (43,45-47) with very different base pairings suggested. Exhaustive mutational analysis proposed a model, which was validated by NMR spectroscopy (42-43). The key to the structure proved to be a 5 base internal loop from nucleotide 53 to 57 across from bases 110-111 (Figure 4.1). The structure of this internal loop in subdomain IIa was later unambiguously determined by X-ray crystallography (44). The 5nt bulge is stabilized by magnesium ions (Figure 4.2) and forms a sharp ( $85^\circ \pm 10^\circ$ )(43) bend in the RNA backbone. This bend segregates the domain into two helices oriented at a right angle relative to one another. This kink in the RNA backbone may function to position domain IIb in the mRNA exit tunnel of the ribosome to achieve 40S conformational change, as suggested in cryo-electron microscopy studies (40).

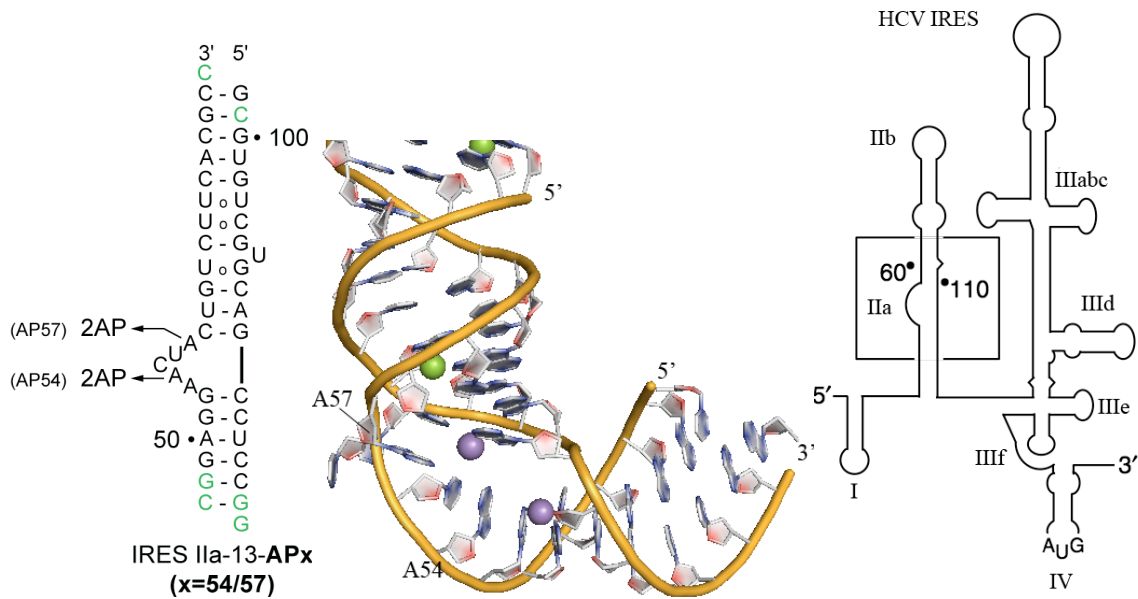


Figure 4.1: (Left) Secondary Structure of IRES IIa RNA constructs. The sequence shown in black is that of the HCV IRES IIa genotype 1(45). Green bases are substitutions made to increase RNA stability. Bases A54 and A57 are shown with arrows that indicate their replacement with 2AP in the Ila-13-AP54 and Ila-13-AP57 constructs, respectively.

Figure 4.2a: (Center) Crystal Structure of IRES IIa RNA. Shown here is a pymol(51) representation of HCV IRES subdomain IIa RNA adapted from PDB 2NOK (44). The IIa RNA forms two short helical stems that are oriented approximately 90 degrees apart from one another. The RNA backbone bends nearly 90 degrees between residues C55 and A57. The unpaired bases within the bend are stabilized somewhat by the presence of divalent metal ions, shown in purple. See Figure 4.3 for more detail.

Figure 4.2b: (Right) Secondary structure of HCV IRES. Shown is the 5' NTR of the HCV genome. The boxed region indicates the location of the IIa subdomain.



### *2AP Fluorescence studies of HCV IRES IIa*

Disrupting the kink in subdomain IIa could ultimately inhibit the spread of HCV by stalling IRES-mediated translation. Targeting the RNA hinge allows small molecules to bind without needing to compete with large interaction surfaces between the small ribosome subunit and viral RNA. To investigate this further, two unpaired adenosine residues at positions 54 and 57 within the hinge were selected for 2AP replacement. As 2AP fluorescence is highly dependent on the local environment (48), the two constructs, IIa-13-54 and IIa-13-57 (figure 4.1) were expected to demonstrate somewhat different responses to the folding process. The IIa crystal structure contains two divalent metal ion binding sites within the bend, which can accommodate either manganese or magnesium.

The two metal ion sites were differentiated by comparison of IIa-13-54 and IIa-13-57 response to titrations with manganese or magnesium. The fluorescence response fits a two-site model for the IIa-13-54 construct, and a single-site model for IIa-13-57. Either construct can be quenched by metal addition, but A54 is sensitive to binding at both sites while A57 responds only to one (44).

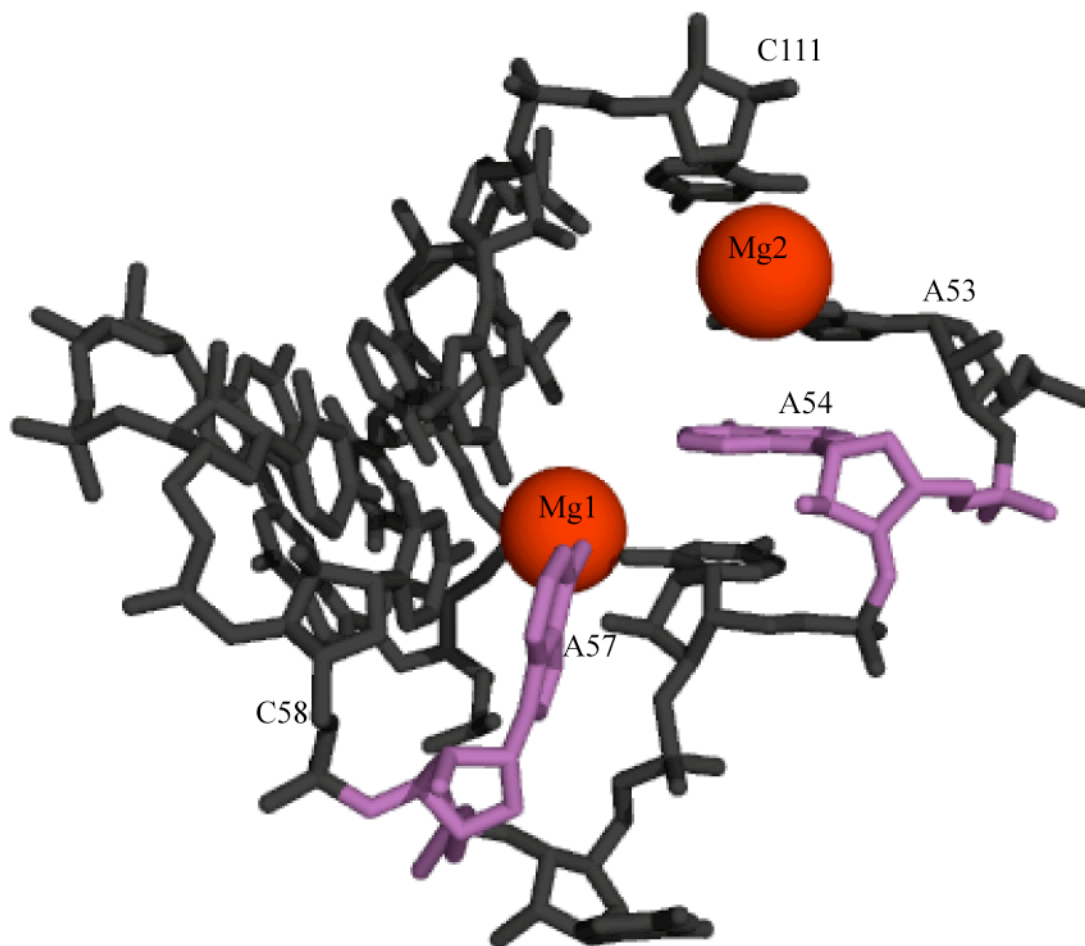


Figure 4.3: IRES IIa hinge region. A pymol representation of PDB 2NOK (44) is shown here, with bases numbered according to their position in the IRES sequence. A54 and A57 are lighter in color. Metal ion binding sites for Mg<sub>1</sub> and Mg<sub>2</sub> are shown as spheres.

## 4.2 Results:

Titration of A54 and A57 constructs (IIa-13-54 and IIa-13-57) with the aminoglycoside neomycin showed that both labels report fluorescence change on the same binding event. (Figure 4.4) In the A57 construct, fluorescence decreases to 75% with an  $EC_{50}$  of  $2.0nM \pm 0.5nM$ . In the A54 construct, fluorescence increases to 185% with an  $EC_{50}$  of  $1.5nM \pm 0.2nM$ . Both responses fit to a single-site binding model.

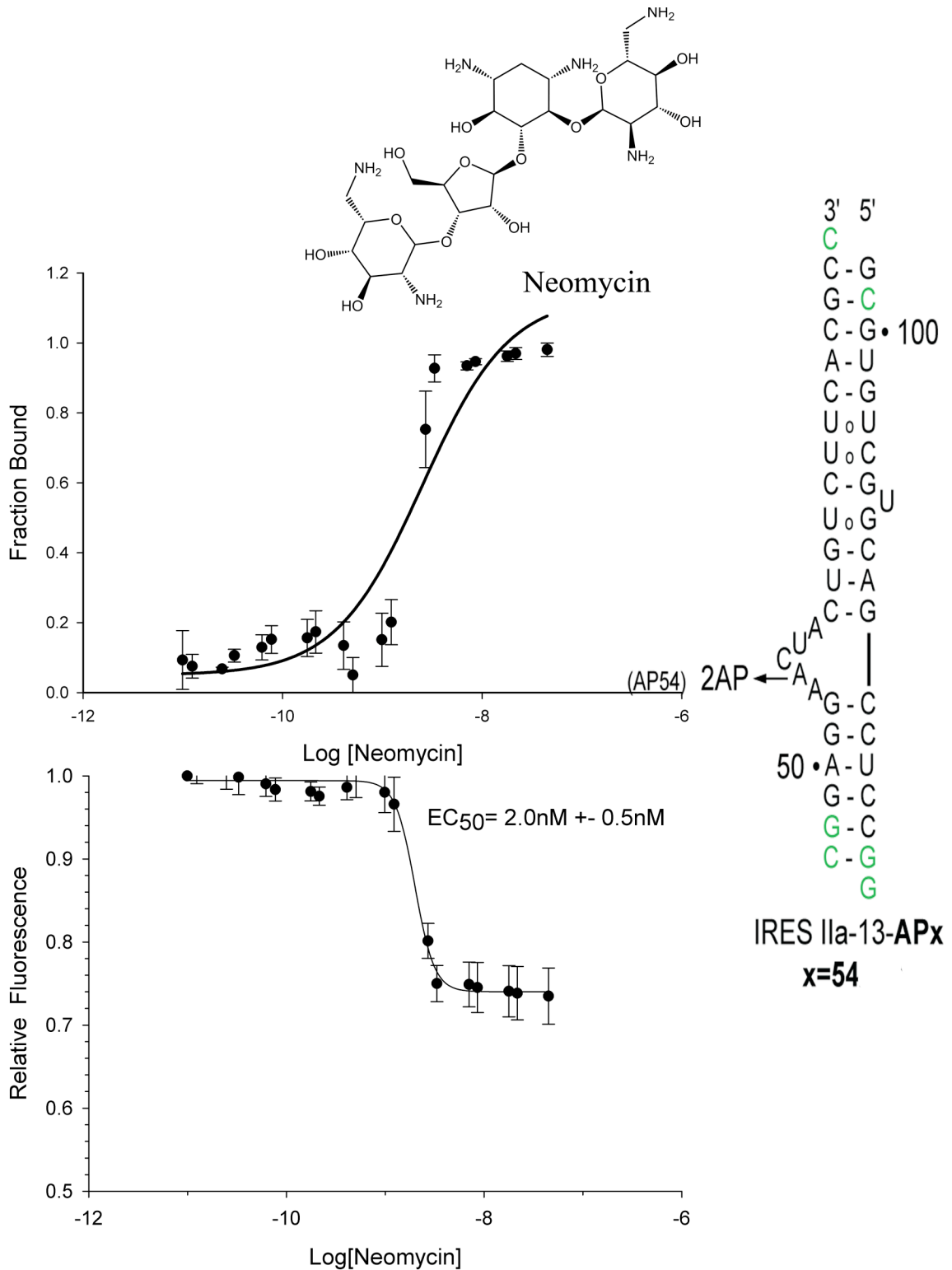


Figure 4.4a: Neomycin titrations in Ila-13-54 RNA. The EC<sub>50</sub> of this fluorescence increase is 1.5nM±0.2nM.

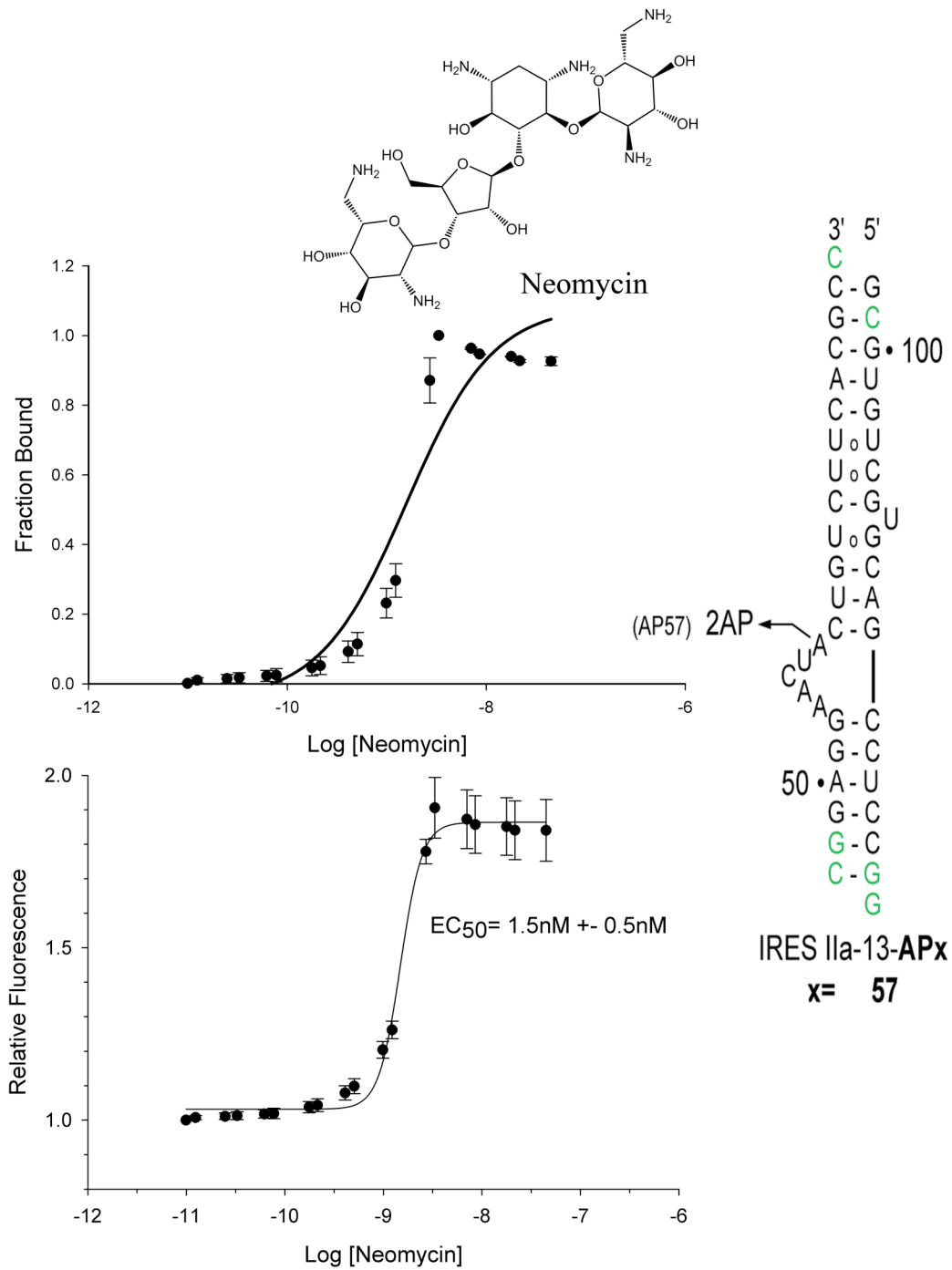


Figure 4.4b: Neomycin Titrations in IIa-13-57 construct. The EC<sub>50</sub> of this fluorescence decrease is 2.0nM±0.5nM.

A series of benzimidazole compounds that bind to the IIa RNA was described previously(49). Structure-activity Optimization of these compounds identified a benzimidazole derivative with sub-micromolar affinity. RNase A protection assays showed protection at bases 55 and 56 in the presence of this compound. (49) This compound was re-synthesized by Paola Castaldi for the Hermann lab and is henceforth referred to as P253. (Fig 4.5)

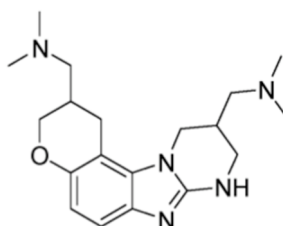


Figure 4.5: P253. The chemical structure (53) of benzimidazole compound P253 is shown. This compound, described by Ibis Therapeutics (49), binds to IRES IIa RNA and demonstrates inhibitory activity in HCV replicon assays.

Titration experiments in the IIa-13-54 and IIa-13-57 constructs (Figure 4.6) demonstrate that P253 binds to this RNA with an affinity of  $510\text{nM} \pm 50\text{nM}$ , comparable to the  $720\text{nM}$  determined by mass spectrometry screening (49). This binding is competitively inhibited by the presence of magnesium ions (Figure 4.7). The onset of competition between magnesium and P253 occurs at  $10\mu\text{M}$ , and the  $\text{EC}_{50}$  of this competition is  $85 \pm 30\mu\text{M}$ . The reported  $K_d$  of the corresponding  $\text{Mg}^{2+}$  site in this construct is  $37 \pm 20\mu\text{M}$ . (44) Auto-fluorescence of P253 at  $365\text{nm}$  precluded testing the compound at concentrations greater than  $30\mu\text{M}$ . This prevented accurate  $\text{EC}_{50}$  determinations for P253 in the presence of very high  $\text{Mg}^{2+}$ .

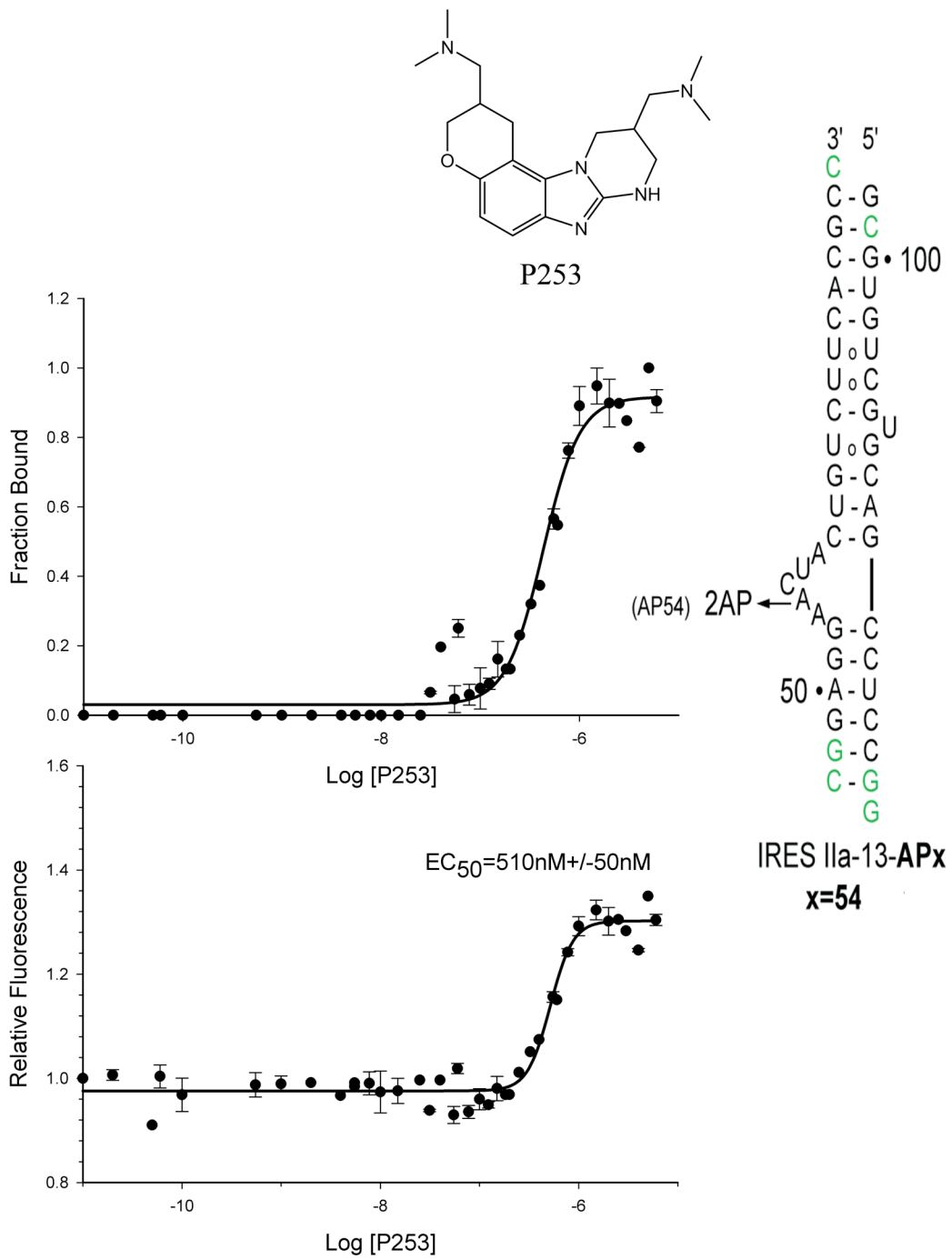


Figure 4.6: P253 titration in IIa-13-54 RNA. The  $EC_{50}$  of this fluorescence increase is 510 nM  $\pm$  50 nM.

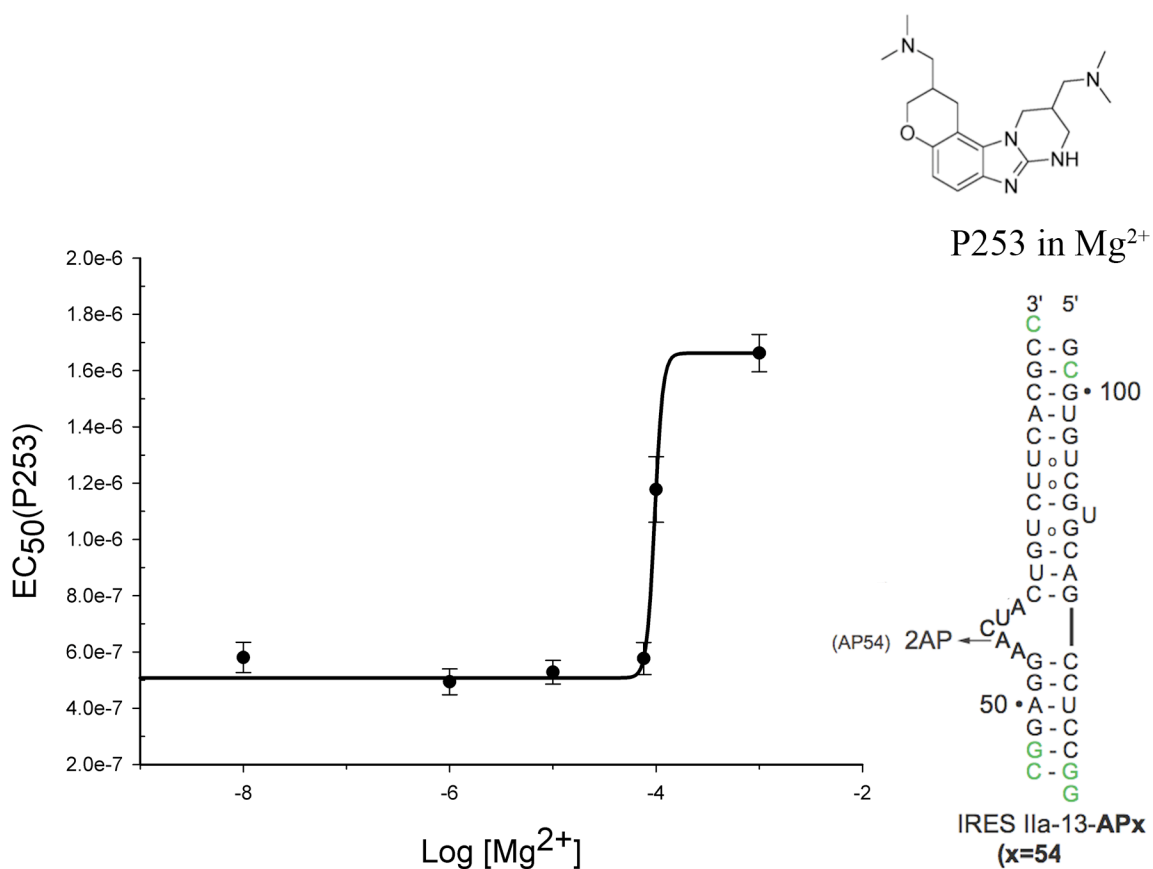


Figure 4.7: P253 competition with magnesium. Plotted is the EC<sub>50</sub> of fluorescence change in IIa-13-54 RNA after P253 titration against the concentration of Magnesium present in the RNA sample during the titration. Magnesium concentrations greater than 7.5 μM cause the P253 EC<sub>50</sub> to shift. The P253 EC<sub>50</sub> shifts from 480 nM at no Mg<sup>2+</sup> to as high as 1.7 μM in the presence of 1mM Mg<sup>2+</sup>.



Figure 4.8 shows the fluorescence responses of Ila-13-54 and Ila-13-57 constructs to a selection of aminoglycosides and other RNA-biased small molecules. Listed at the bottom of this table are seven 3,5-diaminopiperidine (DAP) compounds (MCI0xx) synthesized by M. Carnevali (52). These were titrated into A54-labeled RNA. Of these, three 4-acetylbenzoic acid derivatives - 067, 071, and 076 - showed a dose-dependent decrease of 2AP fluorescence. The presence of high concentrations of either sodium or magnesium salts reduces the affinity of these compounds (52, data not shown).

<b>Compound</b>	<b>2AP Pos.</b>	<b>Rel Min</b>	<b>Rel Max</b>	<b>EC<sub>50</sub></b>	<b>SE(%)</b>
Paromomycin	57	1.00	1.15	N.B.	
Neomycin	57	0.75	1.40	N.B.	
Tobramycin	57	0.85	1.25	N.B.	
Amikacin	57	0.52	1.28	N.B.	
Paromomycin	54	1.00	1.77	-6.65	1
Neomycin	54	0.85	1.19	N.B.	
Tobramycin	54	1.00	1.89	-7.18	3
Tobramycin(100uM SPD)	54	1.00	1.45	-6.15	3
Amikacin	54	0.73	1.71	N.B.	
KCl	54	1.00	1.13	N.B.	
KCl	57	0.90	1.05	N.B.	
MnCl <sub>2</sub>	54	0.51	1.25	-3.419	3
MCI058	54	1.00	1.05	N.B.	
MCI065	54	0.95	1.00	N.B.	
MCI068	54	0.80	1.00	N.B.	
MCI074	54	0.70	1.00	N.B.	
MCI076	54	0.60	1.00	-5.46	6
MCI067	54	0.20	1.00	-5.21	10
MCI071	54	0.20	1.00	-5.67	6

Figure 4.8: Table of results obtained by titration of compounds (column 1) into IRES Ila RNA labeled with 2AP at either position 54 or 57 (column 2). Minimum and maximum fluorescence is reported in columns 3 and 4, while the log of the concentration of half-maximal effect is shown in column 5. Fitting errors are calculated as a percentage of EC<sub>50</sub>. N.B. : No Binding curve can be fit.

### 4.3 Conclusions:

Small oligonucleotide constructs of the IRES Ila subdomain with 2AP replacements were suitable for identifying RNA-binding compounds, including a bona-fide 'hit' compound, P253. Aminoglycosides tobramycin and paromomycin demonstrated affinities of around 1 micromolar to the Ila bend. This affinity reflects the general RNA binding promiscuity of these aminoglycosides (50) and is looser than the affinities reported for the aminoglycosides binding to the bacterial A-site (54-55) or elsewhere (56). These compounds demonstrate the feasibility of monitoring ligand binding by 2AP fluorescence in this construct, but are overshadowed by novel compounds, which also bind tightly to Ila RNA.

Compounds with a diaminopiperidine (DAP) core scaffold were designed with intent to bind to RNA by mimicking the interactions 2-DOS cores make with RNA. All 4-acetylbenzoic acid DAP derivatives tested quenched 2AP fluorescence. This binding was competitive with both sodium and magnesium salts, indicating that electrostatic forces are key to binding. This competition strengthens between 100 $\mu$ M and 1000 $\mu$ M, suggesting competition with the weaker magnesium binding site, possibly in addition to the higher-affinity magnesium site.

Benzimidazole P253 (Figure 4.5) also demonstrates binding activity, substantially increasing fluorescence in Ila-13-54 and Ila-13-57 constructs. Magnesium competition data (Figure 4.7) and RNase protection data (49) support a hypothesis that the compound

binds in the vicinity of the Mg/Mn1 binding site (Figure 4.3) near bases 55-56 and competes directly with the magnesium for access. The fluorescence increase caused by binding of P253 is in sharp contrast to the fluorescence decrease caused by metal ion binding. This suggests the possibility that the binding of the benzimidazole ligand may distort the tightly packed structure in the bend region, exposing the unpaired adenosines to solvent. As a result of this structural distortion, it is likely that the relative orientation of the two domain II helices changes upon P253 binding. To further investigate the structural changes upon compound binding, a series of FRET-based experiments to directly monitor global structural changes were designed. Chapter 5 describes the results of these FRET experiments.

## References:

1. Maheshwari, A.M., Ray, S. and Thuluvath, P.J. (2008). Acute hepatitis C. *Lancet* 372, 321–332.
- 1a. Alter, M.J., Kruszon-Moran, D., Nainan, O.V., McQuillan, G.M., Gao, F., Moyer, L.A., Kaslow, R.A., Margolis, H.S. (1999). The prevalence of hepatitis C virus infection in the United States, 1988 through 1994. *N Engl J. Med.*, 341:556-562.
2. Levrero, M. (2006). Viral hepatitis and liver cancer: the case of hepatitis C. *Oncogene*. 25:3834-3847
3. McCarthy, J.J., Li, J.H., Thompson, A., Suchindran, S., Lao, X.Q., Patel, K., Tillmann, H.L., Muir A.J., and McHutchison, J.G. (2010). Replicated Association between an IL28B Gene Variant and a Sustained Response to Pegylated Interferon and Ribavirin. *Gastroenterology*. doi:10.1053/j.gastro.2010.02.009
4. <http://www.clinicaltrials.gov>
5. <http://www.hevadvocate.com>
6. C.U.T. Hellen. (2009). IRES-induced conformational changes in the ribosome and the mechanism of translation initiation by internal ribosomal entry. *Biochimica et Biophysica Acta* 1789. 558–570
7. Pisarev, A. V. , Shirokikh, N.E., and Hellen, C.U.T. (2005). Translation initiation by factor-independent binding of eukaryotic ribosomes to internal ribosomal entry sites. *C. R. Biologies* 328: 589–605
8. Ji, H., Fraser, C.S., Yu, Y., Leary, J., and Doudna, J.A. (2004). Coordinated assembly of human translation initiation complexes by the hepatitis C virus internal ribosome entry site RNA. *Proc. Natl. Acad. Sci. U.S.A.* 101, 16990–16995.
9. Fraser, C.S., Hershey, J.W., and Doudna, J.A. (2009). The pathway of hepatitis C virus mRNA recruitment to the human ribosome. *Nat Struct Mol Biol.* Apr;16(4):397-404.
10. Tang, H., and Grise, H. (2009) Cellular and molecular biology of HCV infection and hepatitis. *Clinical Science* 117, (49–65)
11. Lindenbach, B. D., Evans, M. J., Syder, A. J., Wolk, B., Tellinghuisen, T. L., Liu, C. C., Maruyama, T., Hynes, R. O. , Burton, D. R. McKeating, J. A., and Rice, C.M. (2005). Complete replication of hepatitis C virus in cell culture. *Science* 309, 623–626.
12. Sakai, A., Claire, M. S., Faulk, K., Govindarajan, S., Emerson, S. U., Purcell, R. H. and Bukh, J. (2003). The p7 polypeptide of hepatitis C virus is critical for infectivity and contains functionally important genotype-specific sequences. *Proc. Natl. Acad. Sci. U.S.A.* 100, 11646-11651
13. Jones, C. T., Murray, C. L., Eastman, D. K., Tassello, J. and Rice, C. M. (2007). Hepatitis C virus p7 and NS2 proteins are essential for production of infectious virus. *J. Virol.* 81, 8374-8383
14. Pestova, T.V., Lorsch, J.R., Hellen, C.U.T. (2007). The mechanism of translation initiation in eukaryotes. In: M.B. Mathews, N. Sonenberg and J.B.W. Hershey, Editors, *Translational Control in Biology and Medicine*, Cold Spring Harbor Laboratory Press, Cold Spring Harbor, New York, pp. 87–128.
15. Pestova, T.V. , Borukhov, S.I., Hellen, C.U.T. (1998). Eukaryotic ribosomes require initiation factors 1 and 1A to locate initiation codons, *Nature* 394, pp. 854–859.

16. Pestova, T.V., and Hellen, C.U. (2000). The structure and function of initiation factors in eukaryotic protein synthesis, *Cell. Mol. Life Sci.* 57 (2000), pp. 651–674.
17. Pisarev, A.V., Kolupaeva, V.G., Yusupov, M.M., Hellen, C.U.T., and Pestova, T.V. (2008). Ribosomal position and contacts of mRNA in eukaryotic translation initiation complexes, *EMBO J.* 27, pp. 1609–1621.
18. Yusupova, G. Z., Yusupov, M. M., Cate, J. H. and Noller, H. F. (2001). The path of messenger RNA through the ribosome. *Cell* 106, 233–241.
19. Siridechadilok, B., Fraser, C. S., Hall, R. J., Doudna, J. A. and Nogales, E. (2005). Structural roles for human translation factor eIF3 in initiation of protein synthesis. *Science* 310, 1513–1515.
20. Merrick, W. C. (2004). Cap-dependent and cap-independent translation in eukaryotic systems. *Gene* 332, 1–11.
21. Brown, E.A., Zhang, H., Ping, L.H., and Lemon, S.M., (1992). Secondary structure of the 5' nontranslated regions of hepatitis C virus and pestivirus genomic RNAs. *Nucleic Acids Res.* 20, 5041–5045.
22. Pestova, T. V., Shatsky, I. N., Fletcher, S. P., Jackson, R. J. and Hellen, C. U. (1998). A prokaryotic-like mode of cytoplasmic eukaryotic ribosome binding to the initiation codon during internal translation initiation of hepatitis C and classical swine fever virus RNAs. *Genes Dev.* 12, 67–83
23. Reynolds, J.E., Kaminski, A., Kettinen, H.J., Grace, K., Clarke, B.E., Carroll, A.R., Rowlands, D.J., and Jackson, R.J. (1995). Unique features of internal initiation of hepatitis C virus RNA translation. *EMBO J.* 14, 6010–6020.
24. Lancaster, A.M., Jan, E., and Sarnow, P. (2006). Initiation factor-independent translation mediated by the hepatitis C virus internal ribosome entry site. *RNA*. May;12(5):894-902.
25. Reynolds, J.E., Kaminski, A., Carroll, A.R., Clarke, B.E., Rowlands, D.J., and Jackson, R.J. (1996). Internal initiation of translation of hepatitis C virus RNA: the ribosome entry site is at the authentic initiation codon. *RNA* 2, 867–878.
26. Otto, G. A. and Puglisi, J. D. (2004). The pathway of HCV IRES- mediated translation initiation. *Cell* 119, 369–380.
27. Rijnbrand, R., van der Straaten, T., van Rijn, P. A., Spaan, W. J. and Bredenbeek, P.J. (1997) Internal entry of ribosomes is directed by the 5' noncoding region of classical swine fever virus and is dependent on the presence of an RNA pseudoknot upstream of the initiation codon. *J. Virol.* 71, 451–457.
28. Kieft, J.S., Zhou, K., Jubin, R., Murray, M.G., Lau, J.Y., and Doudna, J.A., (1999) The hepatitis C virus internal ribosome entry site adopts an ion-dependent tertiary fold. *J. Mol. Biol.* 292, 513–529.
29. Kolupaeva, V.G., Pestova, T.V., and Hellen, C.U., (2000). An enzymatic footprinting analysis of the interaction of 40S ribosomal subunits with the internal ribosomal entry site of hepatitis C virus. *J. Virol.* 74, 6242–6250.
30. Lytle, J. R., Wu, L. and Robertson, H. D. (2002). Domains on the hepatitis C virus internal ribosome entry site for 40s subunit binding. *RNA* 8, 1045–4055
31. Palomares-Jerez, M.F., Guillen, J., and Villalain, J. (2010). Interaction of the N-terminal segment of HCV protein NS5A with model membranes, *BBA - Biomembranes*

32. Friebe, P., Lohmann, V., Krieger, N. and Bartenschlager, R. (2001). Sequences in the 5' nontranslated region of hepatitis C virus required for RNA replication. *J. Virol.* 75, 12047–12057.
33. Fukushi, S., Katayama, K., Kurihara, C., Ishiyama, N., Hoshino, F.B., Ando, T., and Oya, A. (1994). Complete 5' noncoding region is necessary for the efficient internal initiation of hepatitis C virus RNA. *Biochem. Biophys. Res. Commun.* 199, 425–432.
34. Rijnbrand, R., Bredenbeek, P., van der Straaten, T., Whetter, L., Inchauspé, G., Lemon, S., and Spaan, W. (1995). Almost the entire 5' non-translated region of hepatitis C virus is required for cap-independent translation. *FEBS Lett.* 365, 115–119.
35. Zhao, W.D., and Wimmer, E. (2001). Genetic Analysis of a Poliovirus/Hepatitis C Virus Chimera: New Structure for Domain II of the Internal Ribosomal Entry Site of Hepatitis C Virus. *Journal of Virology*, Apr. p. 3719–3730
36. Klinck, R. Westhof, E., Walker, S., Afshar, M., Collier, A., and Aboul-Ela, F. (2000). A potential RNA drug target in the hepatitis C virus internal ribosomal entry site. *RNA* 6, 1423–1431.
37. Locker, N., Easton, L.E., and Lukavsky, P.J. (2007). HCV and CSFV IRES domain II mediate eIF2 release during 80S ribosome assembly. *EMBO J.* 26, 795–805.
38. Lukavsky, P.J. (2009). Structure and function of HCV IRES domains. *Virus Res.* Feb;139(2):166-71.
39. Sizova, D.V., Kolupaeva, V.G., Pestova, T.V., Shatsky, I.N. and Hellen, C.U. (1998). Specific interaction of eukaryotic translation initiation factor 3 with the 5' nontranslated regions of hepatitis C virus and classical swine fever virus RNAs. *J. Virol.* 72, 4775–4782.
40. Spahn, C.M., Kieft, J.S., Grassucci, R.A., Penczek, P.A., Zhou, K., Doudna, J.A., and Frank, J. (2001). Hepatitis C virus IRES RNA-induced changes in the conformation of the 40s ribosomal subunit. *Science* 291, 1959–1962.
41. Boehringer, D., Thermann, R., Ostareck-Lederer, A., Lewis, J.D. and Stark, H. (2005). Structure of the hepatitis C Virus IRES bound to the human 80S ribosome: remodeling of the HCV IRES. *Structure (Camb)* 13, 1695–1706 (2005).
42. Lukavsky, P.J., Kim, I., Otto, G.A., and Puglisi, J.D., (2003). Structure of HCV IRES domain II determined by NMR. *Nat. Struct. Biol.* 10, 1033–1038.
43. Honda, M., Beard, M.R., Ping, L.H., and Lemon, S.M. (1999). A phylogenetically conserved stem-loop structure at the 5' border of the internal ribosome entry site of hepatitis C virus is required for cap-independent viral translation. *J. Virol.* 73, 1165–1174.
44. Dibrov, S.M., Johnston-Cox, H., Weng, Y.H., and Hermann, T., (2007). Functional architecture of HCV IRES domain II stabilized by divalent metal ions in the crystal and in solution. *Angew. Chem. Int. Ed. Engl.* 46, 226–229.
45. Brown, E.A., Zhang, H., Ping, L.H., and Lemon, S.M., (1992). Secondary structure of the 5' nontranslated regions of hepatitis C virus and pestivirus genomic RNAs. *Nucleic Acids Res.* 20, 5041–5045.
46. Honda, M., Brown, E.A., and Lemon, S.M., (1996a). Stability of a stem-loop involving the initiator AUG controls the efficiency of internal initiation of translation on hepatitis C virus RNA. *RNA* 2, 955–968.

47. Honda, M., Ping, L.H., Rijnbrand, R.C., Amphlett, E., Clarke, B., Rowlands, D., and Lemon, S.M., (1996b). Structural requirements for initiation of translation by internal ribosome entry within genome-length hepatitis C virus RNA. *Virology* 222, 31–42
48. Johnson, N.P., Baase, W.A., and von Hippel, P.H. (2004). Low-energy circular dichroism of 2-aminopurine dinucleotide as a probe of local conformation of DNA and RNA. *PNAS* 101:3426-3431.
49. Seth, P.P., Miyaji, A., Jefferson, E.A., Sannes-Lowery, K.A., Osgood, S.A., Propp, S.S., Ranken, R., Massire, C., Sampath, R., Ecker, D.J., Swayze, E.E., and Griffey, R.H. (2005). SAR by MS: Discovery of a New Class of RNA-Binding Small Molecules for the Hepatitis C Virus: Internal Ribosome Entry Site IIA Subdomain. *Journal of Medicinal Chemistry*, 48, 23 Letters pp.7099-7102.
50. Arya, D. P., Xue, L., and Willis, B. (2003). Aminoglycoside (Neomycin) Preference Is for A-Form Nucleic Acids, Not Just RNA: Results from a Competition Dialysis Study. *J. Am. Chem. Soc.*, 125, 10148.
51. Pymol.sourceforge.com
52. Carnevali, M., Parsons, J., and Hermann, T. (2010) A Modular Approach to Synthetic RNA Binders of the Hepatitis C Virus Internal Ribosome Entry Site. *ChemBioChem*, submitted Mar 2010
53. Buntrock, R.E. (2002). ChemOffice Ultra 7.0. *J. Chem. Inf. Comput. Sci.*, 42 (6), pp 1505–1506
54. Wong, C.H., Hendrix, M., Priestley, E.S., and Greenberg, W.A. (1998). Specificity of aminoglycoside antibiotics for the A-site of the decoding region of ribosomal RNA. *Chem. Biol.* 5, 397–406.
55. Griffey, R.H., Hofstadler, S.A., Sannes-Lowery, K.A., Ecker, D.J., and Crooke, S.T. (1999). Determinants of aminoglycoside-binding specificity for rRNA by using mass spectrometry. *Proc. Natl. Acad. Sci. USA.* 96, 10 129.
56. Tran, T., and Disney, M.D. (2010). Two-dimensional combinatorial screening of a bacterial rRNA a-site-like motif library: defining privileged asymmetric internal loops that bind aminoglycosides. *Biochemistry.* 9;49(9):1833-42.

**Chapter 5:**  
**Förster Resonance Energy Transfer Studies of HCV IRES**  
**Subdomain IIa**

Parts of this work are published as:

“Conformational inhibition of the hepatitis C virus internal ribosome entry site RNA”

Nature Chemical Biology 5, 11 823-825 (Nov 2009).



## 5.0: Abstract

The HCV IRES subdomain IIa, which is required for IRES-mediated viral translation, is investigated here by development of a Förster resonance energy transfer (FRET)-based assay. Screening identified 22 RNA-friendly compounds that greatly alter the bent native RNA structure of the IIa subdomain. The most active of these molecules share a similar core structure with one another and contribute to the stability of an inactive, extended conformation of the domain. (1)

## 5.1: Introduction

In biological systems, FRET is most frequently employed as a molecular ruler to experimentally measure distances in the range of 20-70 angstroms. The technique works by taking advantage of non-radiative energy transfer between an excited donor molecule and an acceptor molecule. The process works by exciting a fluorescent donor molecule, which then transfers a fraction of the excited-state energy to an acceptor molecule, which may also be fluorescent.

The rate of energy transfer is equal to the sixth root of the ratio of the distance between the donor and acceptor ( $R$ ) to the Förster radius, a characteristic of the donor-acceptor pair. ( $R_0$ , Figure 5.1) The Förster radius is experimentally verified for most donor-acceptor pairs, provided freedom of rotation for the donor and acceptor in solution. (2,3)

$$E = \frac{1}{1 + \left(\frac{r}{R_0}\right)^6}$$

$r$  is the distance between the donor and acceptor molecule.

$R_0^6 = (8.785 \times 10^{-25}) \Phi^D \kappa^2 n^{-4} J(\nu) \text{ cm}$ .  $\Phi^D$  is the donor emission quantum yield.

$\kappa^2$  is the orientation factor for dipole coupling :  $\frac{2}{3}$  if probes freely and rapidly reorient.

$n$  is the refractive index of the medium (1.4) and  $J(\nu)$  is the spectral overlap integral.

$$J(\nu) = \int (\epsilon^A(\nu) \phi(\nu) \nu^{-4}) d\nu$$

Where  $\epsilon_a$  = molar absorbance of the acceptor at  $\nu$  and

$\phi(\nu)$  is the normalized fluorescence shape function

Figure 5.1: Equations of Förster Resonance Energy Transfer

Cyanine dyes, particularly Cy3 and Cy5 (Figure 5.2) are among the most popular dye pairs used for FRET experiments, due to their high quantum yields and extinction coefficients. Both of these molecules are fluorescent. Cy3 excitation peaks at 550nm, and emission peaks at 570nm with a shoulder out to 610nm. Cy5 excitation peaks at 650nm, with an emission peak at 670nm. Exciting Cy3 just below its peak (535-540nm) prevents most direct excitation of Cy5. Any Cy5 emission based on excitation at 535 nm is almost entirely due to resonance energy transfer from Cy3. (2,5-13)

In the case of IRES subdomain IIa, the function of the domain seems to be related entirely to positioning adjacent domains, making a distance measurement nearly equivalent to a direct functional assay.

*Design of FRET-labeled IRES IIa – “IIa-2”*

Due to the 6<sup>th</sup> order nature of the FRET response, the effective distance measurable by FRET is between 0.5 and 1.5 times the Förster Distance ( $R_0$ ). To maximize the dynamic signal range, a distance of 1.0  $R_0$  (55.8Å for the Cy3-Cy5 pair) (4) in the folded state was desired. Using the X-ray-determined coordinates of the IIa RNA (15) as a guide, the “IIa-2” RNA construct (Figure 5.2) was generated. The 5’ to 5’ distance between the two strands of the crystal construct plus an additional 5’ base and c3 linker was modeled and measured to be just over 58Å. In the absence of magnesium, the construct is expected to form a linear structure of around 80Å end to end. Based on these calculations, the FRET efficiency ( $E_{\text{FRET}}$ ) (7) is expected to be below 0.1 when fully extended and just below 0.5 in a bent conformation as adopted in the crystal structure.

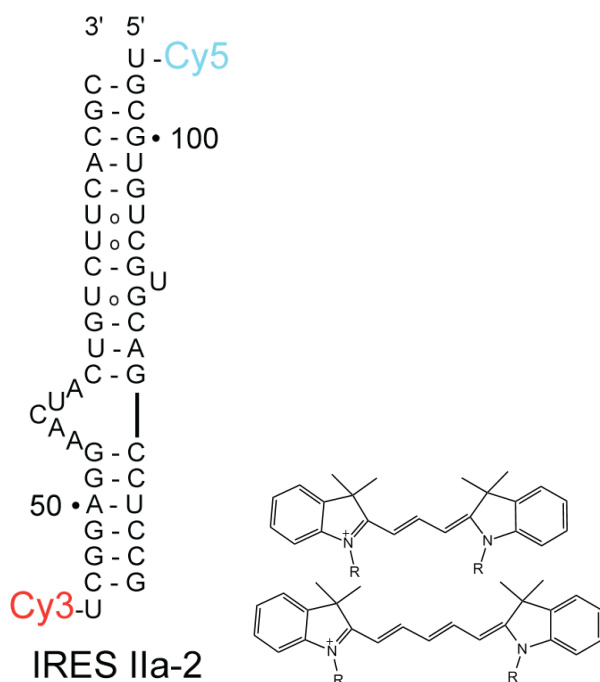


Figure 5.2: IRES IIa-2 construct, and cyanine dyes Cy3(top)-Cy5(bottom)

## 5.2: Results

To verify the modeled FRET efficiency ( $E_{\text{FRET}}$ ) of Ila-2 RNA, a titration with  $\text{MgCl}_2$  was done. Figure 5.3 shows the measured  $E_{\text{FRET}}$  as a function of magnesium concentration. In the absence of magnesium ions,  $E_{\text{FRET}}$  is nonexistent, suggesting a distance greater than  $80\text{\AA}$ . FRET signal grows starting at  $100\mu\text{M}$  and continues rising to around  $10\text{mM}$ . The  $\text{EC}_{50}$  of this response is  $580\mu\text{M}$ . 2AP-based experiments had placed the dissociation constants for the structural metal ions in the Ila domain at  $37\mu\text{M}\pm 20\mu\text{M}$  and  $18\text{mM}\pm 9\text{mM}$ . Titration with  $\text{NaCl}$  and  $\text{KCl}$  did not induce FRET increase, but addition of  $\text{EDTA}$  to the  $\text{Mg}^{2+}$ -containing solution decreased FRET signal at concentrations corresponding to a reverse of the magnesium curve.

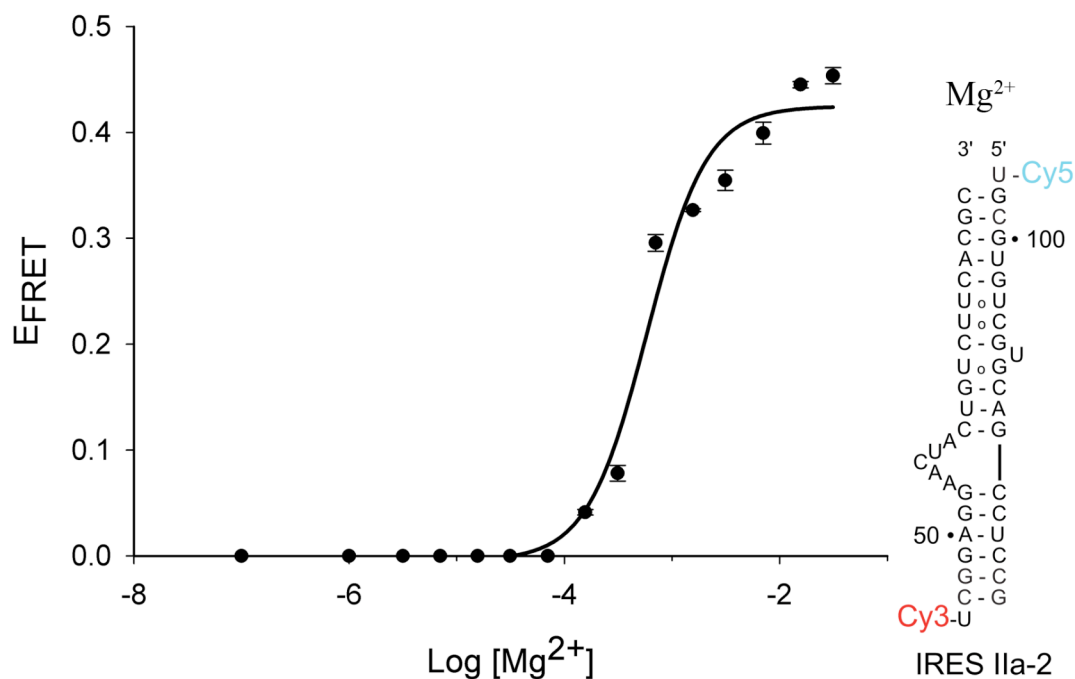


Figure 5.3: IRES Ila-2 titrated with magnesium chloride. The FRET efficiency ( $E_{\text{FRET}}$ ) of Ila-2 RNA is plotted against the concentration of magnesium. FRET response develops at  $100\mu\text{M}$  and stabilizes at .45 at  $10\text{mM}$ . ( $\text{EC}_{50} = 0.58\text{mM}$ ) Distance and angle calculations based on the  $E_{\text{FRET}}$  are described in the text. The FRET effect does not fit exactly to a two-site binding model, indicating that multiple  $\text{Mg}^{2+}$  binding sites are involved in the folding of the Ila-2 RNA.

The benzimidazole compound P253 first described in Chapter 4 was tested in this system. RNA was prepared in the presence of 2mM MgCl<sub>2</sub> to pre-fold the RNA.  $E_{\text{FRET}}$  in this amount of magnesium is  $0.47 \pm 0.02$ . Titration data for P253 is shown in Figure 5.4. The  $EC_{50}$  of binding is  $630 \text{ nM} \pm 290 \text{ nM}$ , in line with the 2AP ( $580 \text{ nM} \pm 100 \text{ nM}$ ) and MS ( $720 \text{ nM}$ ) results.

Repeating the experiment in the presence of unlabeled tRNA at 50-fold excess over Ila-2 RNA had no effect on the FRET response, demonstrating some specificity of the compound for Ila RNA. HCV replicon experiments performed in collaboration with D. Wyles (1) demonstrated that the benzimidazole P253 actively inhibits HCV translation in human HUH-7.5 cells, reducing reporter activity to 50% in  $4.0 \mu\text{M}$  P253. Cytotoxicity assays determined that cell viability is around 90% in the presence of P253 at these concentrations.

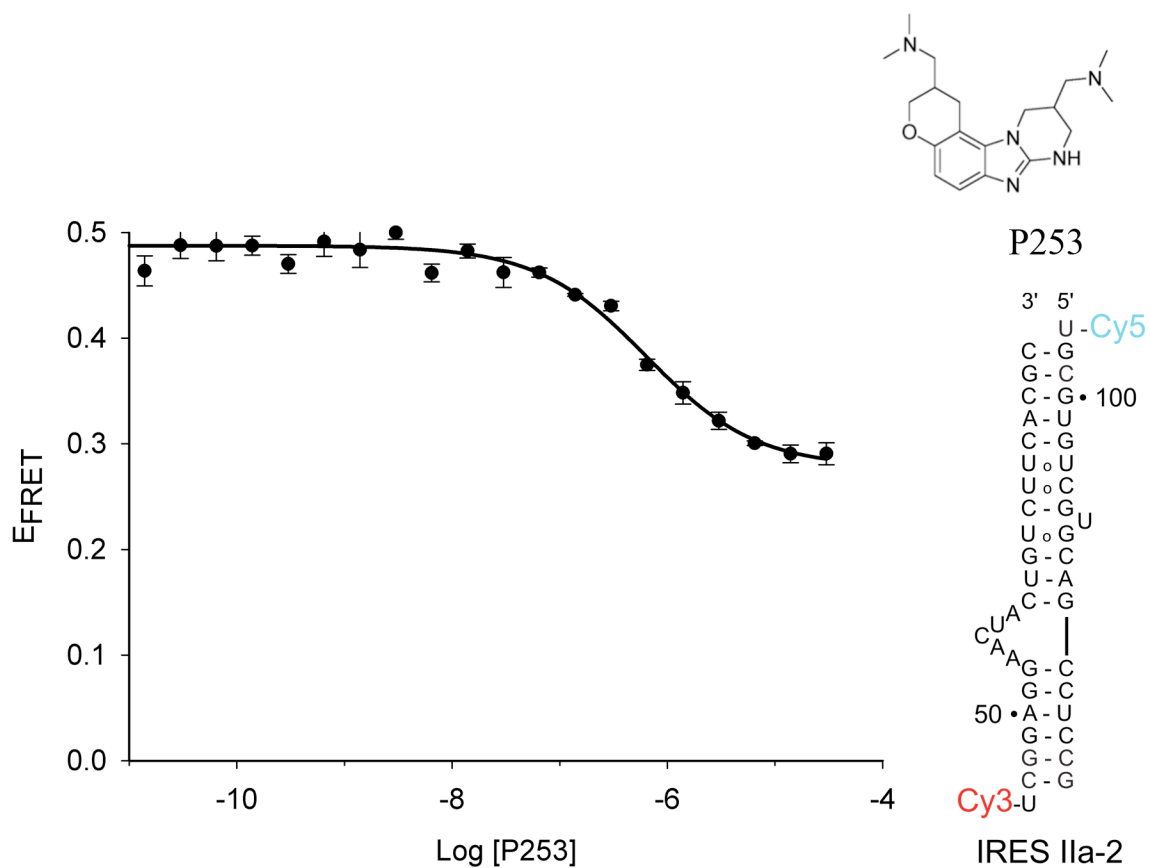


Figure 5.4: IRES Ila-2 titrated with P253. The FRET efficiency ( $E_{FRET}$ ) of Ila-II RNA is plotted against the concentration of compound P253. The  $EC_{50}$  of the FRET response is  $630 \pm 290 \text{ nM}$ .

Benzimidazole compounds have also been described (16,17) as inhibitors of the HCV viral polymerase NS5B. To investigate the potential involvement of P253 in this pathway of viral inhibition, an in-vitro polymerase assay was used (18,19). Polymerase activity in the presence of 10 $\mu$ M of P253 was 104% $\pm$ 8% of control, measured as detection of fluorescent molecules generated by coupled enzymatic activity. A benzimidazole inhibitor previously described reduced activity to 31% in the same assay. (Figure 5.5).

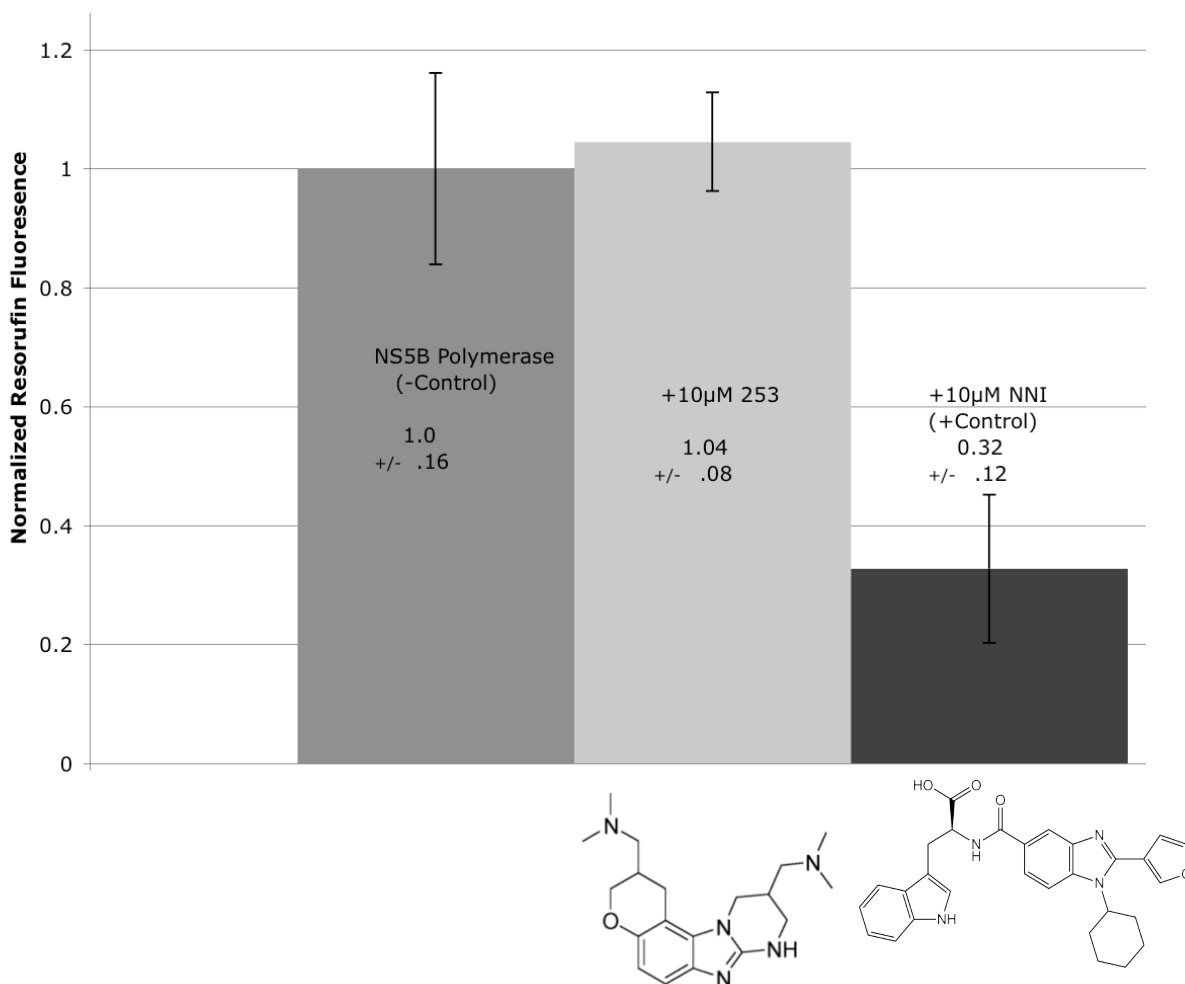


Figure 5.5: P253 is not an NS5B polymerase inhibitor. Level of NS5B polymerase activity in presence of inhibitory compounds. Shown are pyrophosphate levels measured by PiPer pyrophosphate assay kit. (Invitrogen) Pyrophosphate generation by NS5B polymerase in presence of benzimidazole P253 (center) is 104% +/- 8%, indicating no inhibition. In the presence of benzimidazole inhibitor (right, ref.17) pyrophosphate measurement is 32% +/- 12%.

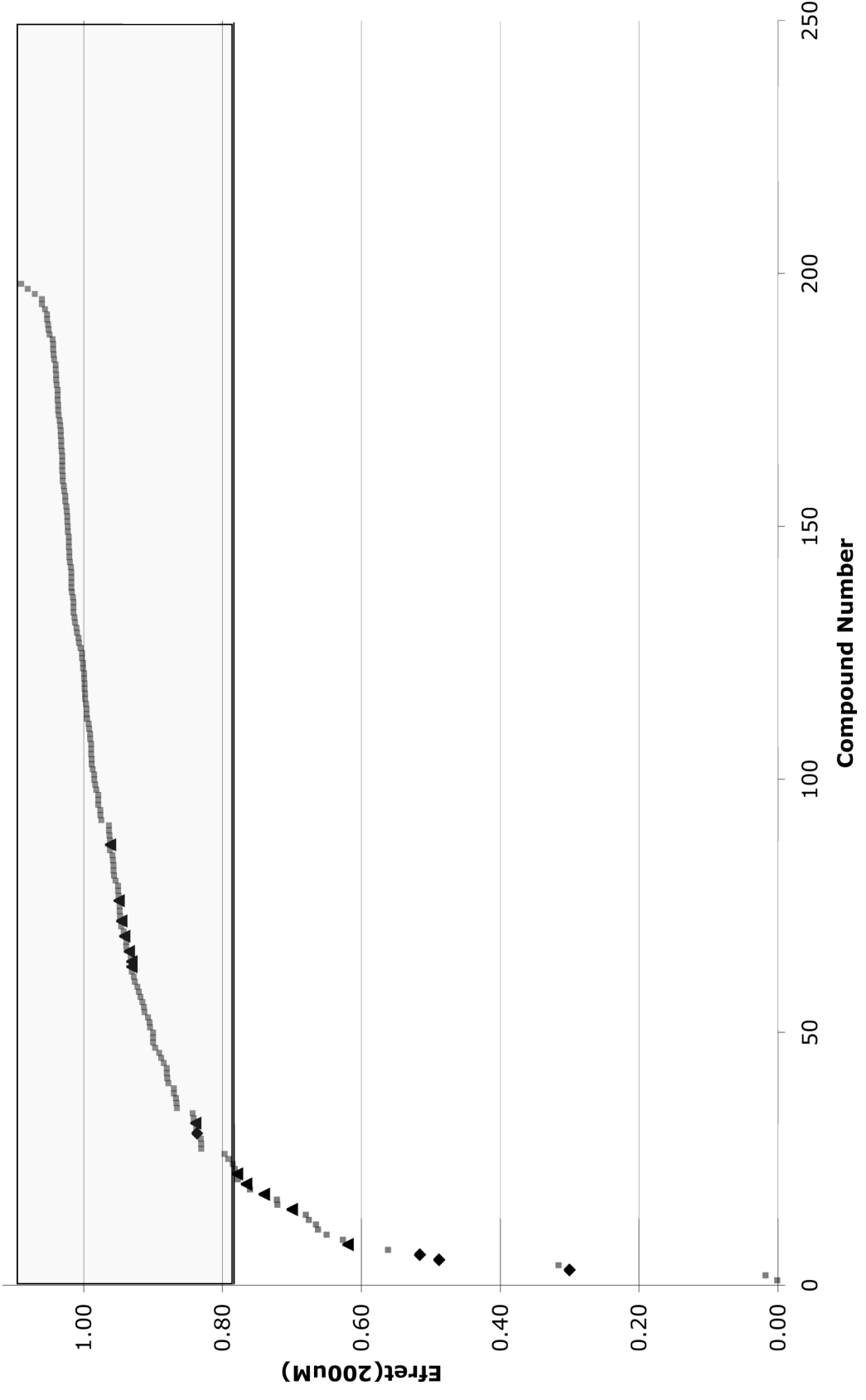


### *Screening*

Having demonstrated the ability to identify the activity of P253, this assay was used for screening a commercial library of compounds. Figure 5.6 shows the  $E_{\text{FRET}}$  of 198 compounds screened at 200 $\mu\text{M}$  concentration. Compounds that decreased calculated FRET response by acceptor quenching were removed from further experiments. On the whole, the screen proved quite effective. The  $Z'$  factor (20), using P253 as a primary control for the assay is 0.83. This reflects the strong signal difference between folded and unfolded Ila-2 RNA and the low variability in signal observed. The  $Z$  factor for the 198 compounds tested is 0.43. The difference between the  $Z$  factor and  $Z'$  factor is due to the small and RNA-biased nature of the library. Twenty two (11% of the total) hit compounds were identified in the screen. Included in this are P253 and two benzimidazole precursors described by Ibis (21). Additionally, five of sixteen hydrazone-linked indole-containing compounds (hydrazones) screened decreased FRET significantly. (Triangles in Figure 5.6 ; Figure 5.7) Titrations of each hit were performed to determine  $EC_{50}$  concentrations. The high proportion of hits within the hydrazone compounds prompted investigation of the structure-activity relationship within the group.

Figure 5.7 shows the hydrazone compounds screened in the Ila-2 RNA, as well as the  $EC_{50}$  concentration of each. The primary determinant of binding activity is the presence of a substituent at the 2 position on the indole ring.

Figure 5.6: FRET efficiencies of 198 compounds screened at 200uM against IRES IIa-2 RNA. Benzimidazole compounds described in the text are shown as diamonds. Hydrazone compounds described in the text are shown as triangles. The grayed-out region represents the variability band - 3 standard deviations from the mean of control IIa-2 RNA. Compounds outside this band are considered hits. P253 is the second diamond from the left and corresponds to 8 standard deviations.



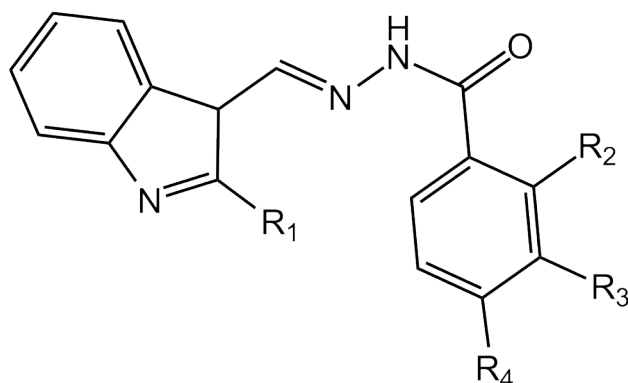


Figure 5.7a: Scaffold of Hydrazone compounds.

Compound	R <sub>1</sub>	R <sub>2</sub>	R <sub>3</sub>	R <sub>4</sub>	Affinity(μM)
1	H	H	OH	H	N.A.
2	H	H	H	OH	N.A.
3	H	H	OH	OH	N.A.
4	H	OH	H	OH	N.A.
5	H	H	H	(CH <sub>2</sub> )OH	N.A.
6	H	H	H	(CH <sub>2</sub> )NH <sub>2</sub>	N.A.
7	H	H	H	CONH <sub>2</sub>	N.A.

Compound	R <sub>1</sub>	R <sub>2</sub>	R <sub>3</sub>	R <sub>4</sub>	Affinity(μM)
8	Me	H	OH <sup>1</sup>	H	N.A.
9	Me	H	H	CONH <sub>2</sub>	N.A.
10	Me	H	H	CH <sub>2</sub> (OH)	N.A.
11,12	Me	H	H	OH	380
13	Me	H	H	CH <sub>2</sub> (NH <sub>2</sub> )	325
14	Me	H	H	NH <sub>2</sub>	120
15,16	Me	OH	H	OH	125
17	Me	H	OH	H	N.A.

Figure 5.7b: Structure-activity relationships for indole-class hydrazone compounds. E<sub>FRET</sub> determinations were made as described in Methods section for each compound at concentrations ranging from 500nM to 1mM. N.A. No decrease in E<sub>FRET</sub> was seen at 1mM. 1: Compound 8 is substituted at both meta positions. Me: Methyl substituent.

### 5.3: Conclusions

FRET reduction and replicon inhibition demonstrate the capacity of benzimidazole P253 to induce an alternate, nonfunctional conformation in the HCV IRES IIa subdomain. Binding of the compound stabilizes a widened interhelical angle, inhibiting HCV translation. Independent NMR studies (22) have since demonstrated that this mechanism of inhibition is shared by related benzimidazole compounds and shown that structural rearrangement occurs within the IIa bend.

Using this assay, a screen of nearly 200 RNA-biased small molecules was performed. In this screen, 22 compounds significantly reduced the FRET efficiencies at 200 $\mu$ M concentration. 3 hits were benzimidazoles, including P253. Most of the remainder were hydrazones linking indole and benzene ring structures (Figure 5.7a). A structure-activity relationship of active hydrazones and related inactive hydrazones, as well as similar isatin-based compounds was determined. Hydrazone molecules showing FRET activity all contain a methyl or carbonyl group at the 2 position of the indole ring (Figure 5.7). In the near future, structural information will become available and allow rigorous modeling of the interaction surfaces of hit molecules. Based on shape similarity, it is likely that the indole and benzimidazole rings would perform the same base-stacking duties. In this case, the required substitution at the 2 position would be located within a large hydrophobic void in the unbent structure. The hydrazone-linked benzene ring would then likely be positioned near the phosphate backbone. The heightened affinity of hydrazones with positively charged substitutions on the benzene ring (Figure 5.7) may be explained in this way. While the benzimidazole compounds

described have better affinities than the hydrazones and isatins (1  $\mu$ M for the optimized benzimidazole versus 60  $\mu$ M for the best isatin), the hydrazones and isatins lack the dimethylamino moiety at the C6 position, which was responsible for a dramatic increase in affinity in the benzimidazoles (21). In the benzimidazoles, this amine is positioned in proximity to the magnesium site, and expansion of the indole ring contained in the hydrazone compounds should similarly increase the affinity of the hydrazone compounds. With an expanded amount of structural and activity information, future synthesis may provide high-affinity IIa-binding molecules with strengthened antiviral activity.

Research described in Chapter 5, in part, has been published in *Nature Chemical Biology* 5, 11 823-825. Jerod Parsons was first author of this paper, in collaboration with Prof. Thomas Hermann, Dr. M. Paola Castaldi, Dr. Sanjay Dutta, Dr. Sergey Dibrov, and Dr. David Wyles.

## References;

1. Parsons, J., Castaldi, M.P., Dutta, S., Dibrov, S.M., Wyles, D.L., and Hermann, T. (2009). Conformational inhibition of the hepatitis C virus internal ribosome entry site RNA *Nature Chemical Biology* 5, 11 823-825.
2. Clegg, R. M. (1992). Fluorescence resonance energy-transfer and nucleic-acids. *Methods Enzymol.* 211, 353–388.
3. Förster, T. (1946). Energiewanderung und fluoreszenz. *Naturwissenschaften* 166–175.
4. Dietrich, A., Buschmann, V., Muller, C., and Sauer, M. (2002). *Reviews in Molecular Biotechnology*, 82:3 Pp. 211-231
5. Hillisch, A., Lorenz, M., and Diekmann, S. (2001). Recent advances in FRET distance determination in protein–DNA complexes, *Curr. Opin. Struct. Biol.* 11, pp. 201–207
6. Clegg, R.M., Murchie, A.I.H., Zechel, A., Carlberg, C., Diekmann, S., and Lilley, D.M.J. (1992). Fluorescence resonance energy-transfer analysis of the structure of the 4-way DNA junction, *Biochemistry* 31, Pp. 4846–4856.
7. Clegg, R.M. (1992). Fluorescence resonance energy transfer and nucleic acids, *Methods Enzymol.* 211, pp. 353–389.
8. Selvin, P.R. (1995). Fluorescence resonance energy transfer, *Methods Enzymol.* 246, pp. 301–334.
9. McKinney, S. A., Declais, A.-C., Lilley, D. M. J., and Ha, T. (2003). Structural dynamics of individual Holliday junctions *Nat. Struct. Biol.* 10 93 97
10. Ha, T. (2001). Single-molecule fluorescence methods for the study of nucleic acids *Curr. Opin. Struct. Biol.* 11 287 292
11. Mollova, E. T. (2002). Single-molecule fluorescence of nucleic acids *Curr. Opin. Chem. Biol.* 6 823-828
12. McKinney, S. A., Tan, E., Wilson, T. J., Nahas, M. K., Declais, A. C., Clegg, R. M., Lilley, D. M. J., and Ha, T. (2004). Single-molecule studies of DNA and RNA four-way junctions *Biochem. Soc. Trans.* 32 41 45
13. Rasnik, I., McKinney, S. A., and Ha, T. (2005). Surfaces and orientations: Much to FRET about? *Acc. Chem. Res.* 38 542 548
14. Dietrich, A., Buschmann, V., Muller, C., Sauer, M. (2002). *Reviews in Molecular Biotechnology*, Volume 82, Issue 3, Pages 211-231
15. Dibrov, S.M., Johnston-Cox, H., Weng, Y.H., and Hermann, T. (2007). Functional architecture of HCV IRES domain II stabilized by divalent metal ions in the crystal and in solution. *Angew. Chem. Int. Ed. Engl.* 46, 226–229.

16. Beaulieu, P.L., Gillard, J., Bykowski, D., Brochu, C., Dansereau, N., Duceppe, J.S., Haché, B., Jakalian, A., Lagacé, L., LaPlante, S., McKercher, G., Moreau, E., Perreault, S., Stammers, T., Thauvette, L., Warrington, J., and Kukulj, G. (2006). Improved replicon cellular activity of non-nucleoside allosteric inhibitors of HCV NS5B polymerase: from benzimidazole to indole scaffolds. *Bioorg Med Chem Lett.* Oct 1;16(19):4987-93.
17. Beaulieu, P.L., Bös, M., Bousquet, Y., Fazal, G., Gauthier, J., Gillard, J., Goulet, S., LaPlante, S., Poupard, M.A., Lefebvre, S., McKercher, G., Pellerin, C., Austel, V., and Kukulj, G. (2004). Non-nucleoside inhibitors of the hepatitis C virus NS5B polymerase: discovery and preliminary SAR of benzimidazole derivatives. *Bioorg Med Chem Lett.* Jan 5;14(1):119-24.
18. Zhou, M., Diwu, Z., Panchuk-Voloshina, N. and Haugland, R.P. (1997). A Stable Nonfluorescent Derivative of Resorufin for the Fluorometric Determination of Trace Hydrogen Peroxide: Applications in Detecting the Activity of Phagocyte NADPH Oxidase and Other Oxidases *Anal Biochem* 253, 162.
19. Mohanty, J. G., Jaffé, J.S., Schulman, E.S., and Raible, D.G. (1997). A highly sensitive fluorescent micro-assay of H<sub>2</sub>O<sub>2</sub> release from activated human leukocytes using a dihydroxyphenoxazine derivative *J Immunol Methods* 202, 133
20. Zhang, J., Chung, T.D.Y., Oldenburg, K.R. (1999). A Simple Statistical Parameter for Use in Evaluation and Validation of High Throughput Screening Assays. 4; 67 *J Biomol Screen*
21. Seth, P.P., Miyaji, A., Jefferson, E.A., Sannes-Lowery, K.A., Osgood, S.A., Propp, S.S., Ranken, R., Massire, C., Sampath, R., Ecker, D.J., Swayze, E.E., and Griffey, R.H. (2005). SAR by MS: Discovery of a New Class of RNA-Binding Small Molecules for the Hepatitis C Virus: Internal Ribosome Entry Site IIA Subdomain. *J. Med. Chem.* 2005, 48, 7099-7102
22. Paulsen, R.B., Seth, P.P., Swayze, E.E., Griffey, R.H., Skalicky, J.J., Cheatham, T.E. III, and Davis, D.R. (2010). Inhibitor-induced structural change in the HCV IRES domain IIa RNA. *PNAS*. DOI://10.1073/pnas.0911896107



**Chapter 6:**  
**Experimental Methods & Appendices**

### *6.0 Materials:*

RNA constructs with 3MI, 6MI, and 2AP fluorescence labels were purchased from Dharmacon and used as received. The Ila-2 construct with cyanine modifications was purchased from Integrated DNA Technologies (IDT) and used as received. All compounds used in titrations were purchased as sulfate salts from Sigma except metal salts, purchased as chlorides such as  $MgCl_2$  and KCl.

### *6.1 Methods:*

UV Melting experiments were performed on a UV-2401PC spectrofluorometer (Shimadzu) equipped with a thermostat. RNA at  $1.6\mu M$  in 20mM sodium cacodylate buffer (pH 6.5) was heated from  $25^\circ C$  to  $85^\circ C$  at  $0.5^\circ / \text{minute}$ . RNA samples were covered with a layer of silicone oil to prevent evaporation. Absorbance measurements at 260nm were read every 6 seconds. Reference 7 contains an excellent introduction to absorbance melting curves of RNA.

Fluorescence measurements were performed on an RF-5301PC spectrofluorometer (Shimadzu) equipped with a thermostat set at  $25^\circ C$ . Emission spectra of 2AP-labeled RNA excited at 310nm were collected from 330nm to 420nm. RNA concentration of around  $1\mu M$  is typically required, although it is important to adjust this figure for each individual construct, adjusting the fluorescence output to a level where both increases and decreases can be observed within the dynamic range of the fluorometer.  $EC_{50}$  calculations were done using sigmaplot software (Systat Software, CA) by fitting one-site (or two-site, where applicable) binding curves to the fluorescence

intensity plotted against the titrant concentration. Normalization of fluorescence signal was done by subtracting the intensity of the highest titrant concentration and dividing by the maximum fluorescence change seen in the titration such that  $N = (I - I_{\min}) / (I_{\max} - I_{\min})$ . Background fluorescence intensity of the titrant can be a concern – in cases where the titrant fluoresces at 310nm, an additional titration of titrant into buffer is performed, and the signal from this background titration (corresponding to the fluorescence of the titrant compound) is subtracted from the signal observed upon addition of compound into RNA.

For experiments with 3MI, 6MI, and 2AP-labeled A-site constructs, Fluorescence measurements and methods are described in (1). For experiments with hygromycin constructs HX-1493 and HX-HX5, Fluorescence measurements, UV melting experiments, crystallization setup, and methods are described in Dibrov 2010. (2) Methods for fluorescence measurements in Ila-54 and Ila-57 RNA constructs are described in Dibrov 2007 (3). Methods for FRET experiments in the Ila-2 construct are described in Parsons 09 (4).

For FRET experiments with the Ila-2 construct, well solutions containing 40nM hybridized Ila-2 RNA, 2mM MgCl<sub>2</sub>, 10mM sodium hepes buffer (pH 7.0) were added to each well of a microplate containing 2.4μL of a 10mM stock of compound, for a final concentration of 200μM compound. The samples were then heated to 65°C and snap cooled to re-anneal in presence of compound. The plate was then read on a Spectra Max Gemini monochromator plate reader (Molecular Devices) at 25°C. The Cy3 label was excited at 520nm in order to reduce direct excitation of the Cy5 label. Cy5 was excited at

620nm. Emission measurements were made at 570nm (Donor emission), 670nm (FRET emission) and 670nm(Cy5 emission). A more complete description of the calculations involved in determining FRET efficiency is contained in appendix 2.

FRET screening experiments in the Ila-2 construct were prepared as 40nM Ila-2 RNA, 2mM MgCl<sub>2</sub>, 10mM HEPES pH 7.0, and sample compound at varying concentrations in 120μL final volumes. 96 samples are prepared in parallel, with positive control RNA (Ila-2 only) and negative control (RNA+P253) present in a total of 6 samples. The samples are heated to 65C for 5 minutes and cooled to 4C before being transferred to a microplate for reading in a Spectra Max Gemini monochromator plate reader (Molecular Devices). Samples were read by exciting Cy3 at 520nm, in order to minimize cross-excitation of Cy5. (5) Cy5 emission was read from 670nm onwards. Excitation and emission filters were used and set at 550nm and 665nm, respectively. Signal calculations are performed as described in reference four (4).  $E_{\text{FRET}}$  was calculated using the acceptor normalization method (6). 50nM was determined as the proper concentration of RNA to achieve desired fluorescence in a microplate reader (Spectramax Gemini, molecular devices). This concentration and excitation settings read around 100 fluorescence units for both dyes in this instrument. Signal variation of 0.5 units in background wells and in sample wells was observed. For EC<sub>50</sub> determinations, compounds were screened in at least 6 concentrations. Averages of three separately prepared samples were used to determine EC<sub>50</sub>. Appendix 1 lists the results of EC<sub>50</sub> determinations and compound structures for all 22 hits in the library used.

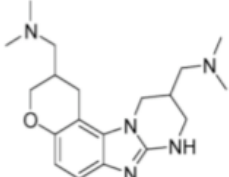
Sigmaplot (Systat software inc) software was used to determine  $EC_{50}$ s in all experiments. Data were fit using the Pharmacology module, fitting primarily to a sigmoidal dose response curve with a Hill coefficient of 1. When sufficient data points (>15) were available, variable Hill slopes were allowed.

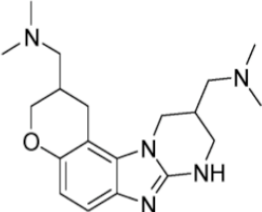
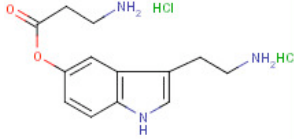
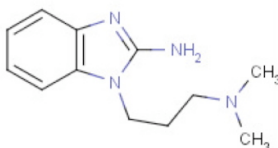
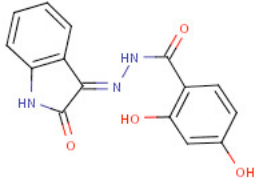
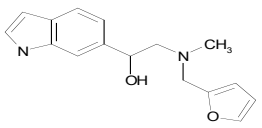
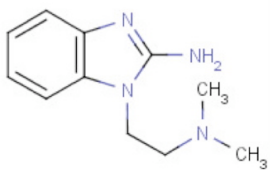
## References:

1. Parsons, J. and Hermann, T. (2007) Conformational flexibility of ribosomal decoding-site RNA monitored by fluorescent pteridine base analogues. *Tetrahedron*, Volume 63, Issue 17, 23. pp.3548-3552
2. Dibrov, S.M., Parsons, J., and Hermann, T. (2010) A model for the study of ligand binding to the ribosomal RNA helix h44. *Nucleic Acids Research*; doi: 10.1093/nar/gkq159
3. Dibrov, S.M., Johnston-Cox, H., Weng, Y.H., Hermann, T., (2007). Functional architecture of HCV IRES domain II stabilized by divalent metal ions in the crystal and in solution. *Angew. Chem. Int. Ed. Engl.* 46, 226–229.
4. Parsons, J., Castaldi, M.P., Dutta, S., Dibrov, S.M., Wyles, D.L., and Hermann, T. (2009) Conformational inhibition of the hepatitis C virus internal ribosome entry site RNA. *Nature Chemical Biology* 5, 11 823-825.
5. Studer, S.M., Joseph, S. (2007). Binding of mRNA to the bacterial translation initiation complex. *Methods Enzymol*, 430:31-44.
6. Clegg, R.M., (1992) Fluorescence resonance energy transfer and nucleic acids, *Methods Enzymol.* 211, pp. 353–389.
7. Puglisi, J.D., Tinoco, I. (1989) Absorbance Melting Curves of RNA. *Methods Enzymol*, 180, pp 304-326.

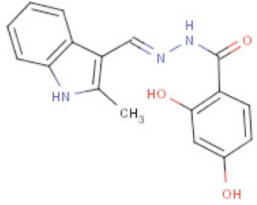
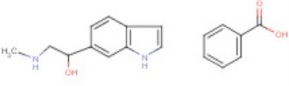
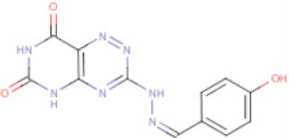
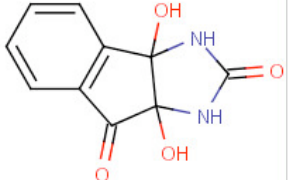
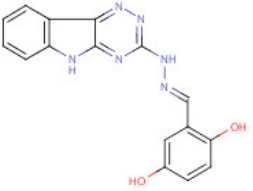
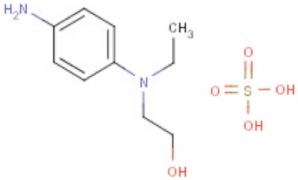
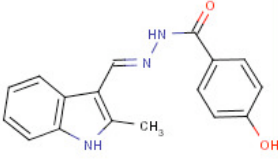
## 6.2: Appendix I.

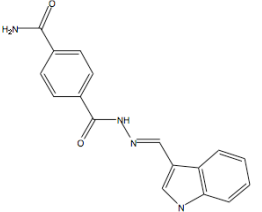
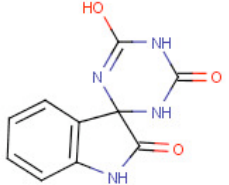
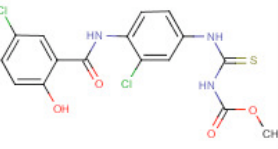
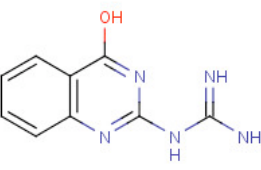
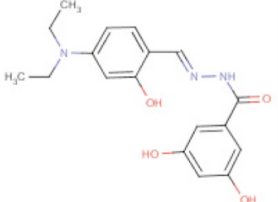
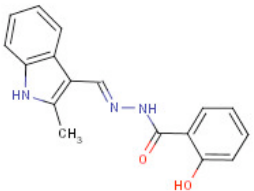
This appendix consists of a list of compounds that decreased  $E_{\text{FRET}}$  in Ila-2 RNA, sorted by calculated  $EC_{50}$ . Presented here is the tool compound P253 as an example. Activity at  $200\mu\text{M}$  is normalized such that the  $E_{\text{FRET}}$  of native Ila-2 RNA is equal to 1.  $EC_{50}$  calculations are all accurate to within  $\pm 15\%$ . RB: Number of rotatable bonds. clogP: logarithm of calculated octanol/water partition coefficient. tPSA: Total polar surface area.  $H_{\text{acc}}/H_{\text{don}}$ : Number of hydrogen bond acceptors / donors. logSw: logarithm of solubility (mg/mL) in water.

ID	Image	"Activity" 200 $\mu\text{M}$	RB	clogP	tPSA	$H_{\text{acc}}$	$H_{\text{don}}$	logSw	Titration $EC_{50}$ ( $\mu\text{M}$ )
P253		0.52	4	2.34	45.56	6	1	N.A.	1

ID	Structure	"Activity" 200μM	RB	clog P	tPSA	ac c	do n	logS w	EC <sub>50</sub> (μM)
P253		0.52	4	2.34	45.56	6	1	N.A.	1
5107240		0.01	6	-0.51	94.13	4	3	0.44	4
5554163		0.49	3	1.65	47.08	3	1	-1.19	50
5276446		0.78	2	2.26	111.02	5	4	-2.72	60
C607-0885		0.65	5	2.01	52.40	4	2	N.A.	70
5544010		0.66	2	1.40	47.08	3	1	-0.88	100



5275548		0.70	3	3.13	97.71	4	4	-3.55	125
5106637		0.72	2	1.86	85.35	4	4	-1.17	150
5937015		0.98	3	0.37	149.01	7	4	-1.55	150
5174412		0.08	0	-1.45	98.66	4	4	-0.88	<200
5308400		0.68	3	2.46	119.31	6	4	-4.17	<200
5106249		0.72	0	-1.42	124.09	5	4	0.70	<200
5227279		0.74	3	2.75	77.48	3	3	-3.11	<200

8827122	 8827122	0.76	4	1.81	100.34	3 3	-2.98	<200
5319927		0.32	0	-0.05	102.82	4 4	-2.16	n/a
5175280		0.66	3	3.96	99.69	4 4	-5.02	n/a
5190842		0.79	2	1.28	107.91	4 4	-1.78	N/A
5227379		0.79	3	2.25	105.39	5 4	-3.05	N/A
5194356		0.62	3	3.70	77.48	3 3	-3.92	N/A

## Using IRES iFRET construct for compound screening

### 1) Preparation and Plate Setup

- Determine desired concentrations and setup of screening compounds:
  - Determine maximum number of wells available per compound:
    - $(90 / (\#Replicates * \# compounds)) * \#plates\ desired$
  - Choose concentrations of compound to suit expectations (Typically 100uM to 100nM)
  - Create stocks of the compound (preferably in PCR tubes for multichannel access) at around 100X final concentrations
- Plate Setup
  - Final Well Contents: 120 uL: 10mM HEPES ph 7.0, 2mM MgCl 50nM iFRET RNA (+compound)
  - 5' Cy5/UGCGUGUCGUGCAGCCUCCGG
  - 5' Cy3/UCGGAGGAACUACUGUCUUCACGCC
  - Controls: 6 wells: 2x No RNA added, 4x No Compound added
  - Prepare well solution with compound in PCR strips, vortex, heat to 65C for 5 minutes and snap cool on ice before transferring to microplate.

### 2) Instrument Setup

- SOFTmax software should be set up to read the following wavelengths:
  - ex540/em670  $\equiv$  FRET
  - ex540/em570  $\equiv$  Cy3
  - ex640/em670  $\equiv$  Cy5
- All settings use automatic filter.
- To minimize effects of crashes, set up software to read each ex/em as a separate plate.

### 3) Data collection/interpretation

- $eFRET = EE / Cy5$
- $EE = FRET - (DE + CT)$
- DirectExcitation:  $.03878 * Cy5$
- CrossTalk:  $.03613 * Cy3$
- DirectExcitation and cross talk terms are derived from single-labeled constructs. To do so, simply measure the same 3 wavelength pairs in single-labeled constructs (one Cy3 and one Cy5-only) and solve for correction factors that zero out the cy5 term in cy3-only construct and vice versa
- eFRET should be in the range of .42-.55 for the only-RNA controls (variability based primarily on  $Mg^{2+}$  concentration)

A significant result would be >3SD (P253 is >15SD) away from the mean of the 4 RNA-only controls. Any signal observed in the 2 No-RNA controls is subtracted from each well.